ACOUSTIC AGGLOMERATION OF POWER PLANT FLY ASH

Final Report

By
G. Reethof
O. H. McDaniel

Technical Information Center
Office of Scientific and Technical Information
United States Department of Energy

DISCLAIMER

This report was prepared as an account of work sponsored by an agency of the United States Government. Neither the United States Government nor any agency Thereof, nor any of their employees, makes any warranty, express or implied, or assumes any legal liability or responsibility for the accuracy, completeness, or usefulness of any information, apparatus, product, or process disclosed, or represents that its use would not infringe privately owned rights. Reference herein to any specific commercial product, process, or service by trade name, trademark, manufacturer, or otherwise does not necessarily constitute or imply its endorsement, recommendation, or favoring by the United States Government or any agency thereof. The views and opinions of authors expressed herein do not necessarily state or reflect those of the United States Government or any agency thereof.

DISCLAIMER

Portions of this document may be illegible in electronic image products. Images are produced from the best available original document.

DISCLAIMER

ACOUSTIC AGGLOMERATION OF POWER PLANT FLY ASH

FINAL REPORT

G. REETHOF, O.H. McDANIEL
NOISE CONTROL LABORATORY
AND
CENTER FOR AIR ENVIORNMENT STUDIES
THE PENNSYLVANIA STATE UNIVERSITY
UNIVERSITY PARK, PA 16802

PREPARED FOR

MORGANTOWN ENERGY TECHNOLOGY CENTER
U.S. DEPARTMENT OF ENERGY
P.O. BOX 880
MORGANTOWN, W. VA. 26505

TABLE OF CONTENTS

EXECUTIVE SUMMARY

Acoustic Agglomeration of Fly Ash

The twenty-five month long research and development program produced important results which will add considerably to our understanding of the processes of sonically induced agglomeration of submicron and micron sized fly ash particles. The work has also shown that acoustic agglomeration at practical acoustic intensities and frequencies is technically and most likely economically viable. The following studies were performed with the listed results:

The physics of acoustic agglomeration is indeed complex particularly at the needed high acoustic intensities in the range of 150 to 160 dB and frequencies in the 2500 Hz range. The analytical model which we developed, although not including nonlinear acoustic efforts, agreed with the trends observed.

We concentrated our efforts on clarifying the impact of high acoustic intensities on the generation of turbulence. Our results from a special set of tests show that although some acoustically generated turbulence of sorts exists in the 150-170 dB range with acoustic streaming present, such turbulence will not be a significant factor in acoustic agglomeration compared to the dominant effect of the acoustic velocities at the fundamental frequency and its harmonics.

Our studies of the robustness of the agglomerated particles using the Anderson Mark III impactor as the source of the shear stresses on the particles show that the agglomerates should be able to withstand the rigors of flow through commercial cyclones without significant break-up.

We designed and developed a 700°F tubular agglomerator of 8" internal diameter. The electrically heated system functioned well and provided very encouraging agglomeration results at acoustic levels in the 150-160 dB and 2000-3000 Hz ranges. We confirmed earlier results that an optimum frequency exists at about 2500 Hz and that larger dust loadings will give better results.

Studies of the absorption of acoustic energy by various common gases as a function of temperature and humidity showed the need to pursue such an investigation for flue gas constituents in order to provide necessary data for the design of agglomerators.

The report ends with a set of conclusions and recommendations for future work in a follow-on program.

I. INTRODUCTION AND STATEMENT OF PROBLEM

The projections for energy of the future as reported in the 1981 Annual Report to Congress by the Energy Information Agency of the U.S. Department of Energy show increasing use of coal as a fuel as given in Table 1 [1]. Also the percentage of coal used relative to domestic energy supplies increases gradually from an actual 28.8% in 1980 to a projected 39.3% in 1995. Oil and natural gas consumption actually show a slight decrease over these years with nuclear energy projected to take up about 10% of domestic production in 1995 compared to 4.2% in 1980.

The history and projections of coal by end use to the year 1995, are given in Figure 1 [1], showing dramatic increase in the use of coal by the electric utilities. These projections reflect the reality of the abundance of coal reserves in the United States. At these consumption levels, coal deposits in the United States are estimated to last at least for 300 years. Since the U.S. coal reserves are estimated to be 475 billion tons with an average annual usage of 1500 million tons over the years, this estimate is certainly not unreasonable.

However, coal fired power plants do emit large amounts of particulates and noxious gases, the removal of which presents major technical challenges and large capital outlays to meet the present stringent environmental protection requirements.

The fine particulate emissions from fossil fueled combustion equipment without any controls have been estimated for typical electric utility boilers on both a number and a mass basis and are given in Figure 2 [2]. Although the data was reported in 1969, power generation has only increased

Table 1. Balance Between Energy Supply and Demand Projections by Type of Energy and Sector, Midprice Case
(Quadrillion Btu per Year)

	History	Projections		
	1980	1985	1990	1995
World Oil Price				
(1980 dollars per barrel)	33.89	33.00	49.00	67.00
Domestic Energy Supply				
Oil	20.6	19.3	20.0	21.2
Gas	19.8	18.6	18.2	18.7
Coal	18.7	21.9	27.1	33.7
Nuclear	2.7	5.4	7.6	8.6
Other (hydropower, solar, and geothermal)[a]	3.0	3.3	3.5	3.6
Subtotal	64.8	68.5	76.4	85.8
Net Imports				
Oil[b]	13.3	14.7	12.0	10.6
Gas	1.0	0.9	0.7	0.7
Coal	-2.5	-2.7	-3.5	-4.2
Subtotal[c]	12.1	12.8	9.2	7.1
Total Energy Supply	76.8	81.3	85.7	93.0
Domestic Energy Demand				
Residential	9.4	9.0	8.9	9.2
Commercial	6.8	7.0	7.3	8.0
Industrial[d]	23.2	26.4	28.3	30.4
Transportation[e]	19.0	18.9	18.2	18.3
Total End-Use Demand	58.5	61.3	62.7	65.9
Stock Changes, Accounting Errors, and Generating and Transmission Losses	18.3	20.0	23.0	27.0
Total Energy Demand[f]	76.8	81.3	85.7	93.0

[a]Includes gains from electricity generation, synthetics production, and petroleum cracking. Historical data excludes solar.

[b]Figure for 1980 includes imports for additions to the Strategic Petroleum Reserve.

[c]Includes 0.2 quadrillion Btu electricity imported in 1980.

[d]Includes refinery consumption of refined petroleum products and natural gas.

[e]Includes gas transmission losses.

[f]Total supply and consumption estimates include the use of wood to generate electrical power. All other fuel use of wood is at approximately 2 quadrillion Btu.

Sources: Historical data: U.S. Department of Energy, Energy Information Administration, Monthly Energy Review, November 1981, and Natural and Synthetic Gas, 1980 (an Energy Data Report). Estimates of energy end-use consumption were based on the State Energy Data System.

Figure 1. Coal Consumption by End Use, History and Projections, Midprice Scenario (Million Short Tons)
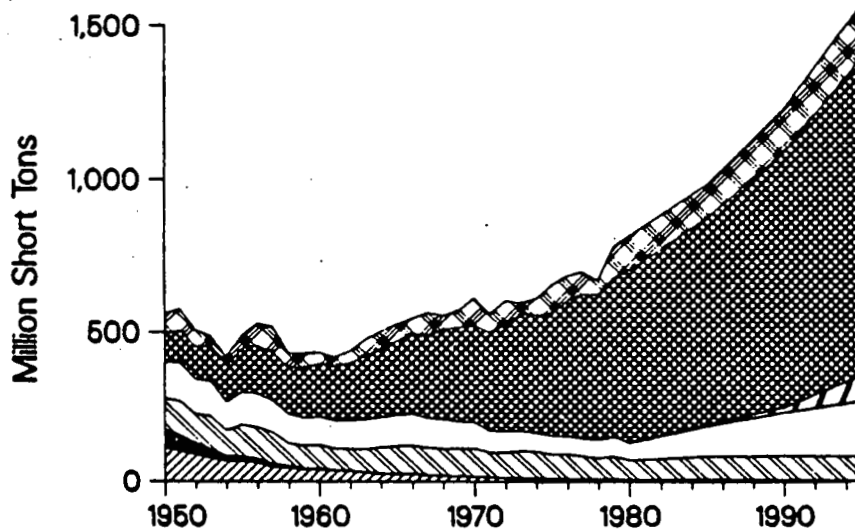
Net Exports and Stock Changes
Electric Utilities
New Technologies
Other Industrial
Domestic Coking
Transportation
Residential/Commercial
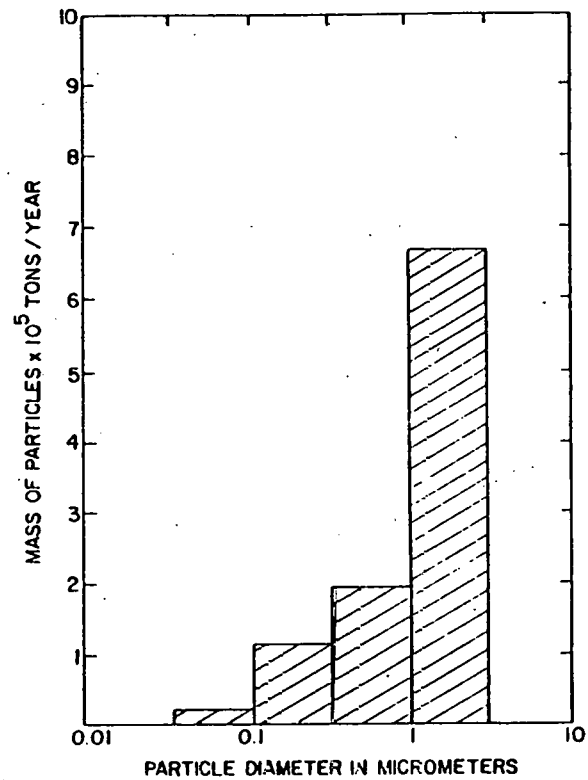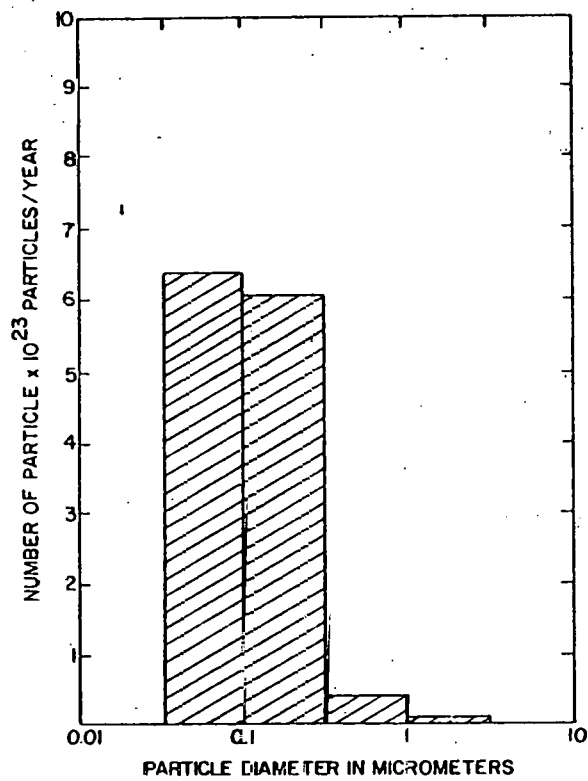
Figure 2. Emission of particles from coal fired Electric Utility Boilers in the U.S.A.

by about 10% since then so that the data is still representative. Although 90% of the mass is above 0.3 μm, we note that better than 90% of the number of particles remain below 0.3 μm. This becomes an important factor when we consider the particle removal efficiency as a function of particle size of various cleaning devices later. Of interest is the fact that particles produced by fuel oil and natural gas are smaller with most of them being smaller than 5 μm. In addition, the mass of particles produced in tons/year is much less for oil and gas as shown in Table 2. These figures are based on average emissions of 17 lb/ton for an 8% ash coal, 10 lb/1000 gallons of oil and 15 lb/million ft^3 of natural gas. Using the predicted coal consumption estimates given in Table 1, we can expect a 41% increase in particulate emissions on a mass basis between 1982 and 1995.

A further concern related to particulate emissions is their impact on the acid rain problem caused by the generation of SO_x and NO_x gases in the coal combustion process. These gases and the particulates generated are sent into the atmosphere in the smoke stack effluents and return to earth in the form of various sulfur based and nitrogen based acids. Much research effort has been, and is being devoted to this SO_x and NO_x problem. One of the more promising methods is to catalize the SO_2 and NO components to SO_3 and NO_2 in atmospheric fluidized bed coal combustors (AFBC). Ammonia (NH_3) gas is then injected into the AFBC thereby neutralizing the sulfuric and nitric acids which are formed as a result of their strong hygroscopic qualities by forming ammonium sulfates and nitrates as the gases cool. Below 513°C, at atmospheric pressures, the gaseous constituents of ammoniums sulfate form very fine, probably submicron sized particulates. The ammonium nitrate constituents similarly form very fine particulates below their

Table 2. Particulate Emissions from Controlled Power
Plants in the United States (Tons/Year).

	Measured 1974	Predicted 2000
Coal	2.66×10^5	6.40×10^5
Gas	2.50×10^2	7.36×10^1
Oil	1.16×10^3	1.50×10^3

decomposition temperature of 210°C. Both the $(NH_4)_2 SO_4$ and the $NH_4 NO_3$ particulates then join the other fine flue gas solids, primarily silica and alumina particles, the so-called fly ash effluents.

We also note from discussions with Dr. Rosa Pena, Professor of Meteorology at Penn State and world renowned expert on acid rain, that much of the acid rain comes from such particulates of ammonium sulfate, ammonium nitrate and sulfuric acid droplets. In fact, Dr. Pena's research on sulfate aerosol production and growth in coal operated power plant plumes [5] has shown that 60% to 70% of the atmospheric acidity correlates with sulfates and 20% to 30% with nitrates. Thus, a method for the removal of the sub-micron sized sulfate and nitrate particles from the power plant effluents would certainly promise to provide substantial gains in the reduction of acid rain causes and respirable dust. As Dr. Pena pointed out to us: "It is much easier to remove the particulates than it is to remove such gases as SO_2, SO_3, NO and NO_2". As will be pointed out later, conventional particle removal methods do not provide efficient entrapment of submicron particles.

Another area of concern is the adsorption of SO_2, SO_3, and NO_2 gases on the surfaces of the escaping fly ash particles. As Dr. Robert Kabel, Professor of Chemical Engineering at Penn State and well known authority on gas adsorption on particles and environmental chemical processes, pointed out to us in several discussions, the remaining submicron particles after clean-up with conventional cleaning methods are the most efficient adsorbers because of their high area to volume ratio. Since SO_3 and NO_2 gases adsorbed on the particle surfaces are highly hygroscopic, they will absorb water vapor as they rise in the atmosphere into inversion layers. These particles

will increase in size and become acidic aerosols which will either fall out or be scrubbed out by rain forming acidic precipitations.

Thus, if we remove these submicron particles from the stack effluents, the ammonium sulfates and the ammonium nitrates and the acid bearing fly ash, we also reduce the acid rain problem and also the to be discussed injurious aspects to the human pulmonary system.

Current techniques to remove particulates in coal fired power plant flues are based on electrostatic precipitators, bag houses and wet scrubbers. Typical collection efficiencies of such devices and the far less efficient cyclones are shown in Figure 3. Of interest is the fact that below 1 μm the efficiencies drop off rather precipitously. Work presented by Davies [3], Figure 4, has shown that the human lower pulmonary system is unfortunately most efficient in absorbing and retaining particles in the 1 μm range. These particles are the primary cause of such respiratory ailments as bronchitis, emphasema and lung cancer.

Observations indicate that currently, approximately 50% of the particles suspended in an urban atmosphere are smaller than 1 μm [2]. This fact appears to be in part the result of the low efficiency of particle collection devices for the removal of these small particles. Therefore, legislation has been under consideration at the Federal level which will include recognition of particle size rather than just mass removal which is the sole criterion in current Federal legislation. California and Maryland have already legislation in effect which, as a result of a "no visible emission" statement, provides some control of submicron particulates.

Based on statements recently made by John Neal, Chief, Control Technology Division, U.S. Department of Energy at Morgantown Energy Technology Center at the 2nd Annual Contractors Meeting on gas stream clean-up, February 17,

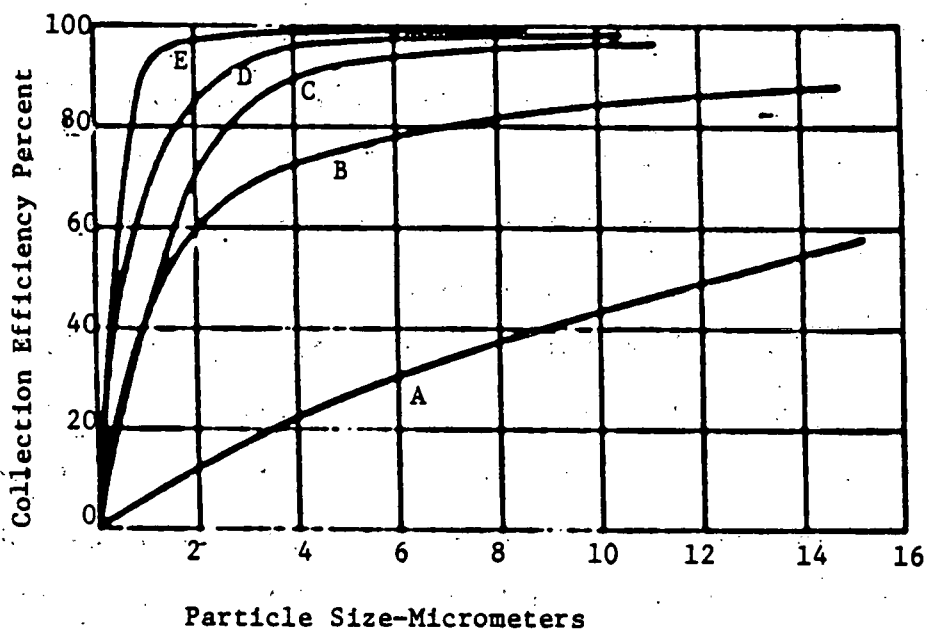Figure 3. Collection efficiencies of several particle removal devices.

A. High Throughout Cyclone
B. High Efficiency Cyclone
C. Dry Electrostatic Precipitator
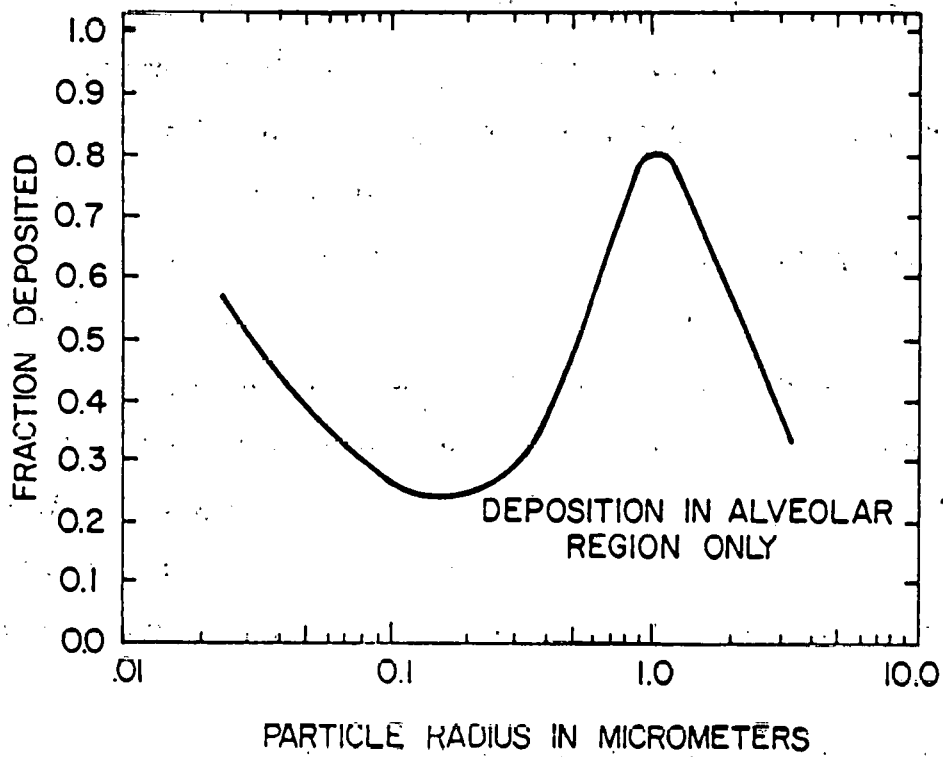D. Spray Tower
E. Scrubber

Figure 4. Absorption of particles in the human
pulmonary system.

1982 [4], most of the emphasis at the Federal level has been on "the simultaneous removal of SO_x, NO_x, constituents and particles based on longer range concerns of acid rain, health effects and visibility problems possibly associated with NO_x in the atmosphere along with SO_x and particulates".

Over the last several years, research has been supported by the U.S. Environmental Protection Agency at Air Pollution Technology, Inc. under Dr. Seymour Calvert's direction to develop much improved wet scrubber technologies (incidentally, Dr. Calvert is former Director for Penn State's Center For Air Environment Studies), with some success reported.

Yeh, Lee and Liu at the University of Minnesota, have performed promising research on the migration of small particulates through various fabrics with the aim of developing much improved fabrics for bag house type cleaning devices.

Other techniques which are being investigated are condensation scrubbers, charged droplet systems, electrified filters and foam scrubbers.

The agglomeration or growth of the submicron and low micron sized particles into 5 to 20 micron sized agglomerates for subsequent efficient removal by conventional particle removal devices, such as those mentioned earlier, is one of the most attractive alternatives and the subject of this proposal.

Accelerated agglomeration of particles in sound fields is not a new idea. William Ostwald first suggested the use of acoustic agglomeration to collect liquid particles although as early as 1866 Kundt [7] had performed experiments which demonstrated the aggregation of dry dust particles to study the speed of sound in a standing wave tube. Since then numerous experiments providing positive results have been conducted. Notable among the early studies is the work of Smoluchowski [8], in Germany in 1915; Andrade [18];

Brandt, Freund and Hiedeman in Germany [6,9] in 1936; St. Clair [10] in the

United States between 1938 and 1950; Stokes [11] in the United States

in 1950. Of much interest is the work of Neumann, Danser and Soderberg

and Fowle [24-29], at Ultrasonic Corporation in Cambridge, Massachusetts

during the early 1950's, who developed commercially available acoustic

coagulators for such diverse applications as cement plants, open hearth gas

dust removal, calcinated soda removal, molybdenum disulfate, ammonium chloride,

carbon black and other dust as well as liquid aerosol agglomeration. The

sound source was a siren with outputs in the 10th of kilowatt ranges. The

company did not prosper apparently because of the lack of interest in

environmental pollution control and economic conditions of the time.

However, much valuable experience was obtained providing important background

to todays revival of the field. The most thorough and often quoted work

was done by Mednikov [12], and others in Russia in the 1960's. More

recent and very thorough work by Volk [13 & 14] in the United States at

Penn State University has shown significant agglomeration of carbon black,

white lead, kaolin clay and fly ash dusts at rather modest acoustic levels,

between 100 and 120 dB with frequencies in the 1000 to 6000 Hz range,

representative dust loadings between 0.5 to 2 gm/m^2, and exposure times

varying from 10 to 40 seconds. The acoustic agglomeration theory developed

by Volk is based on the work of Mednikov [12], Levich [15] and Black [16]

and Fuchs [17]. Scott [19], in Canada performed very interesting and important

studies on the effect of nonlinear acoustic effects on agglomeration.

Shaw [20] through [22], and his associates at the State University of New

York at Buffalo have performed research of both a theoretical and experi-

mental nature on acoustic agglomeration with special emphasis on the

phenomena of acoustically induced turbulence at very high levels of acoustic

intensities and also the effects of acoustically induced shock waves. Dr. Shaw claims that at levels above 160 dB, much enhanced agglomeration occurs for further small increases in sound intensity and that agglomeration rates become largely independent of frequency permitting the use of lower frequencies, i.e. ≈ 800 Hz, than are needed at lower acoustic levels to obtain best acoustic agglomeration performance. In fact, it is suggested that with acoustic turbulence, exposure durations of only a second or two, at frequencies of ≈ 800 Hz and 161 dB are needed to obtain satisfactory agglomeration. Research at Penn State over the last two years under the principal investigators direction, has not been able to identify such high acoustically generated turbulence levels under similar conditions. This important subject will be discussed in considerable detail in this report.

On the other hand, very effective agglomeration of submicron sized particles of fly ash at flue temperatures was obtained by us with similar acoustic levels of 155-165 dB but at frequencies in the 2500 Hz range and exposure times of about 10 seconds. The details of these experiments and the theoretical foundation will be discussed in the several sections of this report.

We must also mention the acoustic agglomeration experiments conducted by the Braxton Corporation [23] in 1974 which did not give good results. In fact, essentially no agglomeration was experienced in this rather large scale facility. These tests which were supported by EPA, were performed at a frequency of 366 Hz and intensities of 165 dB. Redispersed cupola dust of about 4 μm mean size and fly ash of about 6 μm mean size were used as dusts. The results of our research and Dr. Shaw's work clearly show that for the type and size of dust used, frequencies of the order of 2500 Hz and 3000 Hz provide optimum agglomeration. It is, therefore, not surprising that very poor results were obtained by the Braxton experiments.

From these introductory remarks it is apparent that much work has been done on both the theoretical and the practical aspects of acoustic agglomeration.

The research results to date at Penn State University show conclusively that acoustic agglomeration of fly ash can be accomplished yet further research is required on several important acoustic and coagulation phenomena before large scale demonstrations of the technical and economic viability of the process can be accomplished.

II. PRESENTATION OF RESULTS

2.1 INTRODUCTION

The just completed research grant entitled "Acoustic Agglomeration of Power Plant Fly Ash" was a two year and one month program. The program was administered by the Morgantown Energy Technology Center, Morgantown, West Virginia with Mr. William F. Lawson as the Technical Monitor and Mr. Raymond Hill the Contract Administrator. The work was performed under Grant No. DE-AC21-81MC16359.

The knowledgeable support and strong encouragement of the Technical Monitor, Mr. Lawson, and also the appreciation of the technical significance of our work by Dr. Jack Halow, Chief, Gas Clean-up Branch, as well as Mr. Kenneth Markel, Project Manager, Coal Projects are most certainly appreciated.

The work statement for this program is given in Appendix A. This section of the final report will address the items of the work statement in the given order. The reader will note that we have concentrated our efforts in the following areas: 1) Research on acoustically generated turbulence; 2) The design, construction, development and use of the 700°F new agglomerator; 3) The room temperature fragility study and 4) the absorption of acoustic energy by flue gas constituents at the expected conditions in flue gas clean-up systems. We believe that we can state without reservation that good and significant progress has been made.

2.2 ACOUSTIC MODELING OF THE AGGLOMERATION PROCESSES. (TASK I)

The work on a theoretical model of acoustic agglomeration, started under the previous one year contract and was continued under the present research contract. The development of a refined model was completed and the model

was run successfully over a wide range of operating conditions such as
sound intensities, frequencies, particle sizes and gases. This complete
phase of the work was published as a Master's Thesis in Mechanical Engineering
by Mr. Hsu-Chiang Miao in August of 1981. In this section we present the
highlights of the agglomeration model without the mathematical details
yet explaining the physical principles upon which our theory is based.

After a quite complete review and analysis of the literature, we pro-
ceeded to develop an analytical model from fundamental physical principles.
The processes to be described result in:

  1) Particle oscillation;

  2) Particle drift;

  3) Particle collisions;

  4) Particle adhesion.

In deriving the relationships for the particle kinetics we have to develop
equations for the individual forces acting on the aerosol particles. We
considered the following phenomena:

  a) Viscous drag forces (Stokesian forces) due to local velocity
fluctuations and convection flows. These forces are caused by:

      --acoustic velocities,

      --hydrodynamic turbulence due to convection flows,

      --turbulence caused by high intensity acoustic field,

      --acoustic streaming velocities from the nonlinear acoustic

        effects at high intensity levels.

In our model we included acoustic velocities as the primary Stokesian
mechanism. We formulated an acoustically induced turbulent diffusion
coefficient on the basis of Kolmogorov's theory of local isotropic turbulence [30]
and Z. A. Goldberg's formulation of a maximum value of energy dissipation [31].

The resulting turbulence scales at the acoustic levels and frequencies under consideration in Miao's work are about 3 orders of magnitude larger than the particles.

Acoustic streaming was not included in the model and appears not to have been significant at the acoustic levels so far considered. Yet future models must include this factor as higher acoustic levels are considered.

There is no provision for hydrodynamic turbulence due to convection flows in the present model. We feel that this factor should also be included in future models to more realistically represent the expected turbulent flows in practical agglomeration chambers.

b) Forces due to Brownian motion are included in a Brownian diffusion coefficient which is added to the turbulent diffusion coefficient previously discussed.

c) Radiation Pressure Forces. If a soundwave encounters a body in its path of propagation, the wave is scattered as it strikes the body. The radiation pressure is the difference between the momentum transferred to the stricken body by the incident wave and the momentum of the wave scattered by the body. Since the wavelength of the fundamental is much larger than the size of the particle, these forces are quite small for travelling waves, but can become significant for the harmonic components of nonlinear standing waves with forces directed toward antinodes.

d) Average Viscous Forces. Because of the acoustic pressures existing in the sound field, the density variations will result in not insignificant temperature fluctuations. Since the viscosity is roughly proportional to the square root of the temperature, the product of the sinusoidal velocity

fluctuation times the viscosity variation will not vanish and result in a net viscous drag force toward the sound source for travelling waves. This drift velocity is proportional to the average acoustic energy density and inversely proportional to the characteristic acoustic impedance of the gas.

e) Average Oseen Forces. Stoke's viscous drag force expression can be expanded to the second order in relative gas - particle velocity using a Taylor series expansion. This second order term results from the wave shape distortion associated with the large acoustic amplitudes in travelling waves. The coefficient associated with the second order term was derived by Oseen and results in a drift velocity term which is proportional to the mean acoustic energy density, the relative magnitude of the second harmonic, the size of the phase angle between fundamental and second harmonic, the size of the particle and inversely proportional to the gas viscosity. Depending on the phase angle, the drift may be either toward or away from the sound source.

f) Hydrodynamic Forces. If we consider two oscillating particles that are separated by distances of the same order as the particle sizes and if furthermore, an ideal incompressible fluid flows between them such that the mean and oscillating fluid velocity vector is essentially perpendicular to the line seperating the particles, an attractive force will result from the narrowing of the stream and the ensuing increase in local velocity. The attractive force is proportional to the gas density, the square of the gas vibratory velocity, the velocity amplitudes of each particle relative to the medium, the cube of the size of each particle and inversely proportional to the fourth power of the distance between the particles. The phase angle between the direction of the oscillations and the particles centerline also enters the equation.

This "Bernoulli" attractive force will become important for particles in close proximity during the final stage of agglomeration.

g) Hydrodynamically and Acoustically Induced Turbulence. The role of turbulence in enhancing agglomeration of submicron particles has been discussed by Mednikov [12], Levich [15] and more recently by Shaw [20-22] and his researchers. Turbulence is described by its intensity which is the root mean square of the velocity fluctuation and the "scale" in time and space. Only if the turbulence is sufficiently intense and of sufficiently small space and time scales relative to the other causes of particle motion discussed earlier can we expect it to be a significant factor in the collision processes. On the basis of Kolmogorov's [30] theory of local isotropic turbulence and Z. A. Goldberg's [31] development of the turbulent diffusion coefficient for sound intensities of 150 dB in the 1 KHz range we calculate a turbulence space scale of about 100 μm and local velocities which are much smaller than the acoustic velocities at the high intensities considered. We shall discuss this very important topic in Section 2.3 in detail showing that acoustically generated turbulence does not appear to be a significant factor except for acoustic streaming effects.

From the previous discussion it is clear that a complete model of the agglomeration processes will be very complex. Following the work of Mednikov and Levich we have constructed a model which incorporates two mechanisms: the diffusional mechanism which recognizes the coming together of particles from purely random relative motions and the orthokinetic mechanism which results in collisions from the different translational or drift velocities between particles of different sizes. In this sense since relatively large particles are much less affected by the acoustic phenomena than small particles, we can visualize the process as having the large particles sweep out regions where small particles oscillate.

The relationships for diffusional and orthokinetic activities are of necessity very complex and will not be given here. The numerical procedure is formulated to include mass conservation and considerations for the increasing porosity of the agglomerates based on the assumption of particle sphericity. Also it was assumed that all collisions result in adhesion.

The model was only exercised for sound pressure levels up to 140 dB which is a relatively modest level in terms of the impact of nonlinear acoustic effects such as acoustically generated wave steepening and shocks as well as acoustically generated turbulence and acoustic streaming. The results are quite encouraging in that good agreement is shown between predicted agglomeration and test results from our old test facility using the siren sound source. Figure 5 is typical of the results showing significant size increases and agreeing quite well with earlier results by Volk [13 & 14]. Of importance is the fact that we again find an optimum frequency of about 3000 Hz for the fly ash dust with a log normal size distribution; that increasing sound pressure levels should give marked increases in agglomeration; that increased particle density and increased particle sizes will result in lower optimum frequencies.

The spacial characteristics of the sound field resulting from standing wave phenomena in rectangular and circular crossection agglomerator ducts will be discussed in the next section of this report. We now believe that because of the relatively large spatial scale of such standing waves relative to the agglomeration scales, we can estimate the effect of standing waves by dividing the chambers into finite sized rectangular parallelepipeds or annular segments. Each segment is treated as a small agglomerator with
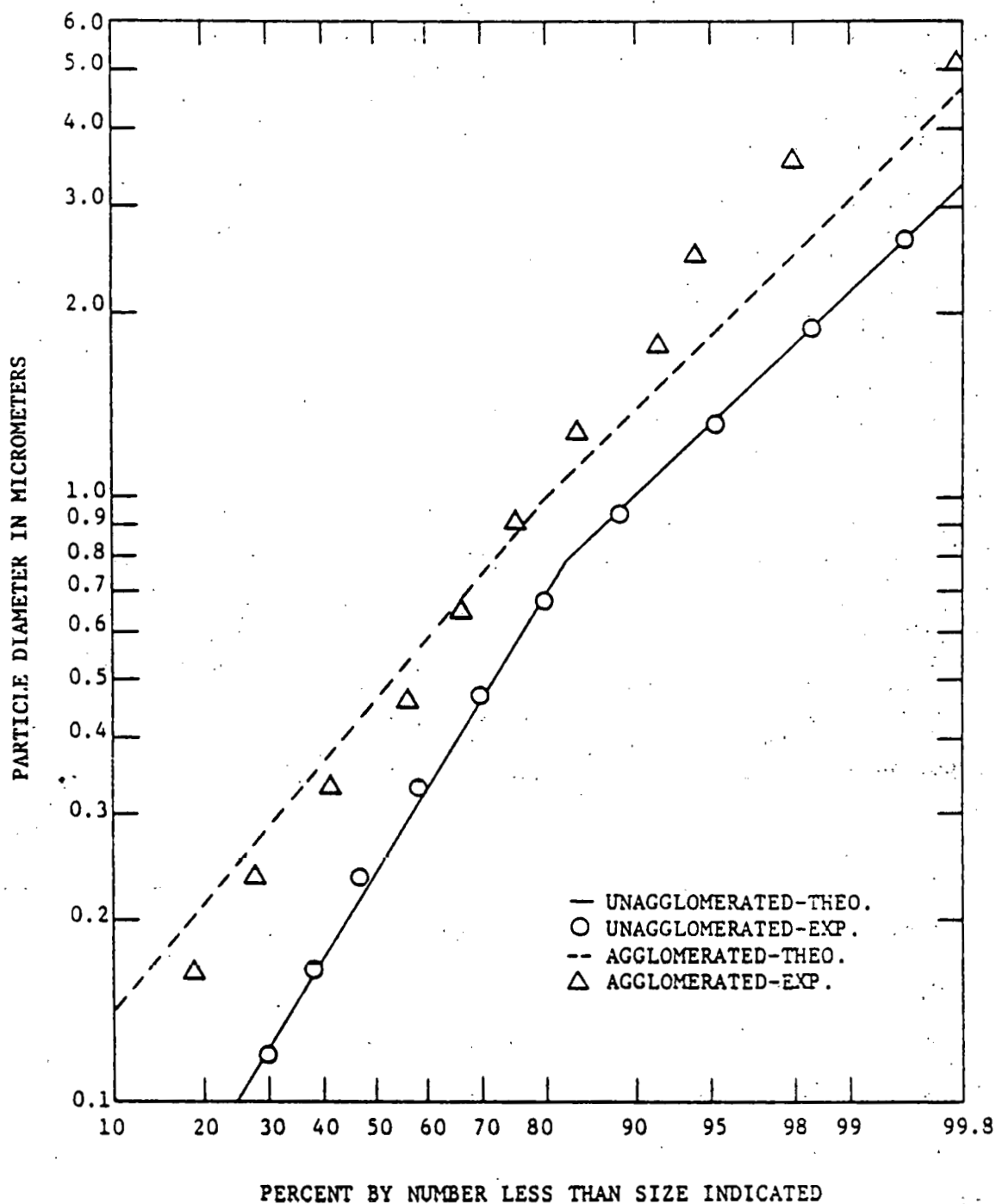
Figure 5. Theoretical and Experimental Particle Size Distributions for Fly Ash Aerosol; Conditions of Agglomeration Were a Sound Pressure Level of 140 dB, Frequency of 2000 Hz, Mass Loading of 2.5 gm/m^3 and an Exposure Time of 26 Seconds.

time exposure determined by the respective size and convection velocity.
Sound pressure levels for each volume will be approximated by the average
value for the particular location and extent. Since the wave length of
the sound wave is given by the ratio of the speed of sound to the
frequency, we find for 700°F gas at 2000 Hz a wave length of 10.0 inches.
We have at last partially accounted for the nonlinear effects by including
wave distortion in the form of the second harmonic term into the model
for the forces on the particle. Much still remains to be done to arrive at
a fully satisfactory model for the high acoustic levels which are clearly
necessary for satisfactory agglomerator performance.

The theoretical and experimental investigation into the potential of
using the parametric acoustic effect to generate both sonic and ultrasonic
acoustic energy show that indeed the nonlinear interaction of two ultra-
sonic acoustic sources operating at a frequency difference in the desired
sonic frequency range does provide high levels of sonic frequency energy
as a result of the high degree of energy exchange. We realize, however,
that the high absorption of acoustic energy by the gases at the temperatures and
frequencies does not make the concept economically viable. Our recent
studies on the topics of acoustic energy absorption of gases have led to
this conclusion. The important preliminary work on this topic is reported
elsewhere in this report.

We must note that we did not continue the development of the agglo-
meration model beyond the work of Miao which was completed in June of 1981
because of the much increased interest expressed by the sponsor in the
topics of particle fragility and the very important question of the signifi-
cance of acoustically generated turbulence on the agglomeration process.

2.3 BASIC ACOUSTIC INVESTIGATIONS.

2.3.1 INTRODUCTION TO ACOUSTIC TURBULENCE STUDIES

Our major emphasis in this task was to study theoretically and experimentally the acoustic and hydrodynamic velocity field in two model chambers at high sound intensities and at frequencies which we expected to encounter in acoustic agglomerators. The motivation was to study further the very important findings reported by Dr. David Shaw and his group of researchers at The State University of New York at Buffalo, New York. There is no question that if indeed acoustically generated turbulence of significant turbulence intensity and sufficiently small scale exists in a high intensity acoustic field the acoustic agglomeration rates can be much enhanced. Mednikov [12] and Levich [15] have shown that both turbulent diffusional and turbulent inertial effects if significant compared to the effects of acoustic velocities will result in the dominance of the turbulence generated kinetic effects. Turbulence of the kind discussed here is a spectrally random phenomenon meaning that much enhanced agglomeration can be obtained at lower frequencies than the hitherto considered diffusional orthokinetic and other effects due to acoustic velocities which peak at frequencies of 2000 to 3000 Hz for typical fly ash aerosols. This aspect is very important as absorption of the acoustic energy by the gases increase typically as the frequency squared as a result of molecular relaxation phenomenon. Thus, lower acoustic powers would be needed if the frequencies could be in the 800 Hertz range rather than 2000 Hz which in turn, would decrease the energy costs of the agglomerator. Furthermore, the much reduced exposure times needed will result in smaller agglomeration volumes reducing the power demands even further. The importance of establishing the existence of

"Acoustic - Hydrodynamic Turbulence - Turbulence Interaction" as termed by Shaw, is an aspect of paramount importance to our understanding of agglomeration processes and the design of agglomerators.

The process whereby particles collide in a velocity field is primarily a diffusion process described by the diffusion differential equation which contains the all important diffusion coefficient D. The portion resulting from turbulence, the turbulent diffusion coefficient D_{turb} is given by [12]:

$$D_{turb} = 0.25 \left[\frac{\varepsilon}{2.5 \, \nu_g}\right]^{1/2} \ell^2$$

on the basis of dimensional analysis considerations where ε is the energy dissipation from any and all sources of turbulence. For acoustic velocity sources it is given by:

$$\varepsilon = \frac{\xi \, I^{3/2} \, f}{(\rho_g C_g)^{3/2} \, C_g}$$

ξ is a constant depending on gas properties;
I is the sound intensity;

ρ_g is the gas density;

C_g is the speed of sound in the gas;

f is the sound frequency;

ν_g is the gas kinematic viscosity;

ℓ is the effective collision radius.

The relationship holds for $\ell < \ell_o$ where ℓ_o is the turbulence microscale.

It is apparent that the higher the energy dissipation due to turbulence, the higher will be the agglomeration rate.

Also contained in the acoustic intensity term is, of course, the r.m.s. acoustic velocity u which in terms of the acoustic intensity is given by: (for plane waves)

$$u^2 = \frac{I}{\rho_g C_g}$$

We note that the above relationships do not consider acoustic turbulence - hydrodynamic turbulence interaction effects in a catalytic sense as noted by Shaw in acoustic agglomeration and to a lesser degree by Morris in acoustically excited small jets [32]. Our intensive research into the nature and magnitude of acoustically generated turbulence in the presence of acoustic streaming caused steady convection velocities showed rather conclusively that acoustically generated turbulence in such a velocity field at acoustic levels up to 165 dB is not a significant factor in acoustic agglomeration. Our approach and results are discussed next.

2.3.2 EXPERIMENTAL FACILITY

The experiments were performed in a rectangular chamber with dimensions of 0.3 x 0.6 x 0.025 meters. The chamber sides were made of 1/2" thick steel plates with 1/4" glass plates at the top and bottom for easy location of measurement positions and for future research using optical methods. Since the lowest frequency in the 0.025 meter direction is about 6900 Hz the chamber can be treated as a two-dimensional chamber with a lowest mode cut-off frequency of 290 Hz. All the experiments were done in the range of 1000 - 3500 Hz so that higher order modes would be excited resulting in standing wave patterns throughout the chamber. As seen in Figure 6, the two JBL series M2470 sound drivers were mounted at opposing locations at one end of the chamber. Six additional small openings were provided for acoustic and velocity probes. When not in use, the openings were closed by flush mounted plugs to prevent leakage and maintain identical boundary conditions from run to run.

Pressure Transducer   Hot Wire Probe
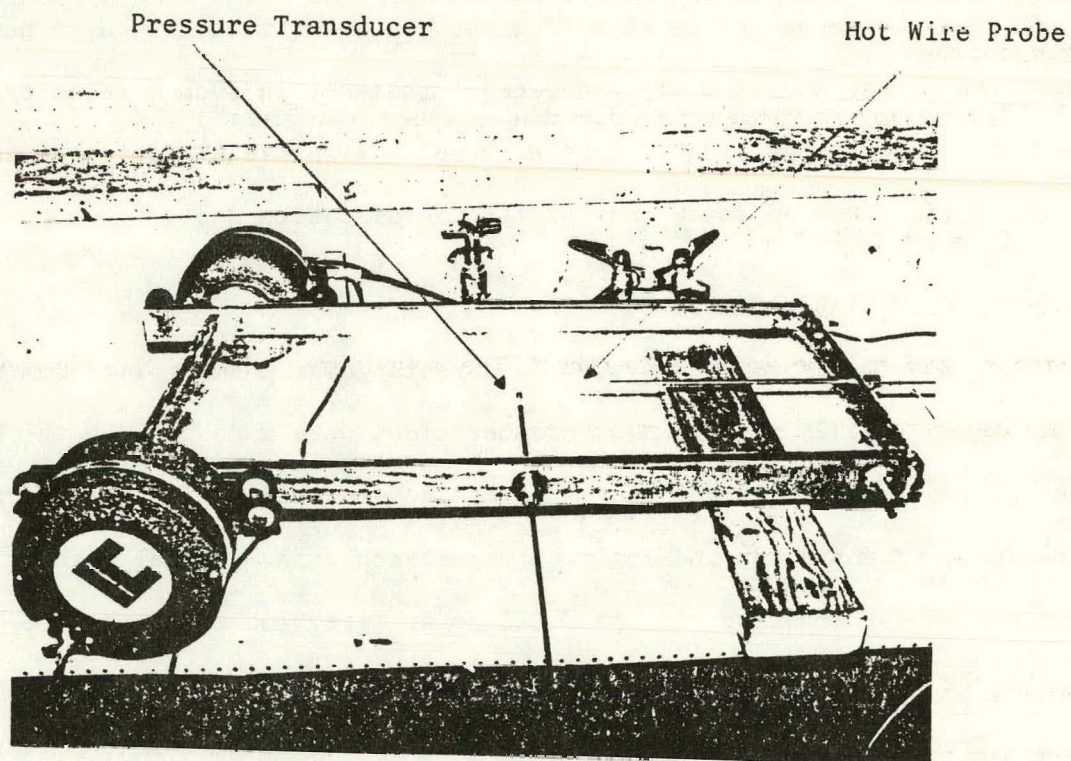

Figure 6.   Experimental Chamber to Study
            Acoustically Generated Turbulence

As can be expected certain predictable modes were strongly excited resulting in very high sound pressure levels at the nodes. The highest acoustic pressures existed at the 4 corners of the chamber. As a result of the standing waves the sound pressure levels varied sinusoidally along the wave paths for the higher order modes. It was possible to excite some plane wave conditions with the resulting wave steepening at certain frequencies.

The resonant frequencies for the chamber are given by:

$$f_n = \frac{C_g}{2} \left[\left(\frac{n_x}{\ell_x}\right)^2 + \left(\frac{n_y}{\ell_y}\right)^2 \right]^{1/2}$$

where n_x and n_y are modal integers. The sound pressure in the chamber's standing wave field is then given by:

$$P_{n_x , n_y} = A \cos \frac{\pi n_x x}{\ell_x} \cos \frac{\pi n_y y}{\ell_y}$$

where A is the wave amplitude which is determined by the acoustic power developed by the drivers and the absorption of the walls and the air; x and y are the distances from the origin at the center of the chamber. Typcial sound fields are illustrated in Figure 7 showing nodes and loops.

We observe, and this is very important, that higher order modes are dispersive meaning that they will not exhibit wave steepening in either progressive or standing waves as will be shown in wave form figures. Earlier research at Penn State has demonstrated this fact for, particularly, circular ducts excited at very high acoustic intensities.
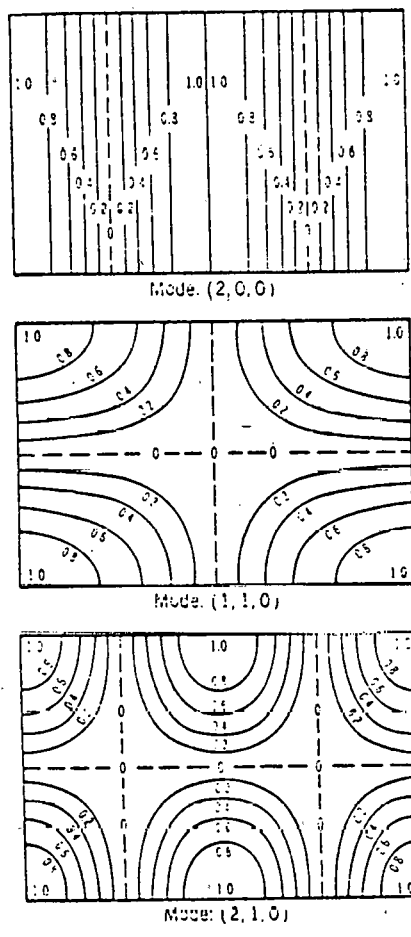
Figure 7. Sound Pressure Contour Plots in a Rectangular Chamber For
Some Simple Acoustic Modes. Modes Are Specified as
(n_x, n_y, n_z).

As a result of these high acoustic levels in the chamber and the opposing location of the acoustic drivers, a nonlinear phenomenon called acoustic streaming was present. This second order effect resulted in a steady velocity circulation in the chamber with magnitudes which assured turbulent flow circulation. The acoustic streaming velocities represented a steady velocity component which changed from one mode to the next upon which was superposed the local acoustic velocity and the acoustic turbulence velocity. Both the latter velocities have zero mean components.

A Spectral Dynamics Model SD 104-5 sweep oscillator was used to produce the pure tone electrical signal and a Biamp Model 2500 power amplifier provided the input to the sound drivers. High pass filters were used to eliminate any 60 Hz line caused signals.

The sound pressure signals were measured by a Celesco Model LD-25 and a Massa Model M-213 microphones. The vibration isolated Celesco pickup was used for wall pressure fluctuations and the Massa unit was used as a movable probe to measure acoustic pressure distribution patterns inside the chamber. Both microphones were calibrated with a B & K Model 4220 piston phone. Preamplifiers were used before the signal was sent to B & K Model 2604 microphone amplifiers and sound level meters.

The fluid velocity was measured with 5 micron Tungsten hot wire anemometers. The hot wire anemometer was mounted on a 1/8" stainless steel probe tube to permit traversing the chamber. Both probes were isolated from the steel side plates by soft plastic tube sleeves to prevent solid born transmission to the probes. The DISA Model 55 D01 constant temperature anemometer and DISA Model 55 D10 linearizer were used to process the hot wire signal. Frequency response of the system was up to 100 KHz. The hot wire anemometers were carefully calibrated before and after each run

using a TSI Model 1125 calibrator. The hot wire signals could be further

filtered by Ithaca Model 450 P11 band pass filters.

The microphone and hot wire signals were analyzed with a Nicolet

Scientific Model 660 A Dual Channel FFT analyzer to obtain instant spectra,

r.m.s. spectra, power spectra, autocorrelation, cross correlation, coherence

amplitude, probability density etc. The signal was also displayed on a

Nicolet Scientific Model 206 digital oscilloscope. The signals were

stored for further computer analysis on floppy disks either on the FFT

analyzer or the digital scope. A photograph of the system is shown in

Figure 6 and a shematic diagram is shown in Figure 8.

The velocity signal was the sum of three velocities: the essentially

steady acoustic streaming velocity, the acoustic velocity occurring at the

excitation frequency and its harmonics and the rather (although not completely

so) random turbulent velocity caused by the acoustic streaming. We

considered the streaming velocity a d.c. component which was easily

separated by high pass filtering. The acoustic velocities were separated

by using digital notch filtering at the fundamental and the harmonic

frequencies. An example of this process is shown in Figure 9. In Figure

10, we show turbulent and non turbulent spectra of the velocity signal

taken at the same frequency of excitation but at different locations

in the chamber. The random signal in the "non turbulent" spectrum is the

noise threshold of the instrumentation.

2.3.3 CALCULATION OF TURBULENT PARAMETERS

Levich [15], and Staffman and Turner [33], have related turbulent

parameters to the rate of agglomeration. The experiments confirming the results

were done in the absence of sound and it is expected that the results would
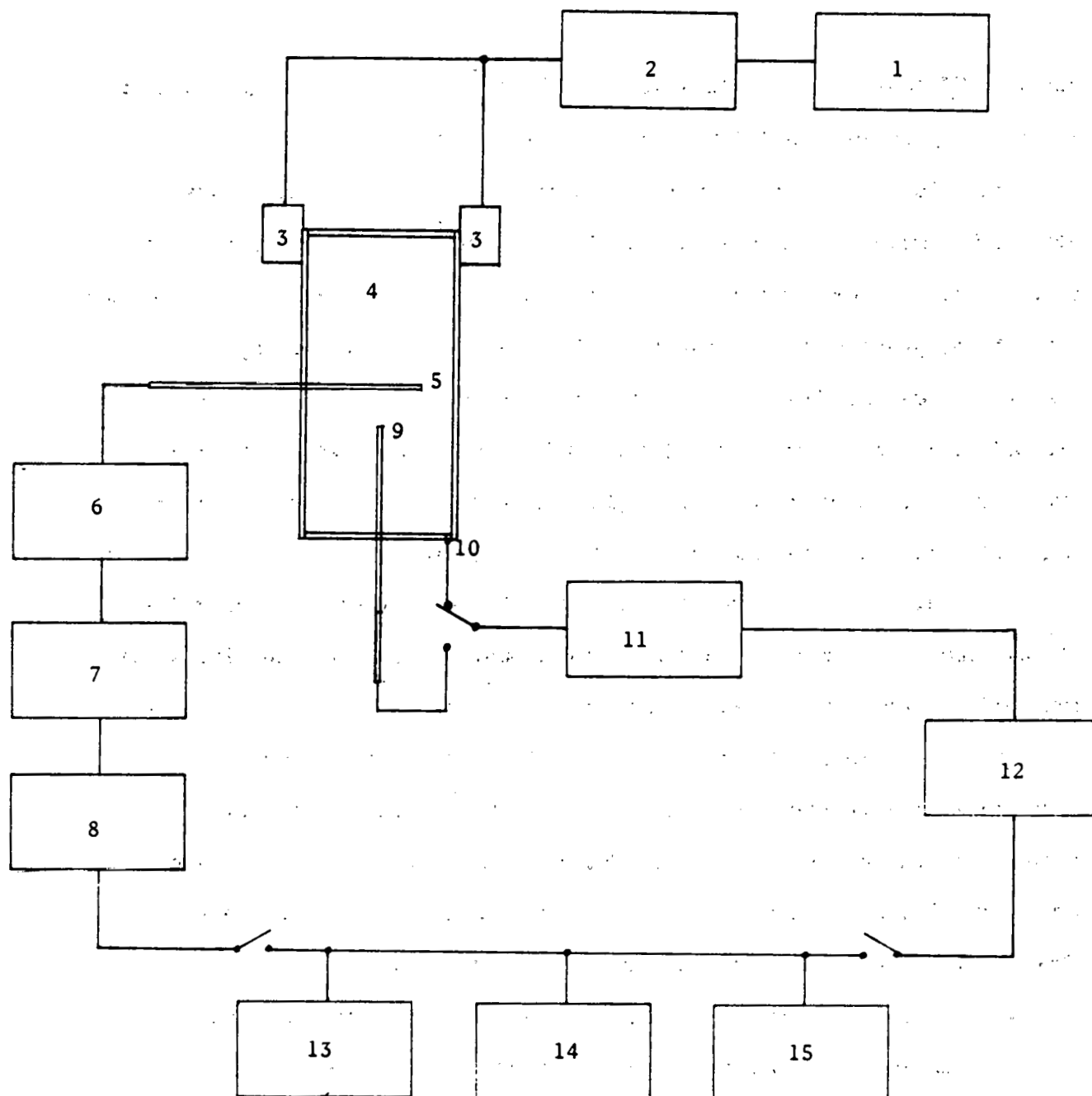
Legend:

1 - Oscillator
2 - Sound Amplifiers
3 - Sound Drivers
4 - Rectangular Chamber
5 - Hot Wire
6 - Hot Wire Anemometer
7. - Linearizer

8 - Filter
9 - Massa Microphone
10 - Celesco Microphone
11 - Preamplifiers
12 - Microphone Amplifier and Sound Pressure
     Level Meters
13 - True RMS Meter
14 - FFT Analyzer
15 - Oscilloscope

Figure 8.   Schematic Diagram of the Experimental
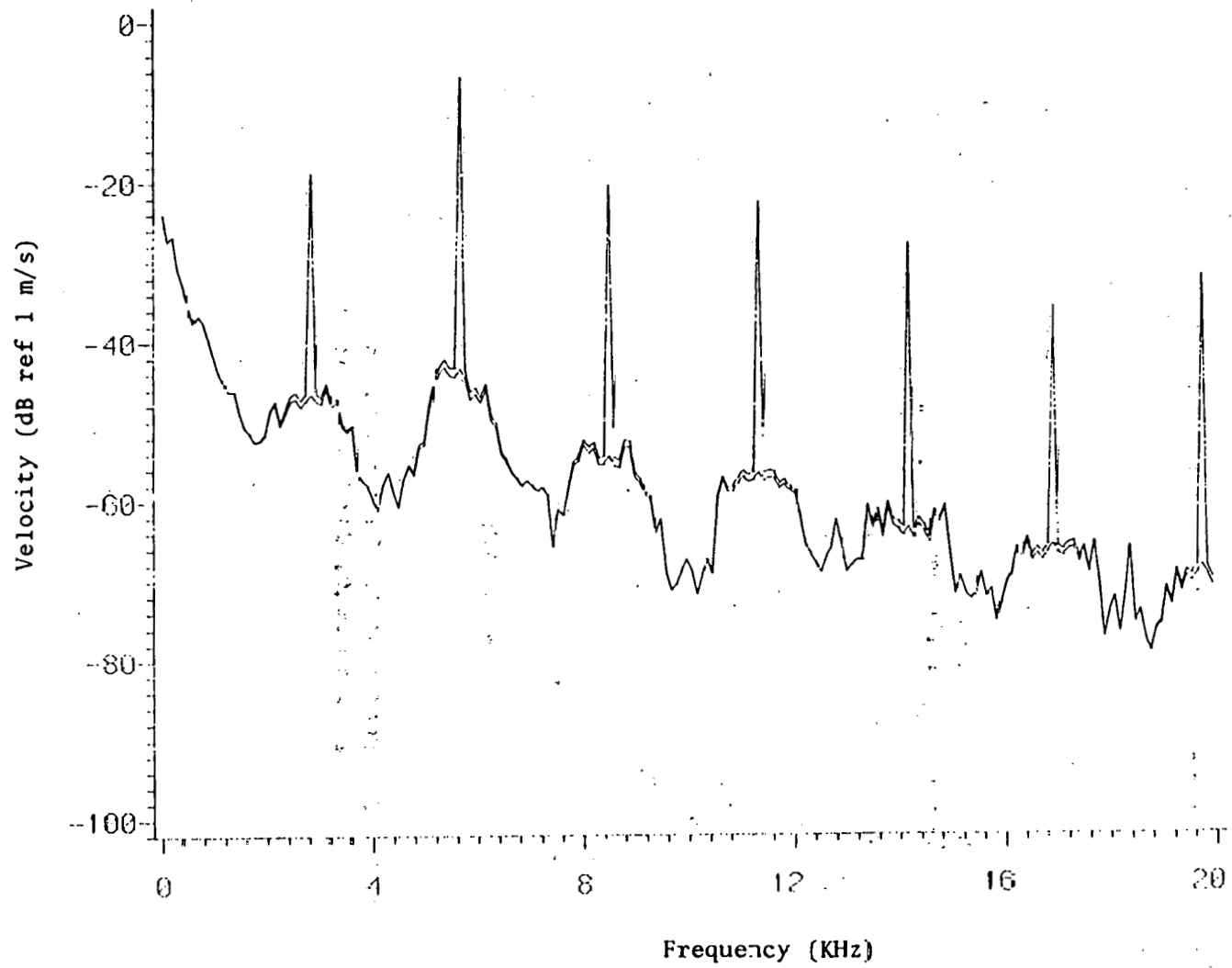   Arrangement for the Rectangular Chamber

Figure 5.   Spectra of a Turbulent Velocity Signal Before and
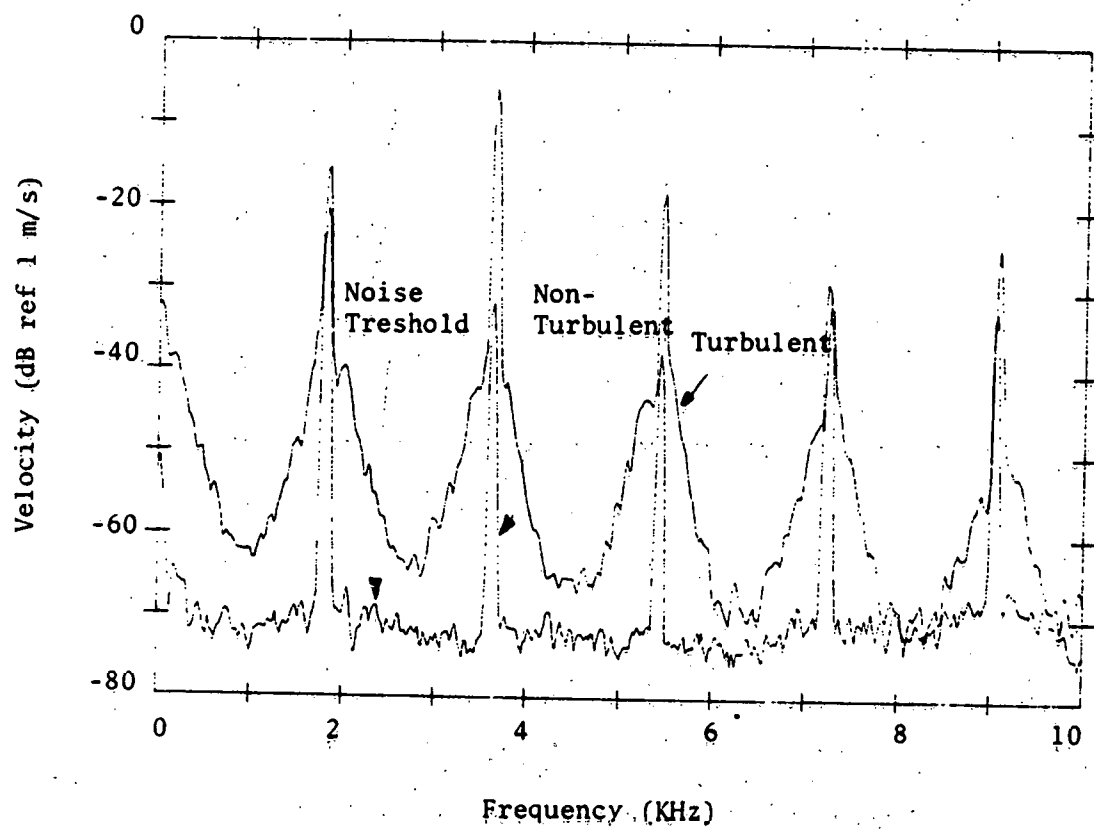After Filtering of the Acoustic Velocities

Figure 10. Spectra of Two Velocity Signals
One Turbulent, One Non-Turbulent

hold also for the situation where the turbulence is generated by sound.
Since the derivation of the equation does not assume the source of turbulence,
this seems to be a reasonable assumption. The equations relate the agglo-
meration rate to the turbulence levels by a turbulence parameter called
the energy dissipation rate. Higher energy dissipation rates give rise
to higher agglomeration rates. Hence, to determine the effect of turbulence
on the agglomeration rate, the energy dissipation rate needs to be
measured.

The energy dissipation rate is a very difficult parameter to measure.
The correct measurement requires triple correlation measurements of
turbulent velocities. To do that at least a double hot wire needs to be
used and very extensive experiments are needed. Even after all that the
results would not necessarily be very accurate, since quite a few averaged
values need to be summed and hence, errors propagate fast. Because of this
reason researchers have shied away from calculating energy dissipation
rate and whatever values are available, are given as estimates. Nevertheless,
estimates of energy dissipation rate can be made if some assumptions are
taken. The first assumption is that the turbulence is isotropic. This
assumption is not strictly correct since the sound field, which gives rise
to the turbulence, is non isotropic and hence the turbulence produced can
not be isotropic. However, since the hot wire measures turbulence in a
very small space, the scales involved in the measurements are very small
and the turbulence may be considered to be approximately isotropic. The
second assumption is that Taylor's Frozen Turbulence Approximation
holds. This approximation is true if the ratio of turbulent velocities to
the mean velocity is very small. This assumption is justified here since
the turbulent velocities are at least an order of magnitude lower than the
mean acoustic streaming velocities.

The first step is to calculate the averaged value of the square of the rate of change of the turbulent velocity, that is:

$$\overline{u_t^2} = \overline{\left(\frac{du}{dt}\right)^2} = \frac{1}{N} \sum_{n=1}^{N} \left(\frac{du}{dt}\right)_n^2$$

where u is the turbulent velocity and t is time. The average is to be taken over a sufficiently large sample length at small time intervals, so that a correct value is obtained. To ensure calculation of a correct value, the above quantity was calculated by two methods. The first method was to fit a cubic spline to the digital values of the turbulent velocity. This gave a curve which was differentiated at a large number of points and $\overline{u_t^2}$ was calculated by averaging the square of the first derivatives. The second method used the properties of the autocorrelation coefficient. The autocorrelation coefficient of the digital values was calculated at one and two time differences. Then a curve was fitted for the autocorrelation coefficient near the origin (time = 0). The curve was differentiated twice at the origin and the second derivative related to $\overline{u_t^2}$ by:

$$\overline{\left(\frac{du}{dt}\right)^2} = -\overline{u^2} \left.\frac{d^2\rho}{d\tau^2}\right|_{\tau = 0}$$

where $\overline{u^2}$ is the averaged value of the square of turbulent velocity, ρ is the normalized autocorrelation coefficient and τ is the time difference in the calculation of the autocorrelation coefficient. The value of $\overline{u^2}$ was simply calculated by averaging the square of turbulent velocities.

It was found that for the type of turbulence being investigated, a sampling time (for velocity) of 5 microseconds was a good compromise to get the best value of $\overline{u_t^2}$. If a slower sampling rate was used, the curve of

velocity against time was too discontinuous and hence the values calculated by the two methods were quite different. When a higher sampling rate was used, the information in lower frequencies, where most of the turbulent energy was contained was suppressed. This happens because only a finite number of values can be digitized in a waveform at a time. The Nicolet digital oscilloscope, which was used to digitize the data, stores 4096 points in a waveform. It was found that the two values of $\overline{u_t^2}$, when calculated from the waveform sampled at 5 microseconds, were within 10% of each other, which is sufficiently accurate for this type of measurement.

In short, the method of calculation was this: The values of the turbulent velocity, from the hot wire, were sampled at the rate of 5 microseconds. For each calculation 8 or 16 such waveforms, of 4096 points each, were taken one after another, digitized, and stored on floppy disks. The data from these floppy disks was transferred to the main computer (IBM 370) of the University. The acoustic velocity levels at various harmonics were determined and subtracted from the waveform by digital notch filtering. The filtered waveform was the turbulent velocity, and for each turbulent waveform $\overline{u_t^2}$ was calculated by the two methods. Then the averaged value of the quantity was calculated. The spectrum, mean value, mean turbulent velocity and the value of $\overline{u_t^2}$ for each waveform was compared with the average value to make sure that conditions in the chamber had not changed while the measurements were being made.

From Taylor's Frozen Turbulence Approximation:

$$t = \frac{x}{U} \quad \text{where x is a characteristic distance}$$

hence

$$\overline{\left(\frac{du}{dt}\right)^2} = U^2 \overline{\left(\frac{du}{dx}\right)^2}$$

where U is the mean velocity which in our case is the streaming velocity.

Assuming isotropic turbulence, the value of energy dissipation rate ϵ is given by:

$$\epsilon = 15 \; \nu \overline{(\frac{du}{dx})^2} = \frac{15 \; \nu}{U^2} \overline{(\frac{du}{dt})^2} \quad \text{where } \nu \text{ is the kinematic viscosity}$$

Several well known measures of turbulence scale can be calculated from the following relationships:

Taylor's microscale λ:

$$\lambda = \frac{\overline{u^2}}{\overline{(\frac{du}{dx})^2}} = \frac{15\nu \; \overline{u}}{\epsilon} = U \frac{\overline{u^2}}{\overline{(\frac{du}{dt})^2}}$$

Kolmogorov's length scale η:

$$\eta = (\frac{\nu^3}{\epsilon})^{1/4}$$

Kolmogorov's velocity scale: v
$$v = (\nu\epsilon)^{1/4}$$

Values for each of the three scales were calculated from the filtered time histories of the hot wire signals using the University's computer.

2.3.4 EXPERIMENTAL RESULTS

Test were run at a number of frequencies and various pressure levels up to 170 dB in one of the corners of the chamber. In Figure 11a through 11e we show a typical set of results taken at 2800 Hz with a level at the corner of 170 dB. The plots are narrow band spectra with a 25 Hz bandwidth of the hot wire anemometer signal taken at several locations in the chamber to illustrate the appearance and nature of acoustically generated turbulence. The high pressure spectra are taken at pressure loops (a and d) and the low pressure spectra at nodes (b, c, and e). It is clear that only Figure 11e
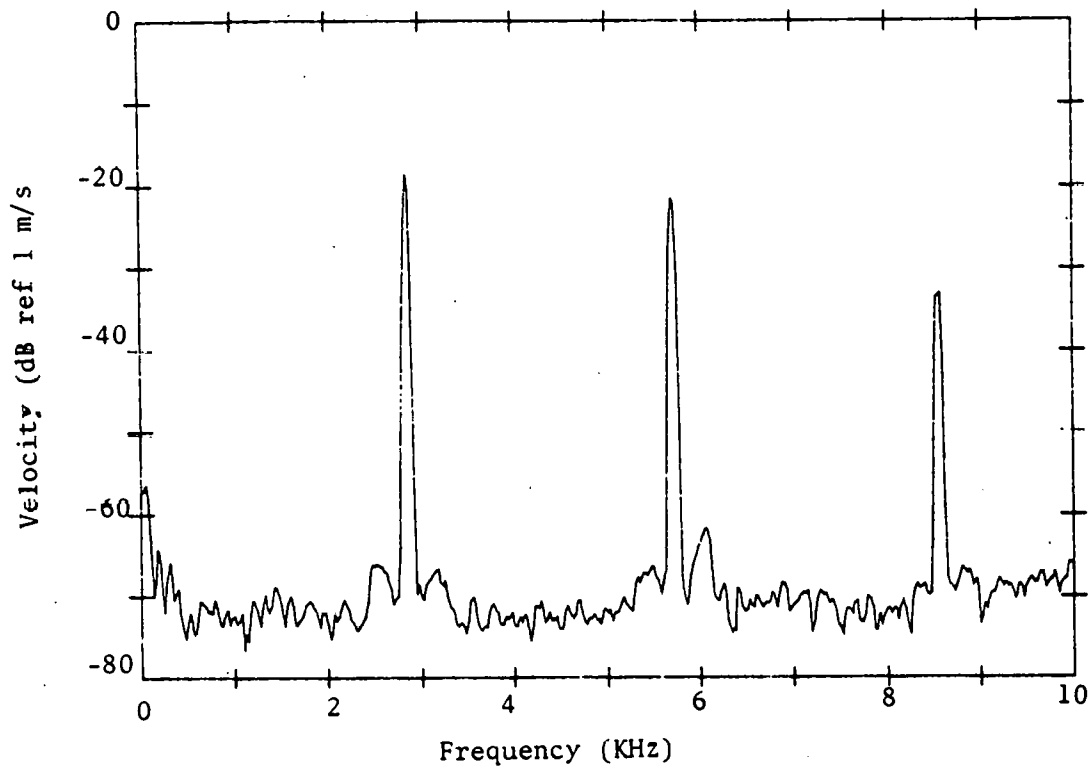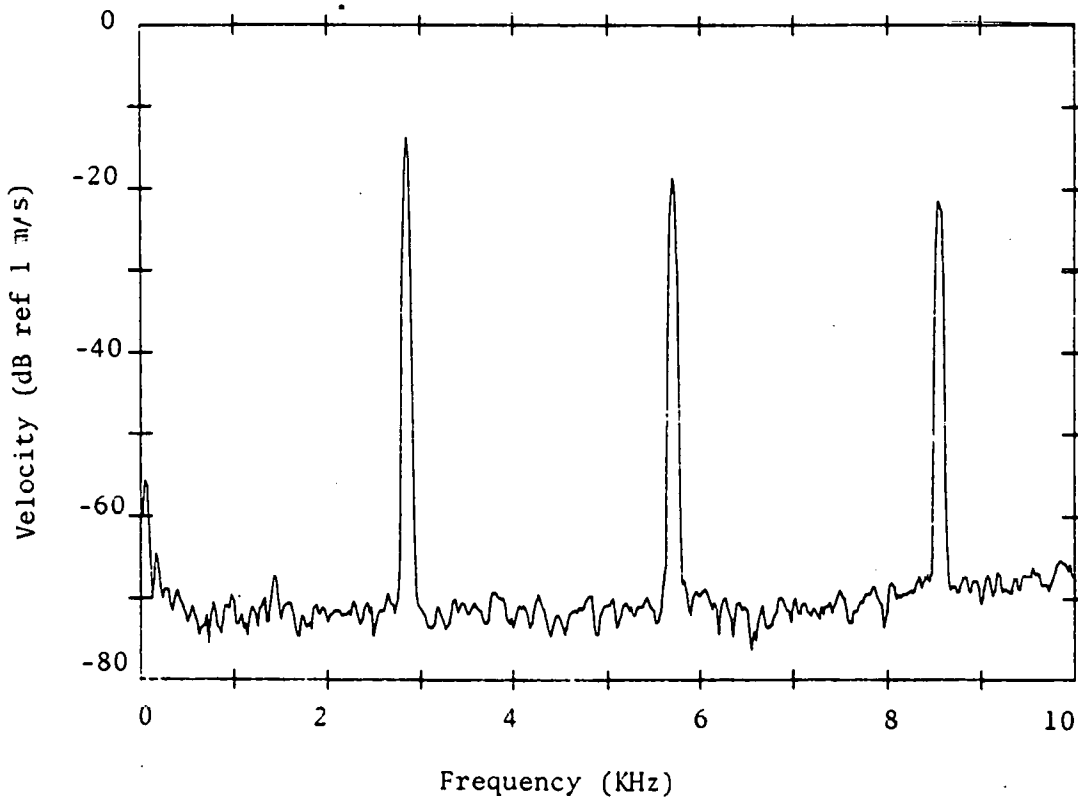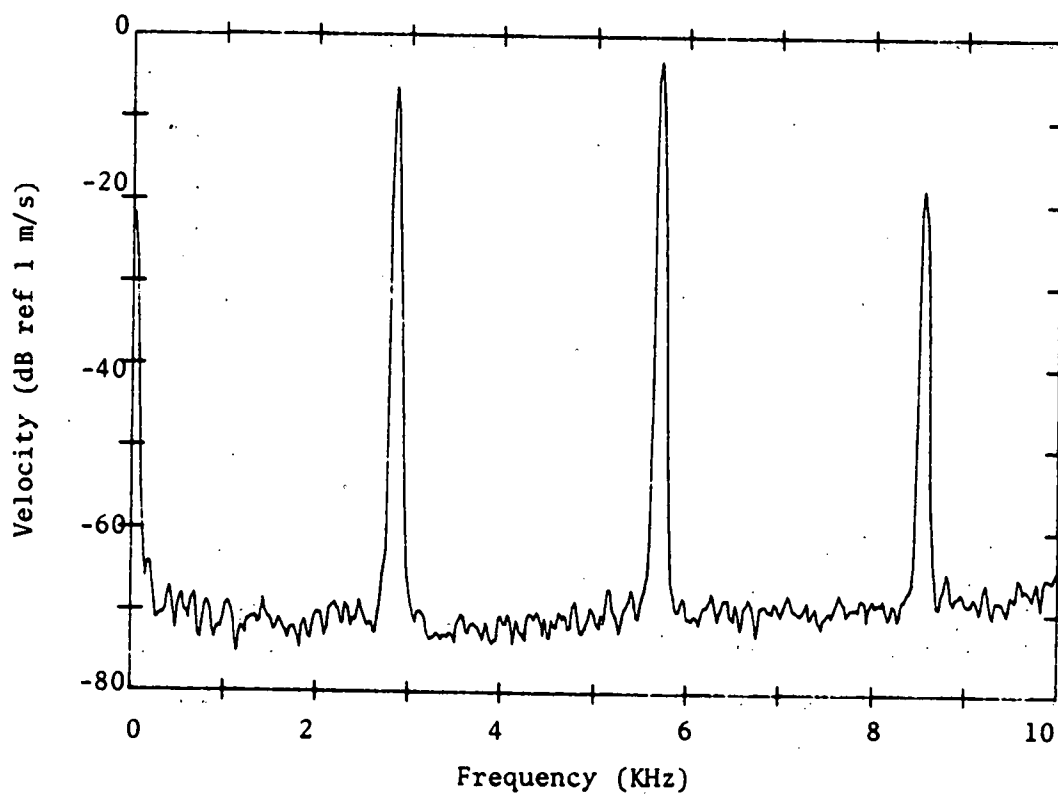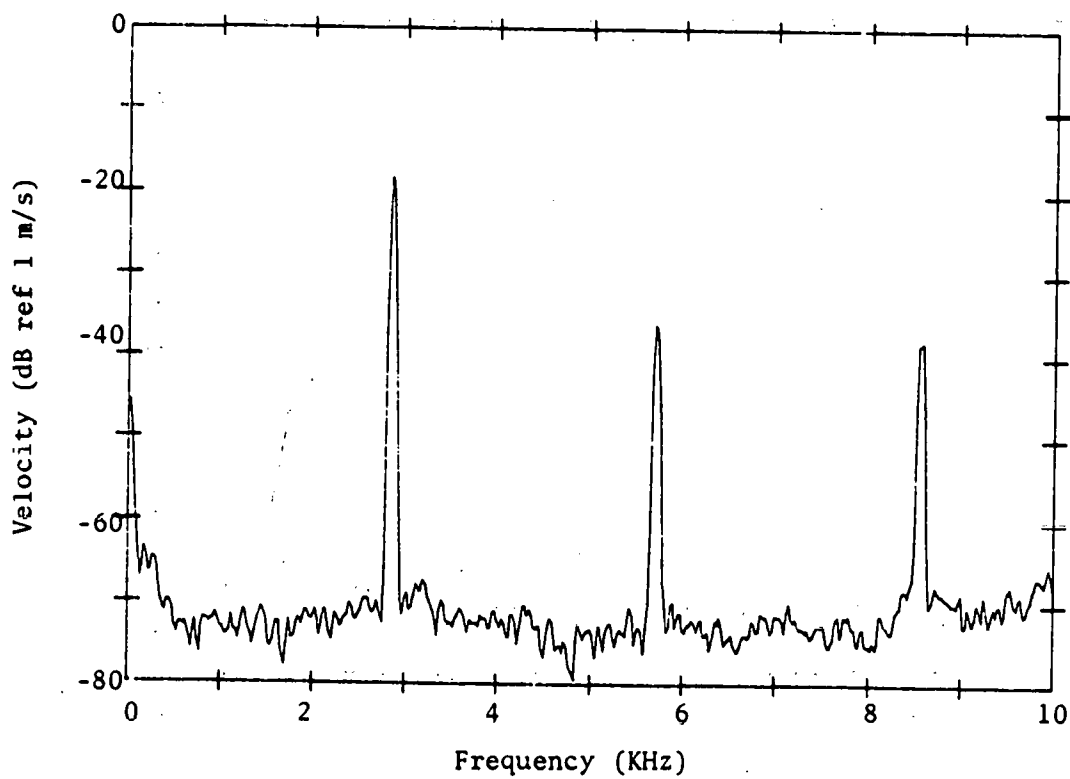
Figure 11(a)

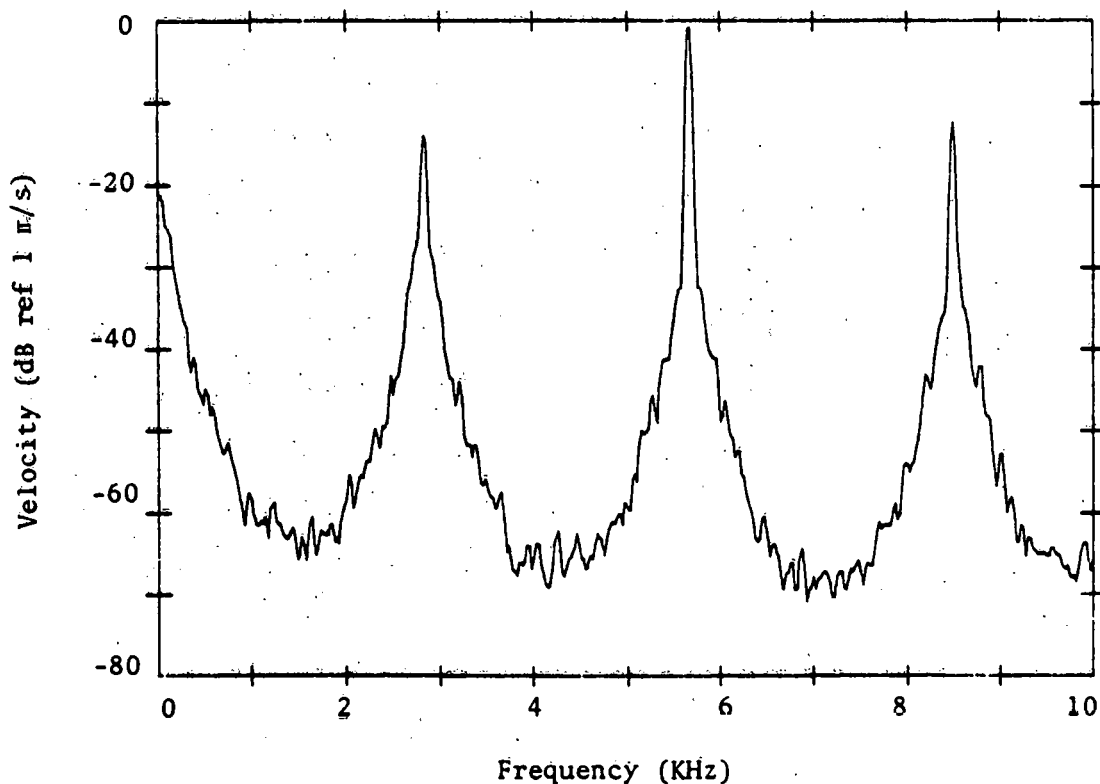Figure 11(b)

Figure 11(c)

Figure 11(d)

Figure 11(e)

Figure 11. RMS Spectra of Velocity Signal from Hot Wire at
Various Positions in the Chamber. Excitation
Frequency - 2800 Hz. Sound Pressure Level at the
Corner of Chamber - 167 dB. Sound Pressure Levels
at the Point of Velocity Measurement: (a) 166 dB,
(b) 150 dB, (c) 154 dB, (d) 164 dB, (e) 153 dB.

shows an onset of turbulence. From other results we noted that turbulence was prominent at pressure nodes, but not <u>all</u> pressure nodes. The pressure loops were non turbulent. We must recognize that a pressure loop corresponds to a velocity node thus the pressure node spectrums show the higher velocities.

We must show in Figure 12 a series of velocity spectra at the same location in the chamber and of course at the same frequency of 2262 Hz but at increasing sound levels starting with 153 dB at the point at which the velocity was measured. We note that at 153 dB no thickening of the base at the pure tone frequencies occured indicating that no turbulence was generated. We then increased the power to the drivers obtaining levels of 155, 158 and 160 dB. It is clearly evident that for very small increases in acoustic pressure such as 3 dB variations we obtained about 10 dB increases in the "turbulent" component at the pure tone velocities with only the last increase showing a significant rise in the in-between levels. We also draw attention to the changes in the spectra in the 0 to 1000 Hz frequency range. We have established that this portion of the spectrum is caused by the turbulence generated by the acoustic streaming.

We believe that this rather unexpected spectral characteristic of the velocity is the result of nonlinear acoustic phenomena which cause the acoustic streaming and the rich harmonic content of the spectra. The interaction of the low frequency spectrum of the acoustic streaming velocity with harmonics causes a phenomenon akin to intermodulation distortion in electric circuits, known to acousticians as the parametric effect, with the resulting thickening and rise of the random signal at the harmonic frequencies.

In Figures 13 through 18 we give a set of acoustic pressure and local velocity measurements for a point in the model chamber where the acoustic pressure was 150 dB and the frequency 1815 Hz. The wave form plots of pressure and velocity do tell us much about the processes. The velocity. wave form is reasonably linear showing some high frequency components and the frequency doubling due to the hot wire anemometer. The spectrum is reflecting this character. The spectrum also shows some of the parametric effects. The pressure spectrum and wave form show much more high frequency content.

Of interest is the observation that even at the highest levels of excitation (170 dB) these very low levels of turbulence were found to be present over less than 20% of the area.

2.3.5 DISCUSSION OF RESULTS OF ACOUSTIC TURBULENCE STUDIES

It was found that the flow did become turbulent when the acoustic pressure levels become very high. The onset of this, strictly speaking, not truly random velocity started at local acoustic levels of about 150 dB yet in some instances not until much higher levels were reached.

The evidence started as a broadening at the "base" of the pure tone elements in the spectrum which then rose and broadened for relatively small increases in sound pressure level. A typical example of this facet was given in Figure 12. It is clearly evident from these results that the average broadband levels are several orders of magnitude below the acoustic velocity levels at the excitation frequency and its harmonic.

Table 3 summarizes the results using only the examples of highest energy dissipation rates for the turbulent velocity component. The last column of the table gives the most important and conclusive result. The
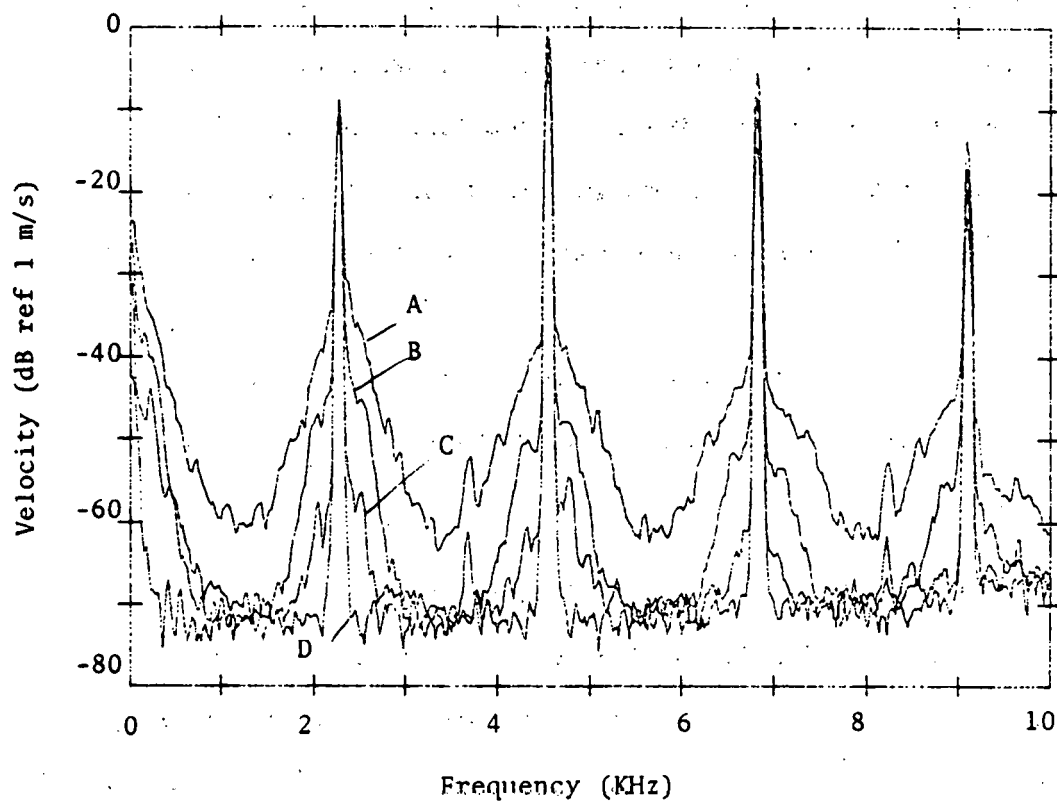
Figure 12. Velocity Spectra at the Same Measurement Location and Frequency of Excitation (2262 Hz) but at Different Sound Levels. The Sound Pressure Level at the Corner of Chamber and at the Location of Measurement Were: Spectrum A - 168 and 160 dB; Spectrum B - 166 and 158 dB; Spectrum C - 164 and 155 dB; Spectrum D - 162 and 153 dB.
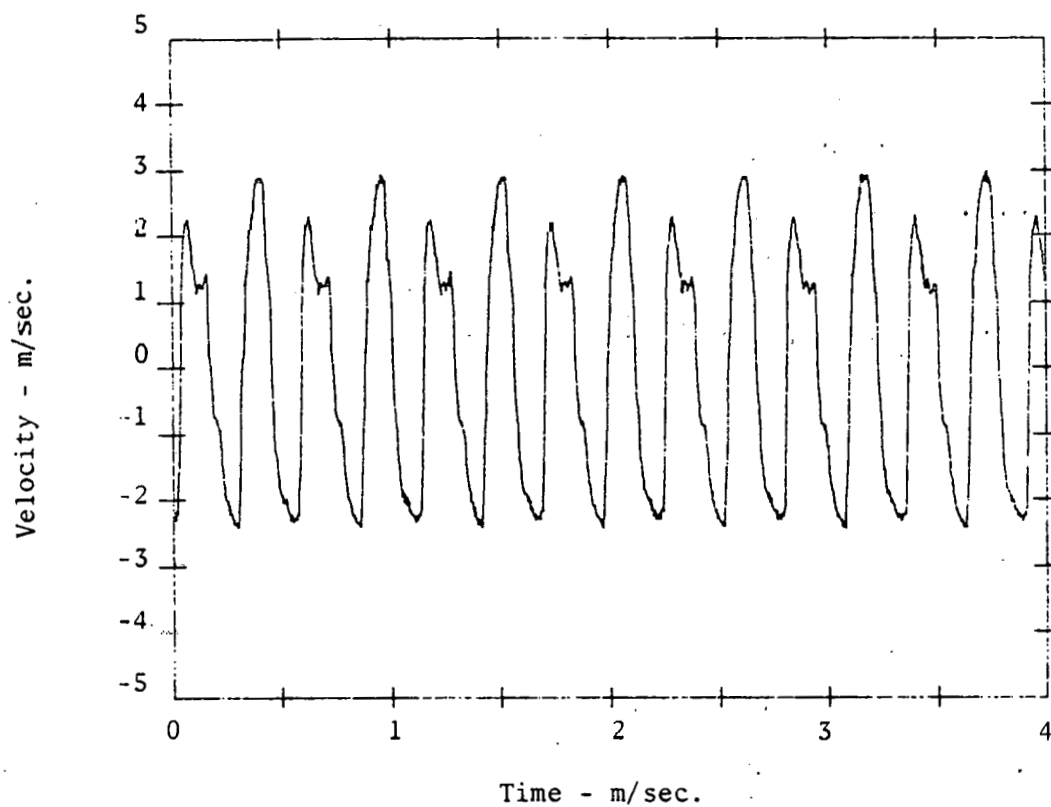
Figure 13. Plot of Velocity Wave Form (AC Component) versus
            Time (taken in two-dimensional rectangular
            chamber).
            Excitation Frequency - 1815 Hz.
            Sound Pressure Level at Corner - 170 dB.
            Sound Pressure Level at Measurement Location - 150 dB.
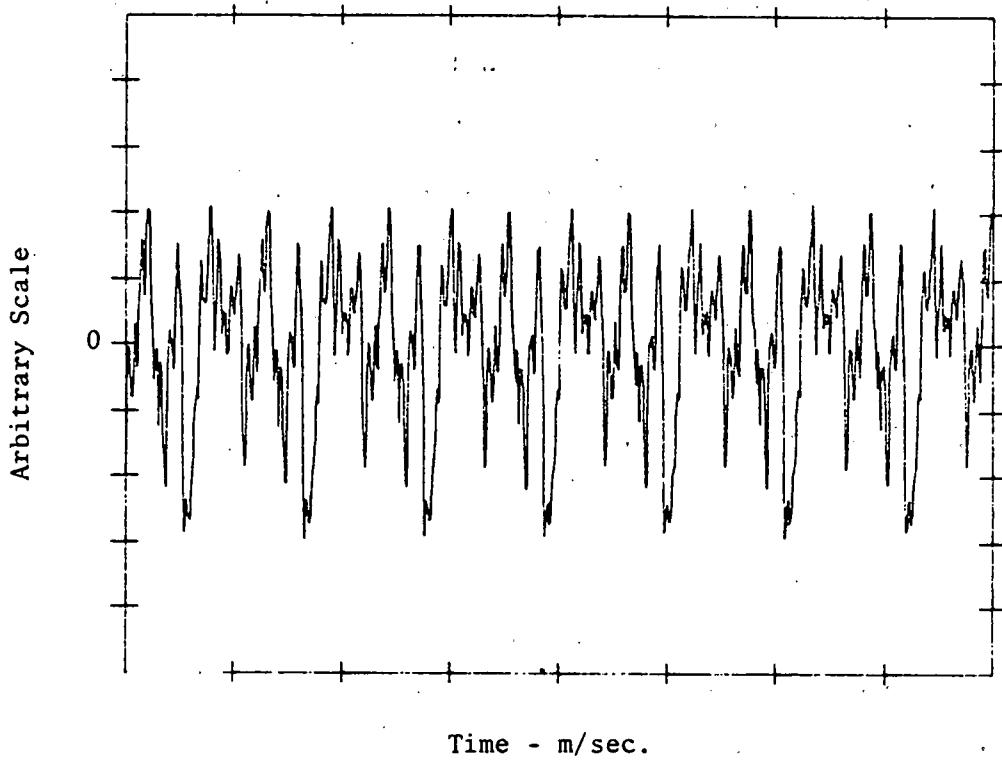
Time - m/sec.

Figure 14. Plot of Sound Pressure Wave Form versus Time.
            (taken in two-dimensional rectangular chamber).
            Excitation Frequency - 1815 Hz.
            Sound Pressure Level at Corner - 170 dB.
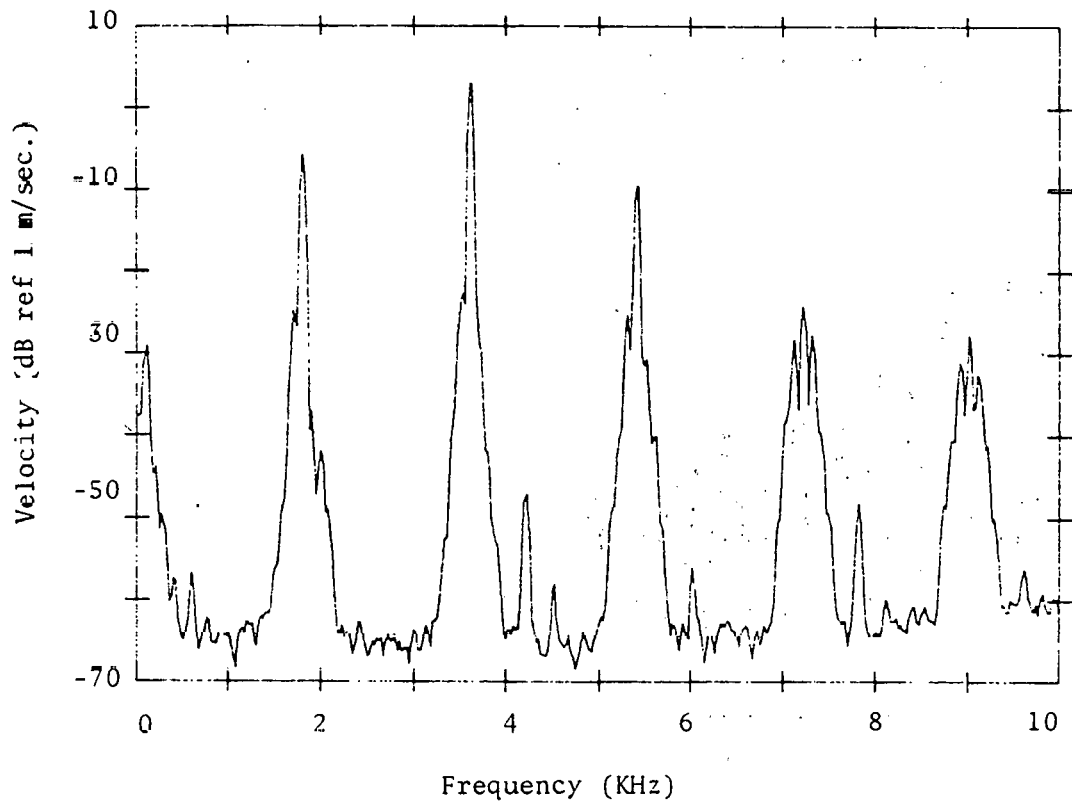   Sound Pressure Level at Measurement Location - 150 dB.

Figure 15. Plot of Velocity versus Frequency (taken in two-
dimensional rectangular chamber).
Bandwidth - 25 Hz.
Excitation Frequency - 1815 Hz.
Sound Pressure Level at Corner - 170 dB.
Sound Pressure Level at Measurement Location - 150 dB.

Figure 16. Plot of Velocity versus Frequency (in two-
dimensional rectangular chamber).
Bandwidth ~ 250 Hz.
Excitation Frequency - 1815 Hz.
Sound Pressure Level at Corner - 170 dB.
Sound Pressure Level at Measurement Location - 150 dB.

Figure 17. Plot of Sound Pressure Level versus Frequency (in two-dimensional rectangular chamber).
Bandwidth - 25 Hz.
Excitation Frequency - 1815 Hz.
Sound Pressure Level at Corner - 170 dB.
Sound Pressure Level at Measurement Location - 150 dB.

Figure 18. Plot of Sound Pressure Level versus Frequency (in
two dimensional rectangular chamber).
Bandwidth - 250 Hz.
Excitation Frequency - 1815 Hz.
Sound Pressure Level at Corner 170 dB.
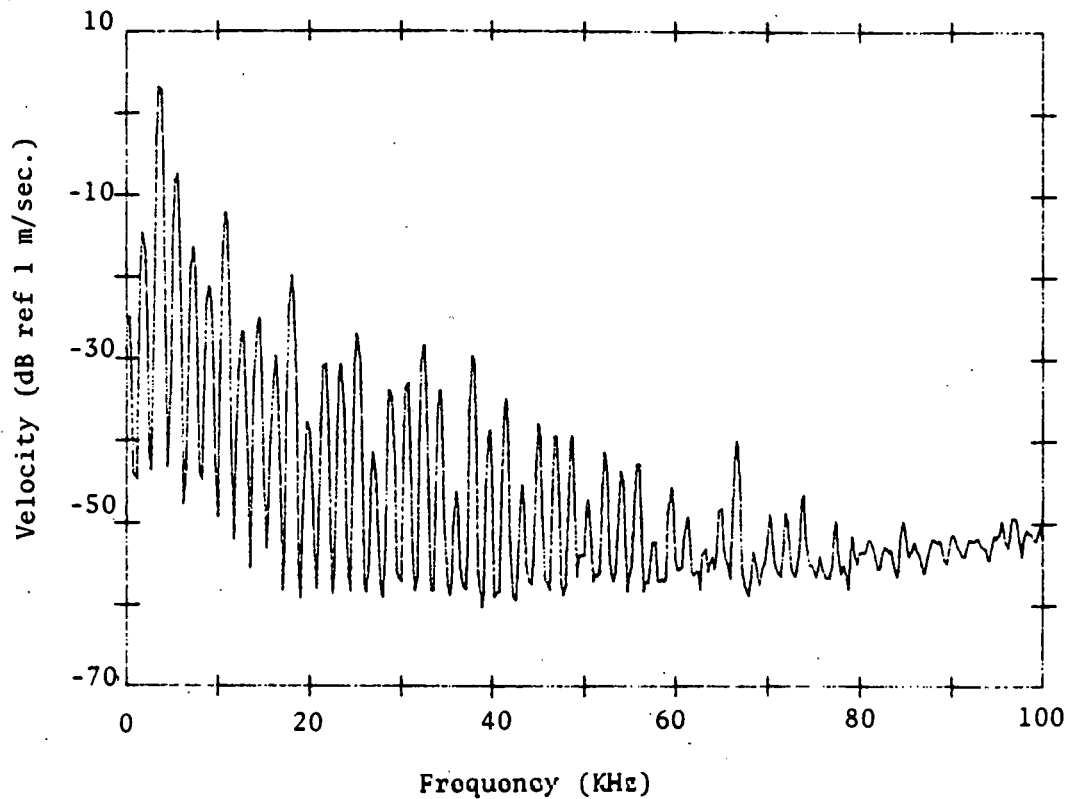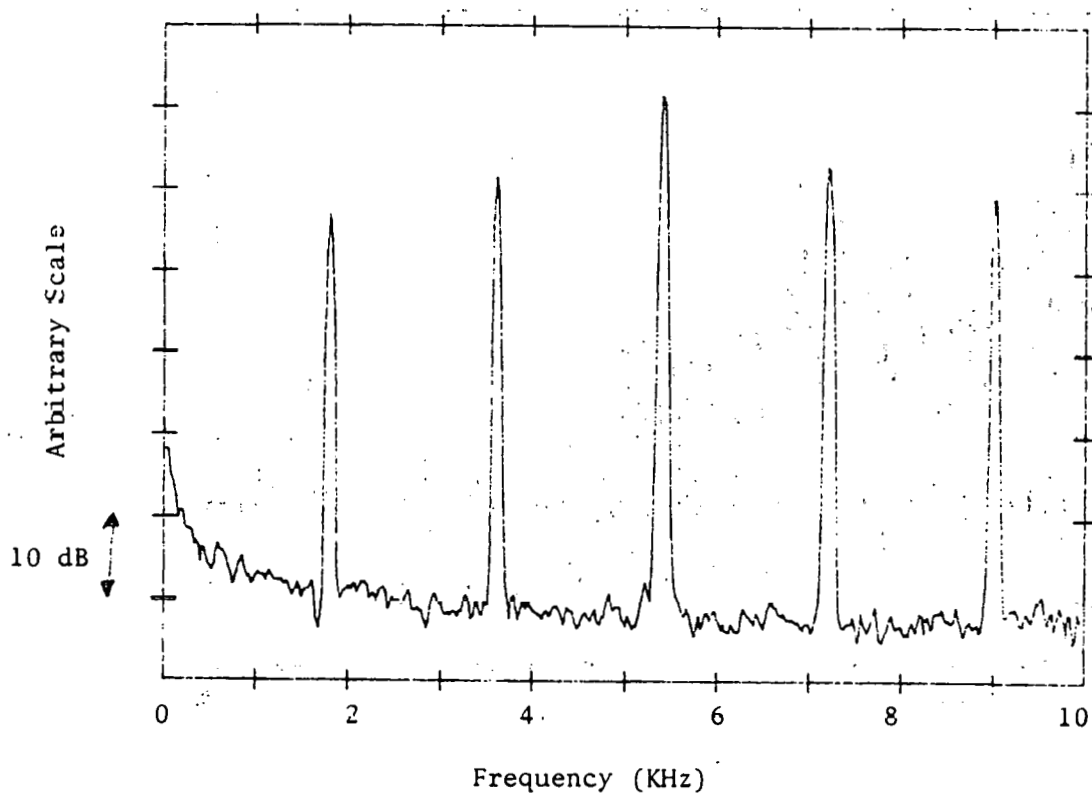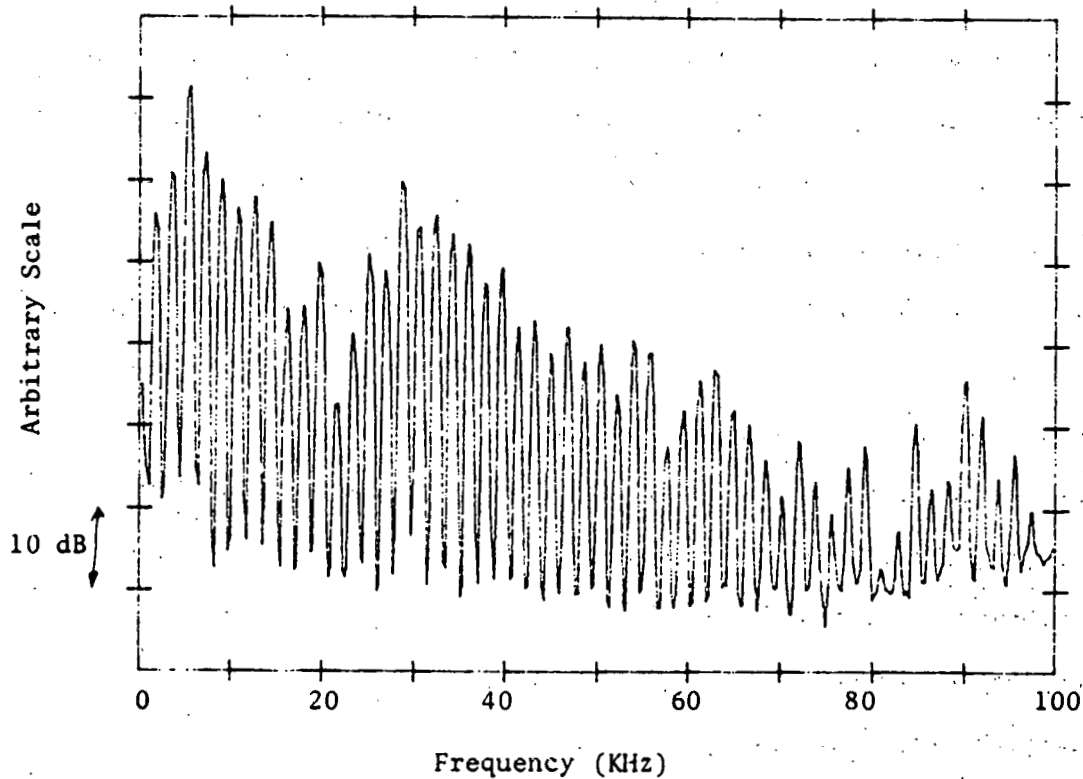Sound Pressure Level at Measurement Location - 150 dB.

TABLE 3

EXPERIMENTAL CONDITIONS IN RECTANGULAR CHAMBER AND TURBULENT PARAMETERS FOR POSITIONS WHERE
THE HIGHEST VALUES OF ENERGY DISSIPATION RATE WERE CALCULATED

FREQUENCY Hz	ACOUSTIC PRESSURE dB		MEAN VELOCITY m/s	RMS TURBULENT VELOCITY m/s	ENERGY DISSIPATION RATE (ε) m^2/s^3	$(\frac{\partial u}{\partial t})$ m^2/s^4	TAYLOR'S MICROSCALE (λ) m	KOLMOGOROV'S SCALES		RATIO OF TURBULENT ENERGY TO ACOUSTIC ENERGY
	Measurement Position	Corner Of Chamber						Velocity (v) m/s	Length m	
1815	161	170	5.79	0.127	50.5	4.54×10^5	3.59×10^{-4}	0.144	3.79×10^{-5}	1.54×10^{-3}
2050	159	167	4.30	0.088	55.1	2.93×10^5	2.20×10^{-4}	0.151	9.85×10^{-5}	1.03×10^{-3}
2262	155	167	3.82	0.101	29.6	1.88×10^6	1.89×10^{-4}	0.141	1.07×10^{-4}	1.06×10^{-3}
2800	153	167	4.77	0.109	57.7	5.88×10^6	2.26×10^{-4}	0.169	8.83×10^{-5}	3.53×10^{-3}

ratio of turbulent energy to acoustic energy was obtained by integrating the

energy narrow band spectral data over the frequency band from 500 to 100,000

Hz and taking the ratio of total turbulent energy to total acoustic energy

(energy in the excitation frequency and harmonics bands). It is quite

clear that the turbulent component is 3 orders of magnitude lower than the

acoustic component. We also note that the r.m.s. turbulent velocity

is better than an order of magnitude less than the mean velocity due to

acoustic streaming. The indication is that we have fully turbulent steady

flows over most of the chamber as a result of the acoustic streaming. The

steady velocities are quite comparable to the convection velocities we

expect to see in an agglomerator.

It is only in the last few weeks that we have obtained a satisfying

understanding of the cause of the thickening of the base of the pure tone

components of the velocity spectra and the general rising of the broad band

levels as shown in, for example, Figure 12. The phenomenon is the result

of an intermodulation distortion due to the simultaneous presence of a

low frequency turbulence from acoustic streaming and the pure tone components

and harmonics. We have actually simulated the process electronically with

quite conclusive results.

2.3.6 CONCLUSIONS

The acoustically generated turbulence in disperse acoustic fields

although observed was on the order of 3 order of magnitude less than

the acoustic velocity generated energy even at the highest acoustic levels

of about 170 dB at the corners of the chamber. Such acoustic levels do

not appear to be practical for use in agglomerators because of the require-

ment for immense energy to provide the acoustic power to fill the large

agglomeration chambers. Also for clean-up of power plant flues the agglomeration chamber sizes will be so large that the acoustic field will always be dispersive. For dispersive acoustic fields we will not experience a significant fraction of plane wave energy so that the wave steepening and acoustic shocks will be essentially non existent.

We must conclude, therefore, on the basis of this study that acoustically generated turbulence is not a significant mechanism in the agglomeration process for the conditions expected in coal fired power plants.

2.4 ROOM TEMPERATURE FRAGILITY STUDIES (TASK III)

The scanning electron microscope photo-micrographs of the agglo- merates as captured by an electro-static precipitator type device showed very lacy, fragile looking agglomerates in our earlier studies. These observations gave rise to questions by EPRI and DOE personnel about the ability of the agglomerated particles to withstand the rigors of flow through, particularly, cyclones without breaking up into much smaller particles, thereby undoing the acoustic agglomerators work.

We were, therefore, asked to develop a method to establish the robust- ness of the agglomerates and relate such a measure to the conditions existing in cyclones. We investigated many possible methods such as subjecting the particles to known fluid shear forces or impacting the particles at known velocities on flat plates or actually flowing the agglomerated aerosols through simple cyclones. In each case the before and after exposure measure- ment appeared to present formidable if not impossible difficulties.

Since we were using Anderson Mark III impactors for particle size distribution determination in our research, we decided to investigate the shear forces that particles would be subjected to in these inertial separation devices. In fact, there is a certain similarity between the inertial separation principles in impactors and cyclones. If we could establish that the velocity gradients and resulting shear forces on the particles in the impactor were of the same order of magnitude or larger than the shear forces in cyclones, we would be able to prove that the agglomerates would be able to withstand the rigors the agglomerates are subjected to in typical cyclones.

A literature search and subsequent analysis of the kinetics of the Anderson Mark III impactor flows and the flows in cyclones was undertaken. The results are reported in our report entitled: "Fragility of Acoustically Agglomerated Submicron Fly Ash Particles" authored by Wallace George and submitted as CAES/NCL Report No. 655-82 dated August 28, 1982 [34].

The results show clearly that the representative shear forces agglomerates are subjected to are considerably larger in impactors than in cyclones. Thus, for example, the particles in stage zero of the impactor with a "cut-off" diameter of 7.23 μm are subjected to shear stresses of 6.7 N/m^2 whereas the shear stresses on equivalent size particles in typical cyclones are of the order of 2 N/m^2. For smaller particles the relative velocity in cyclones decrease whereas the impaction velocities and velocity gradients in impactor increase markedly.

Since we have used the impactor to establish agglomerator performance the agglomerates that survive impaction in the impactor can be expected not to be broken up in cyclones. In fact, we believe that our agglomerator performance measures are rather conservative.

As a further means to provide us with a "feel" for the nature of the agglomerates and some indication of the bonds we studied a large number of photomicrographs of the sound agglomerated particles and the non sound exposed particles from the seven stages of the Anderson Mark III impactor. The results were indeed revealing. For the samples which came from runs without sound, we observed jagged rock-like type of single particulates with very little bridging. On the other hand, we observed very complex particles made up of many clearly "stuck-together" tiny particles from the aerosols which had been exposed to sound at 130 dB at 3000 Hz.

In several cases we were able to identify bonds between particles. Such agglomerates were clearly identifyable down to the stage 5 (1.1 μm) photomicrographs.

As a result of these studies, we believe that the agglomerates are quite robust and should be able to survive the rigors of travel through cyclones. We are, at the time of this writing, completing the high temperature tests up to 700°F and will report on these results later. Based on earlier studies by us and others, we do expect to see a deleterious effect as a result of the increased temperature as van der Waal's forces of attraction are inversely proportional to absolute temperature and increased viscosity will increase drag forces on the particles. The issue is, by no means resolved and further study is necessary.

2.5 MODERATE TEMPERATURE AGGLOMERATION TESTS (TASK IV)

2.5.1 INTRODUCTION

The agglomeration facility designed, developed and used by Dr. Michael Volk [14] in 1973 permitted tests at room temperature and acoustic sound pressure levels up to 120 dB. The acoustic frequencies ranged from 1000 Hz to 6000 Hz.

However, the temperatures existing in typical coal fired power plant flues range from 700°F without air preheaters down to about 300°F if air preheaters are installed. Although substantial agglomeration was reported by Volk for the typical fly ash and other aerosols, the exposure times of 40 seconds are unrealistically long. Volk's results show, as was to be expected, a sharp drop-off in agglomeration to the more realistic exposure times of 10 to 20 seconds. We, therefore, decided to design and build a new acoustic agglomeration facility to provide for higher acoustic intensities and aerosol temperatures up to 700°F for further exploration of the acoustic agglomeration processes. Since we learned many useful lessons from the experience with our first agglomerator, the new facility should incorporate several important new features such as an improved aerosol generation system, a better sampling system based on impactor technology rather than manual counting and sizing of particles from many transmission microscope photomicrographs, an improved siren and much higher power sound source and a modern data acquisition, processing and display system.

The specifications for the system were as follows:

Sound Pressure Levels: 130 - 160 dB

Sound Frequencies: 1000 - 4000 Hz

Aerosol Flow Rates: 0.1 - 1 ft/sec.

Aerosol Loading: 2 gr/m^3 - 20 gr/m^3

Agglomeration Section: 8" ID x 8' Long

Temperature: Controllable to 700°F

Sound Source: Electric Motor Driven Siren Producing up to 600 Acoustic
                Watts.

2.5.2   DESCRIPTION OF AGGLOMERATOR DESIGN

A detailed description of the new P.S.U. 700°F agglomerator facility

is given in Reference [36] which is published both as a Penn State University

Master of Science in Mechanical Engineering Thesis by Peter An Lu, November

1982 and as a report to D.O.E.

The description presented here incorporates several improvements which

have been incorporated as a result of our experience with the system

covering about 500 hours of testing. We can say without reservation that

the system has been functioning reliably and predictably with only the

usual developmental problems. All the original performance specifications

have been met or exceeded (CAES Report #649-82).

The agglomerator is shown in the partial sectional view in Figure 19 and

the system is shown in Figure 20. Starting from the left we have the 600

acoustic watt siren designed by Dr. G. Reethof and Mr. S. J. Shane [37,38].

Compressed air is provided by a Roots type blower. Pressure to the siren is

controlled by means of a bypass valve. Because of its importance, the siren

design will be discussed in more detail later. We note that the siren is

acoustically coupled to the 8 inch internal diameter agglomerator chamber by

an exponential area increase acoustic coupler. The coupling starts at the 40

circular holes in the siren stator expanding to an annulus through the 4.5" long

hard wood flanged section continuing through the exponential wooden conical

section to the full 8" opening. The 9.25" long tubular section has 16 - 0.5"

diameter exhaust holes for the siren air. The acoustically transparent

barrier prevents the cold siren air from flowing into the heater section.

ACOUSTIC TANSPARENT
BARRIER

COOLING
SECTION

AGGLOMERATION
CHAMBER

ACOUSTIC COUPLER

HEATER

GOOSE NECK PROBE

SIREN

AEROSOL FROM
DUST GENERATOR
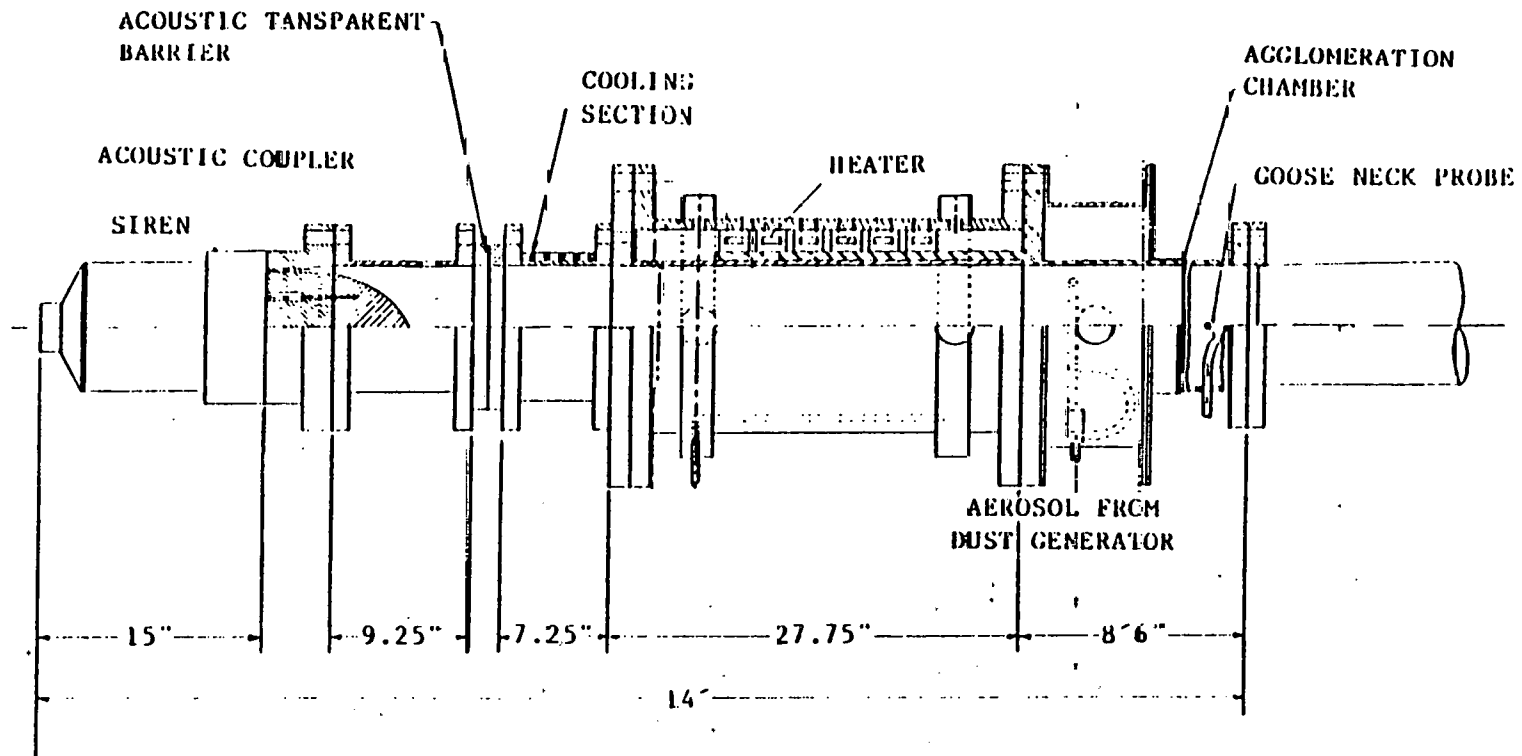
15"   9.25"   7.25"   27.75"   8'6"

14'

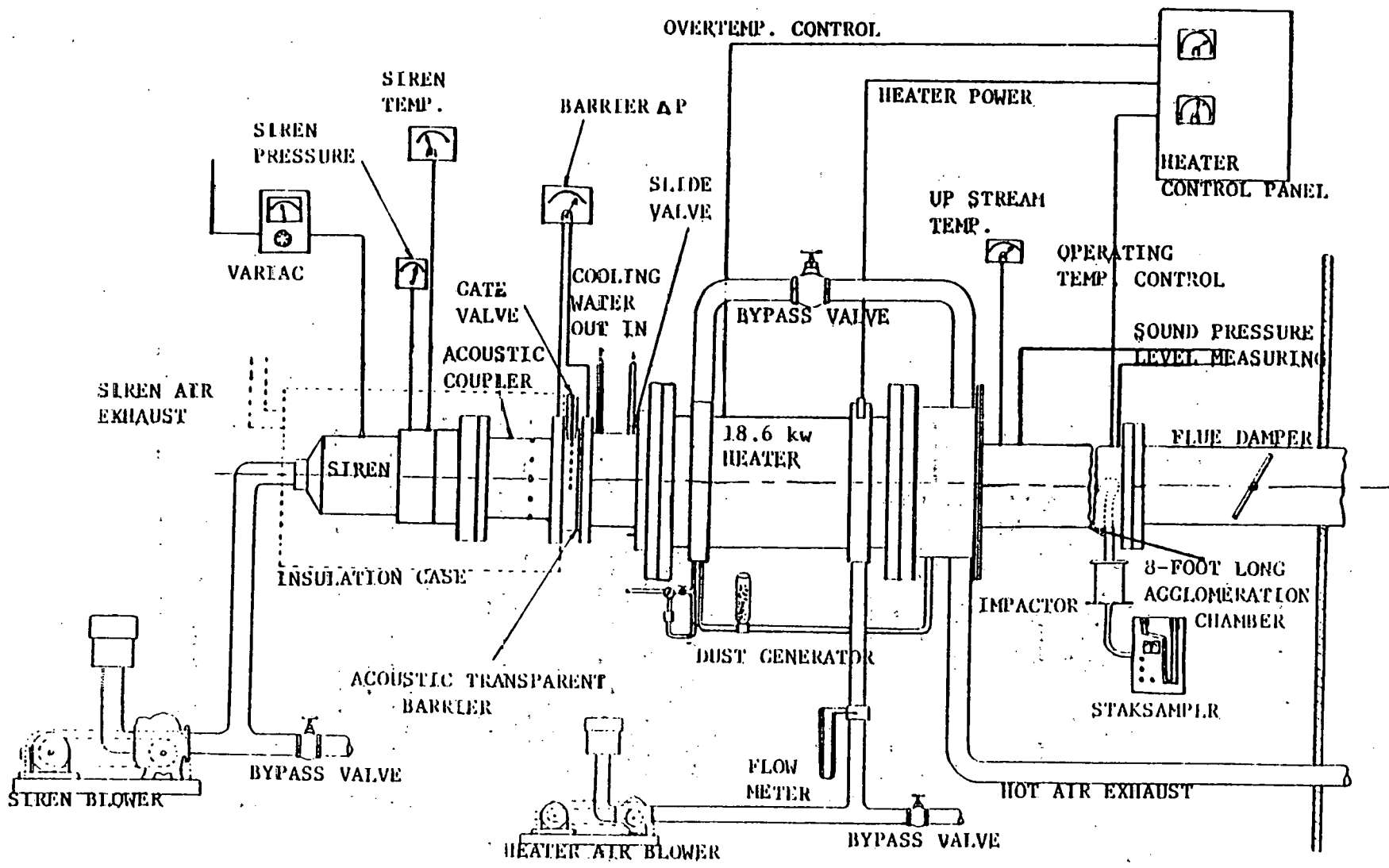Figure 19.   Moderate Temperature Acoustic Agglomerator

Figure 20. Final Setup of Moderate Temperature Acoustic Agglomeration Facility

The sheet of felted, woven and sintered stainless steel has a flow resistance of 110 MKS rayls giving an acoustic transmission loss of only 4 dB. By automatically controlling the pressure drop across the barrier to about 1 inch of water, we are able to minimize cold siren air flow into the agglomeration chamber. Control is obtained by an automatically controlled damper valve in the final exhaust section of the system. We sense the pressure drop by means of a Valedyne differential pressure sensor which in turn, through appropriate electronics, controls the stepping motor activated damper valve. A sluice type gate valve is installed as noted to prevent hot air backflow during the many hours of heater-only time to reach the desired system temperature.

The 7.25 inch jacketed, water cooled section prevents heat conduction to the siren system thus protecting the wooden horn and siren from over-temperature. The heater section consists of a 14" schedule 40 pipe with 150 lb flanges welded to each end. Six Chromolox Model KSEF- Koilfin electric heating elements generate 18.6 KW of heating power which is transferred to the airflow by convection. Power to the heaters was obtained from the solid state Silicon Controlled Rectifier (SCR) Chromolox Model 4231 power source and control system. The on-off control includes overtemperature sensors mounted on the heating coil fins and an operating temperature thermocouple sensor mounted in the agglomeration section. The system can be cycled at 3 Hz holding the temperature within just a few degrees. Air velocity over the heaters is 10 ft/sec. to maintain proper heating element temperatures. System schematic diagram Figure 20 shows the Roots type blower with bypass flow control and orifice meter flow sensor providing

the heating air to the system. Only about 10% to 20% of the heated air actually enters the agglomerator through 24 - 1/8" diameter angled holes. An adjustable sleeve valve controls the exposure of these holes. The excess hot air is then passed through the bypass control valve (shown in Figure 20) into the aerosol distribution section to heat the aerosol to the gas temperature. Finally the hot air is exhausted to the out of doors. We note on Figure 19 that the finned heating elements are tightly enclosed on their inner and outer surfaces to assure maximum heat transfer to the air. The flow rate through the heater is about 63 cfm. The aerosol concentrate distribution system is attached to the heater flange as shown in Figure 19. Four equal length copper tubes from the aerosol manifold are connected to the four 90° spaced holes on the 8" diameter tube.

The aerosol generator is shown schematically in Figure 21. Carrier air, introduced from the main air supply, is cleaned by passing through three separate filters, each serving a particular purpose. A condensate filter removes oil and moisture from the air stream. Next is a primary filter which removes large solid impurities such as rust, scale, and dirt. The third filter removes submicron particles, ensuring a clean, uncontaminated air supply.

The aspirator shown in the figure is a simple plated standard aspirator of the type used in laboratories to obtain a vacuum source from a water supply. It is modified by removing the original vacuum line attachment and is connected to a cylindrical glass tube as the reservoir for the dust. A pulse of air traveling through the aspirator creates a short time duration low pressure which causes a controlled amount of dust from the reservoir to be sucked down the pipe line and into the agglomeration chamber. The pulsed
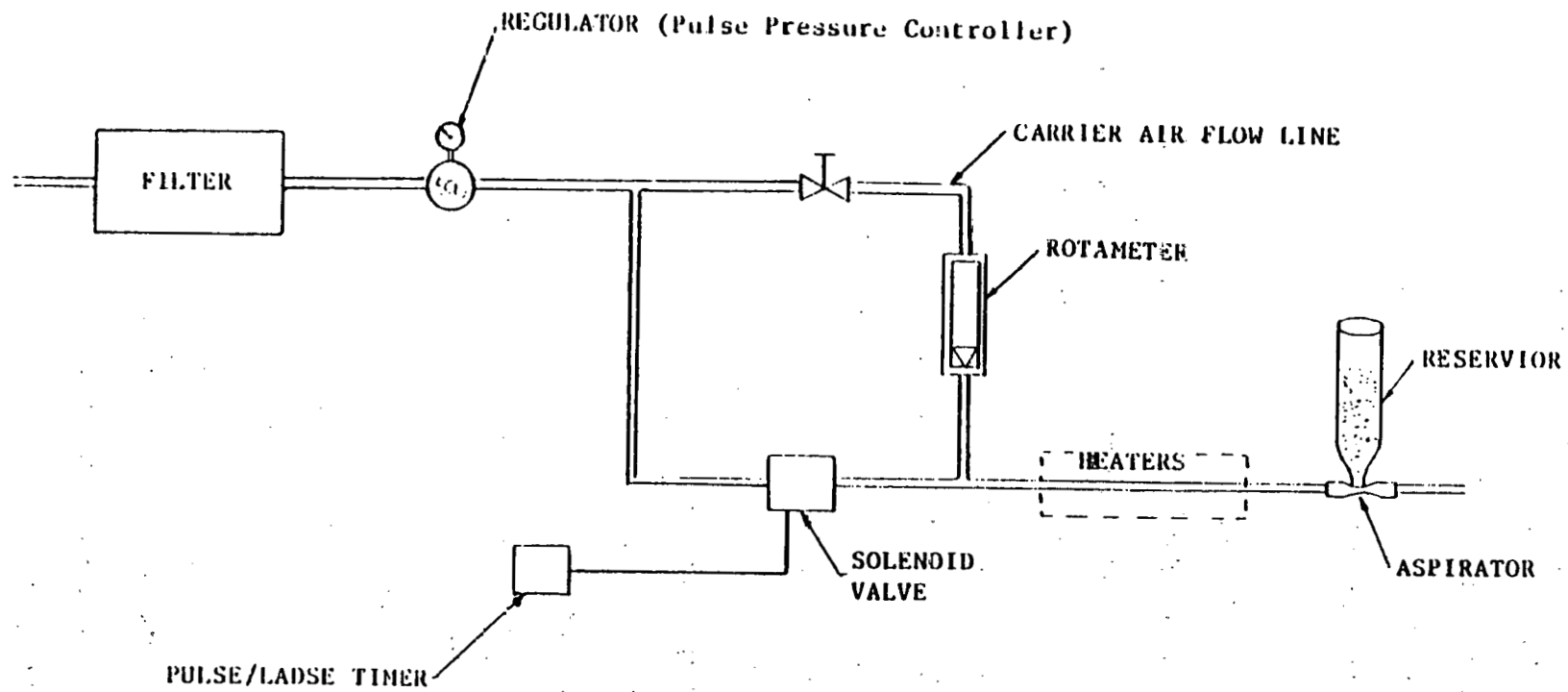
Figure 21. Schematic of Aerosol Generating System

air is produced by passing the compressed air through a solenoid valve.
The pulsed air then passes through heaters. Therefore, the temperature
inside the agglomeration chamber will not drop when the pulsed air goes into
the chamber. The time that the air is permitted to flow through the aspirator
(pulse time) and the pulse frequency are controlled by a Pulse/Lapse Timer
connected to the solenoid valve.

Agglomeration takes place in the 8 foot long 8" schedule 40 pipe. A
1/2" gooseneck sampling probe is located in the end of the section. Iso-
kinetic samples were drawn by the RAC Staksampler into an Anderson Mark III
particle-sizing stack impactor shown in Figure 22 which is designed for use
up to 1500°F. The impactor consists of a series of plates with a number
of holes arranged as shown in Figure 23. The holes are displaced on
successive plates so that a gas stream, after going through the holes in a
plate, impacts a surface and must make a sharp turn to enter the holes in the
next plate. The impactor operates on the theory that at each stage
smaller particles flow with the air stream during the sharp turn; larger
particles, due to their greater inertia, will go straight and deposit on to
the plate. As shown in Figure 23 each plate has holes smaller than those
in the previous plate and, therefore, the velocity increases at each stage,
depositing particles of given size ranges at each level. A final filter
collects any particles which remain after the last plate. A glass fiber
substrate with properly located cutouts is placed on each stage as the
collection medium. Each substrate is weighed before and after exposure to
determine the mass of particles of each size collected; and it is dehydrated
before weighing to eliminate the factor of the weight of moisture. The
range of particle diameters that will collect on a plate at each stage is
determined by the aerosol flow rate through the impactor.
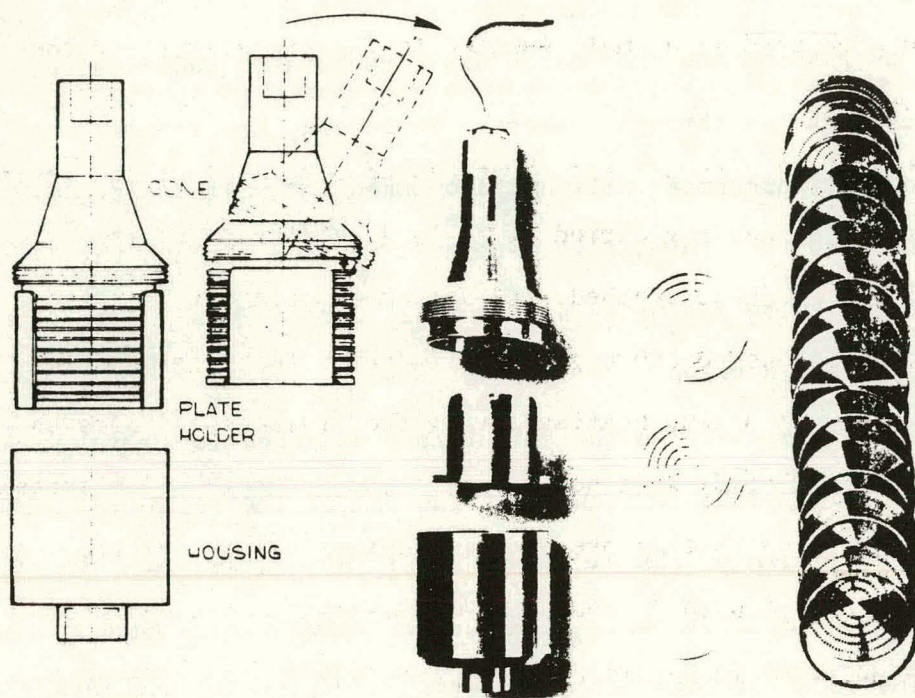
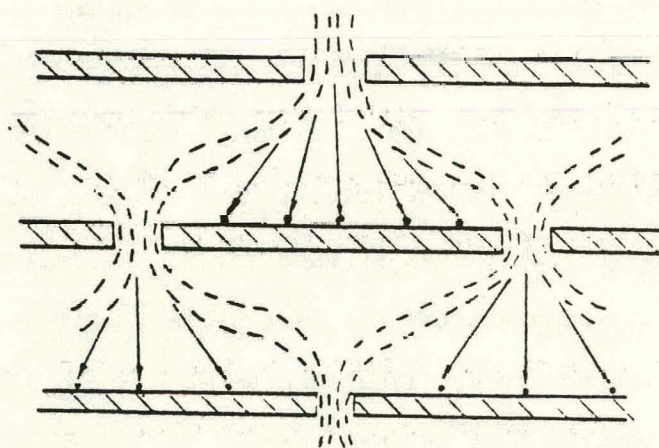Figure 22.   Anderson Mark III Stack Impactor

Figure 23.   Schematic of Impactor Stage

The impactors are preheated in a small furnace to the temperature of the aerosol being tested.

Because of the large mass of steel that has to be heated to the desired operating temperature, a heating period of as long as four hours is required to reach 700°F. Once reached, the system temperature is quite stable providing a rather small temperature gradient in the 8 foot agglomerator of about 30°F. During this long heating period the sluice gate valve is shut tightly preventing backflow of hot air into the upstream siren system. The water jacketed cooling section prevents conduction heating of the upstream system which is housed on acoustically treated wooden enclosure. The enclosure was designed to assure acceptable levels in the work area. The siren air is exhausted through an acoustically lined long duct into the work space again to assure acceptable sound levels. The sound level in the work space reaches a value of about 105 dBA with 168 dB in the agglomerator necessitating the wearing of high quality muff type ear protectors by the operating personnel.

The piping from the upstream heater flange to the end of the 8 foot agglomerator tube is covered completely with 2 inch thick thermal insulation (calcium silicate or Epytherm) and aluminum sheeting to reduce heat loss, increase acoustic transmission loss and reduce temperature gradients in the test section.

The acoustic pressure sensors were attached to small water jacketed coolers which were screwed into the hot agglomeration chamber pipe wall to provide protection from the high temperatures.

In order to prevent overtemperature of the siren from a combination of internal heating by the high powerful electric motor and the very hot air from the Roots blower, we installed a one foot long water cooled coil of
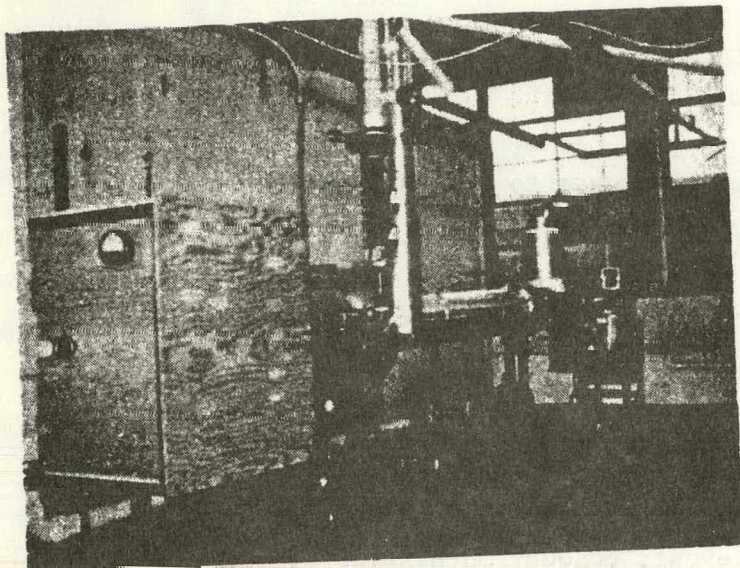
Figure 24.   View of 700°F Agglomerator

Figure 25.   View of Computer Controlled Area
For P.S.U. 700°F Agglomerator

copper wire into the 3" PVC pipe from blower to the siren to cool the air to the siren. Figures 24 and 25 are photographs of the facility.

2.5.3 THE SIREN

Because of the importance of the sound source in terms of its overall efficiency, reliability and cost, we shall describe the siren design in somewhat greater detail. Before deciding on the siren as a very promising sound source, we investigated several other potential high acoustic sound pressure sources. Hartmann Whistles (generators) provide efficiencies of about 5%. Air powered, electrically driven oscillating sleeve valve type drivers are on the market with acoustic outputs in the 2 KW to 40 KW range. Their efficiencies are in the 8% to 10% range. These latter sound sources can provide the broad band sound required in the acoustic fatigue test installations for which they were designed. Generally, they are not designed for long life applications. These sources work at considerably lower frequencies than needed for acoustic agglomeration. Another well known high power source is the St. Clair generator which is basically a resonant cylinder vibrating in an axial mode. Kilowatt range powers in the 1 to 15 KHz range have been produced with overall efficiencies in the vicinity of 6%. Sirens have been shown to be the only sound source which promises to provide the high overall efficiencies required for economically viable acoustic agglomerators in power plant applications. Also, properly designed sirens offer the promise of the required long life, high reliability, low operating costs and relatively low initial cost compared to other systems.

Almost all commercial sirens are used for fire and air raid warning systems. They have frequencies in the 250-500 Hz range and produce acoustic powers in the 100-1000 watt range.

The most definitive early work on the design of high power sirens was done at Bell Telephone Laboratories by Jones [39] under Defense Department auspices during the second world war and published in 1946. The siren produced 37,000 watts at a frequency of about 500 Hz and an acoustic efficiency of about 70%. The siren, output exponential horn and compressed air source are represented as lumped parameter electric circuits. Stator and rotor port shapes are related to acoustic efficiency and design criteria for optimum efficiency are established. Allen and Rudnick [40], used much of the theory of Jones to develop a siren with outputs up to 2000 watts of acoustic power at frequencies in the 50 to 2,000 Hz range and acoustic efficiencies of about 35 to 45%. Several of the features of this successful work were incorporated into our design. Commercial high power sirens for acoustic agglomeration applications were developed by Ultrasonic Corporation in the 1950's [41]. A siren with several independently driven rotors was developed by the Air Force to produce broad band sound for sonic fatigue testing of aircraft and missile structures [42] in 1962, but efficiencies were very low.

Mednikov [12], in a chapter in his text on acoustic agglomeration in 1965, pulls together the work of the above authors. Some very interesting work was published recently by researchers in Poland relating to the effect of port shape on siren efficiency [43]. Similar to Jones, they found that rectangular shaped ports, which produce much shorter opening and closing times than round ports, provided higher efficiencies although Puch's efficiencies were very low. In 1978, Puch [44], published a four terminal electric network analogy of the siren with encouraging agreement with experiment as long as plane wave conditions existed.

The literature on siren design and experience applicable to acoustic agglomeration gives a very encouraging picture:

1) The large acoustic powers needed can be produced.

2) Overall efficiencies in excess of 50% are achievable with good aerodynamic and acoustic design.

3) The siren is primarily a pure tone with higher harmonics-type sound source.

The siren was to be used as the sound source in our acoustic agglomeration research facility. Although we were not looking for highest efficiencies at the expense of high complexity, we were hoping to learn from this experience how to predict siren performance, to verify scaling laws, and to obtain experience for the design of more efficient sirens.

Power: 600 acoustic watts, maximum.

Frequency: Controllable from 1000 to 4000 Hz.

Acoustics: Pure tone and warble tones with 2nd harmonic at least
10 dB below fundamental.

Pressure Drop: 7 psi, maximum.

Overall Efficiency: In the 25% range.

Physical Features: Small size, reliable service for 2000 hours,
easy maintenance.

The relatively low overall efficiency of 25% for this research type siren was accepted first of all, to meet the pure tone requirment for the agglomeration studies, to perform over a wide frequency band, and to assure a reliable sound source for our agglomerator obtainable in a short time at low cost and minimum risk.

The siren has to be treated as a system as shown in Figure 26. We recognize the compressor as a pressure-flow source, the upstream chamber complex impedance, the time varying flow resistance of the rotor-stator,
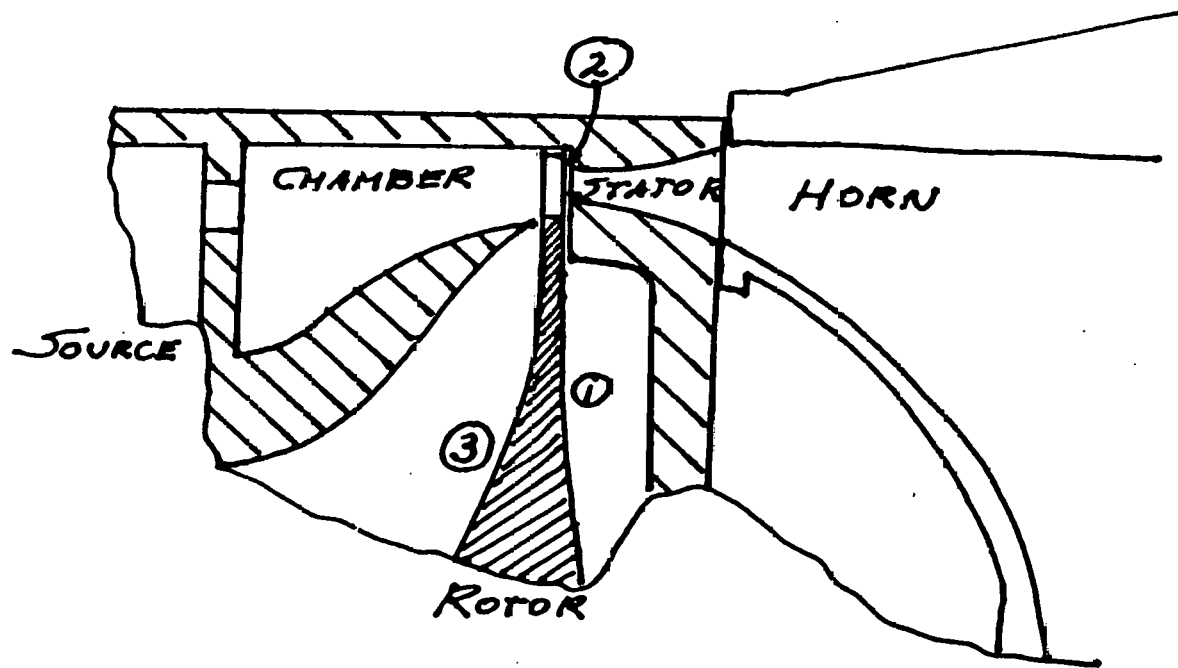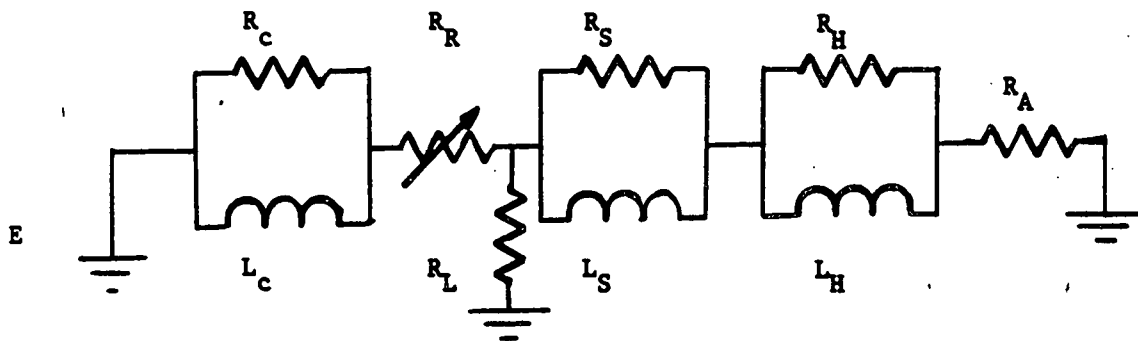
FIGURE 26

Schematic Diagram of Siren System

E   —   Pressure Source (Compressor)

R_c, L_c —   Complex Impedance of Siren Chamber

R_R —   Rotor-Stator Time Varying Impedance

R_L —   Rotor Leakage Resistance

R_S, L_S —   Stator Port Impedance

R_H, L_H —   Horn Coupler Impedance

R_A —   Agglomerator Resistance

FIGURE 27

Equivalent Circuit of Siren System

stator with a leakage shunt, the complex impedance of the acoustic coupler to the agglomerator. We shall use the lumped electric analogy first proposed by Jones as shown in Figure 27.

The purpose of this analysis is to properly size the various components so that high acoustic power output can be achieved at the desired frequency and at a high acoustic efficiency.

Acoustic efficiency is here defined as the ratio of sound power radiated divided by the power of the compressed air flow. The acoustic power is given by the product of volume velocity, U_H, into the horn squared times the horn resistance R_H. The power to provide the mass airflow at pressure ΔP, by isentropic compression assuming small pressure ratios is given by (i.e. 1.3) the product of volume velocity through the siren opening times the pressure drop so that the acoustic efficiency is given by:

$$\eta_{ac} = \frac{W_{ac}}{W_c} = \frac{U_H^2 R_H}{U_o \Delta P}$$

where U_o is the average volume velocity through the time varying flow resistance of the rotor-stator.

We can draw two rather important conclusions from this simple relationship:

1) The lower the pressure difference across the cut-off ports of the siren, the higher the acoustic efficiency. But, experience has shown that there appears to be an optimum pressure ratio P_c/P_o of 0.35 beyond which the dissipation of energy by turbulence becomes excessive.

2) In comparing average volume velocities through the rotor-stator flow resistance for sinusoidal area variation (to obtain a sinusoidal output with minimum distortion) and the square wave case we find that the

square wave case passes a higher volume velocity. Jones established that the maximum acoustic efficiency for sine waves ($\Delta P \approx 0$) is 50% whereas it is 100% for square waves. Or realistically, we can expect a two to one ratio between acoustic efficiencies from square wave relative to sine wave outputs.

The impedance relationships for the various circuit elements are as follows:

a) Agglomeration chamber resistance R_A,

$$R_A = \frac{\rho c}{S_A}$$

where S_A is the cross-sectional area of the agglomeration chamber, ρc is the characteristic impedance of the gas. Also the agglomeration chamber is treated as an infinitely long pipe (anechoically terminated).

b) Stator port and horn impedance as seen at horn,

$$Z_{SH} = \frac{\rho c}{S_H} \frac{\cos(bl + \theta) + j(\sin bl)}{j(\sin bl) + \cos(bl - \theta)}$$

where S_H is the horn's throat area

    l is the length of the horn

$$b = \frac{1}{2} (4k^2 - m^2)^{1/2}$$

    m is the horn's expansion coefficient

    k is the wave number $= \frac{\omega}{c}$

    θ is $\tan^{-1} \frac{m}{2b}$

c) The impedance as seen at the throat of the stator port including the horn and the agglomeration chamber is given by:

$$Z_{SA} = (\frac{\rho c}{S_1})(\frac{S_1 Z_{SH} (\cos k l_1) + j \rho c \sin k l_1}{j S_1 Z_{SH} (\sin k l_1) + \rho c \cos k l_1}) - \frac{\rho c}{S_A}$$

where l_1 is the length of the stator ports and S_1 is the stator ports cross-sectional area.

d)   We can now combine the equations and determine the expressions for the resistance and inductance for the stator-horn combinations. The lengthy expressions are not given here.   One point of interest is that both R_{SA} and L_{SA} are functions of frequency and have been determined by means of our computer for the particular siren design.   A brief discussion is given later.

e)   The impedance of the siren chamber was derived considering the entrance to the rotor (the chamber exit port) as a hole radiating into a free field which considers the hole to be a vibrating piston.   We have thus, assumed that the chamber walls are fully absorptive so that the chamber dynamics have no effect on the bulk flow through the siren.

The impedance for such a hole with 2ka < 1, is:

$$Z_C = \frac{\rho c}{\pi a^2} \left[\frac{(ka)^2}{2} + j \frac{8ka}{3\pi}\right]$$

where a is the radius of the exit port.   The real and imaginary components will form the resistance and reactance.

f)   The term for the rotor flow resistance must be determined using actual dimensions of a proposed design.   The configuration is illustrated in Figure 26.   The change in resistance with rotation will determine the wave form produced.   We have assumed a sine wave formulation:

$$R_S = \overline{R}_S + R_a \sin \omega t$$

The calculation of flow resistance treats the flow by a combination of empirical flow orifice relations and isentropic recovery in the expanding stator section.

The analysis was programmed on Penn State University's digital computer to provide at least better qualitative understanding.   The results

are discussed in the section on the mechanical design where specific physical quantities are determined for a particular design configuration and analytical trials were run. The equivalent circuit model presented is an essentially untried model and contains many simplifying assumptions. Thus, we shall take recourse to some empiricisms based on the experience with similar sirens.

The performance specification calls for an acoustic power of 600 watts. We have to determine the air flow and pressures needed to provide this power.

The acoustic power developed by a siren is expressed by the following relationship:

$$W_{ac} = \Gamma \, Q_m \, L_{ad} \, \eta_{ac}$$

Where Γ is the siren flow coefficient which combines the flow orifice coefficient and the leakage in the space between stator and rotor radially inward. It is the reduction in the theoretical volume flow rate, Q_m, at siren chamber pressure, P_S. Using test data from [40] and correcting for differences in configuration, we estimated Γ to be about 0.34.

L_{ad} is the adiabatic work term per unit of mass with w being the isentropic velocity from the stator ports resulting from a pressure drop P_S/P_o

$$L_{ad} = \frac{1}{2} \rho_c \, w^2$$

and

$$w^2 = 2(\frac{\gamma}{\gamma-1}) \, (\frac{P_c}{\rho_c}) \, [1 - (\frac{P_o}{\rho_c})^{\frac{\gamma-1}{\gamma}} \,]$$

where γ is the ratio of specific heats.

The acoustic efficiency of a siren is a complicated function of the shape of the rotor teeth and ports, chamber pressure P_c, the frequency, the type of horn and various engineering features such as leakage gap and rotor wobble.

For the case of square wave modulation, which is shown to be the most efficient system, Jones [39], suggested simplifying the circuit of Figure 27 by letting $L_C = 0$ and $R_H \approx 0$, thus arriving at an idealized siren efficiency expression given by:

$$\eta_{ac} \cong \frac{[(1 + 2y)^{1/2} - 1]}{y} = \psi(y)$$

where $y = \frac{4}{\gamma} (\frac{P_c - P_o}{P_o})$

For a suggested optimum pressure drop ratio of 0.35, the value of y for $\gamma = 1.4$ becomes one and the acoustic efficiency becomes 73.2%.

A suggested correction to the above relationship is given by [45]:

$$\eta_{ac} \approx \frac{\psi (\frac{4\Delta P}{\gamma P_o})}{1 + 0.5 (ka^2) + 1.68 \, ma}$$

where a is the width of the port opening in the stator, m is the exponential horn's expansion coefficient, and ψ designates a function.

For sirens with relatively small stator ports and an exponential horn with appropriately low cut-off frequency, the last two terms in the denominator will become small compared to one so that we return to the earlier relationship.

For the round stator ports, (giving sinusoidal output) and a pressure drop ratio of 0.3, the acoustic efficiency should be expected to be approximately $\eta_{ac} \approx 0.379$.

We can now calculate the required flow rate. L_{ad} is found to be 33,296 $\frac{N-m}{m^3}$ for the pressure drop ratio of 0.3. Thus Q_m = 0.14 m^3/sec at $\frac{\Delta P}{P_c}$ = 0.3. The air supply source requirements are specified.

The rotor-stator design and the specification for the siren drive power are done concurrently. The rotor operating speed is determined by the number of rotor slots and stator ports to provide the required frequency. The number of rotor slots and stator ports define the rotor diameter which in turn, defines the torques required to overcome drag and fluid acceleration.

The flow area S_1 into the stator is given by the flow requirement Q_m,

$$Q_m = \varepsilon \, S_1 \, \omega \, (\frac{P_c}{P_o})^{1/\gamma}$$

where ε gives the fraction of the rotation, the stator ports are cut-off by the rotor. We shall use wider slots in the rotor than the diameter of the stator holes such that $\varepsilon \approx 0.34$ following the results of [40]. The area, S_1 can thus be calculated.

The rotor was given 40 slots and the stator 40 holes so that we would obtain 4000 Hz at 6000 r.p.m. The rotor design can be seen in Figure 28. The exponential thickness will make the rotor a constant stress design. We chose stainless steel to minimize axial tooth deflections under pressure so that we could reduce rotor-stator axial clearance to a minimum. The axial operating clearance of 0.001" required a true running and well balanced rotor. The axial location is fixed by two preloaded ball bearings which are located as close to the rotor as possible. The bearing at the other end is, of course, floating.

The electric motor was chosen to overcome the frictional drag forces and to provide sufficient torque to permit warbling at up to 4 Hz. The

drag torque results from skin friction drag and the acceleration of the air mass as it enters the rotor. In Figure 26 we have identified three rotor regions 1, 2, and 3 where drag calculations have been performed. The skin friction was calculated using an empirical relationship due to Daily and Nece [46], for enclosed rotating disks. Most of the drag comes from the close spacing (0.001") between stator-rotor at the cut-off ports. The total drag power was about 30 watts. The power to accelerate the air mass was 256 watts. Thus, a total steady state power of about 300 watts is called for.

We are using a 2 horse power 120 volt Dumore Universal motor which provides adequate excess torque for an effective warble tone generation.

The motor is cooled by passing the compressed and cooled air through the field coils and over the armature into the siren. In order to obtain a warble tone, we alternately turned the motor on and off at a rate of 4 Hz. From the mass moment of inertia of 10 lbm-in^2 and the available torque at a particular speed, we calculated the band width of the warble. For example, at 4000 Hz center frequency and a warble rate of 4 Hz, we calculated a band width of 125 Hz. The purpose of the warble tone was to substantially reduce the very large amplitude variations in the hard walled rectangular cross-section agglomeration chamber.

The exponential horn was fabricated in three pieces. The throat of the horn was made of a 4.510 inch long, 10.5 inches in diameter, piece of hard maple with 40 holes circumferentially arranged of the exact size and location of the stator exit peaks shown on Figure 19. The 40 holes were circumferentially enlarged so as to smoothly merge into a circumferential annulus. The change in area with axial distance conformed to the horn equation.
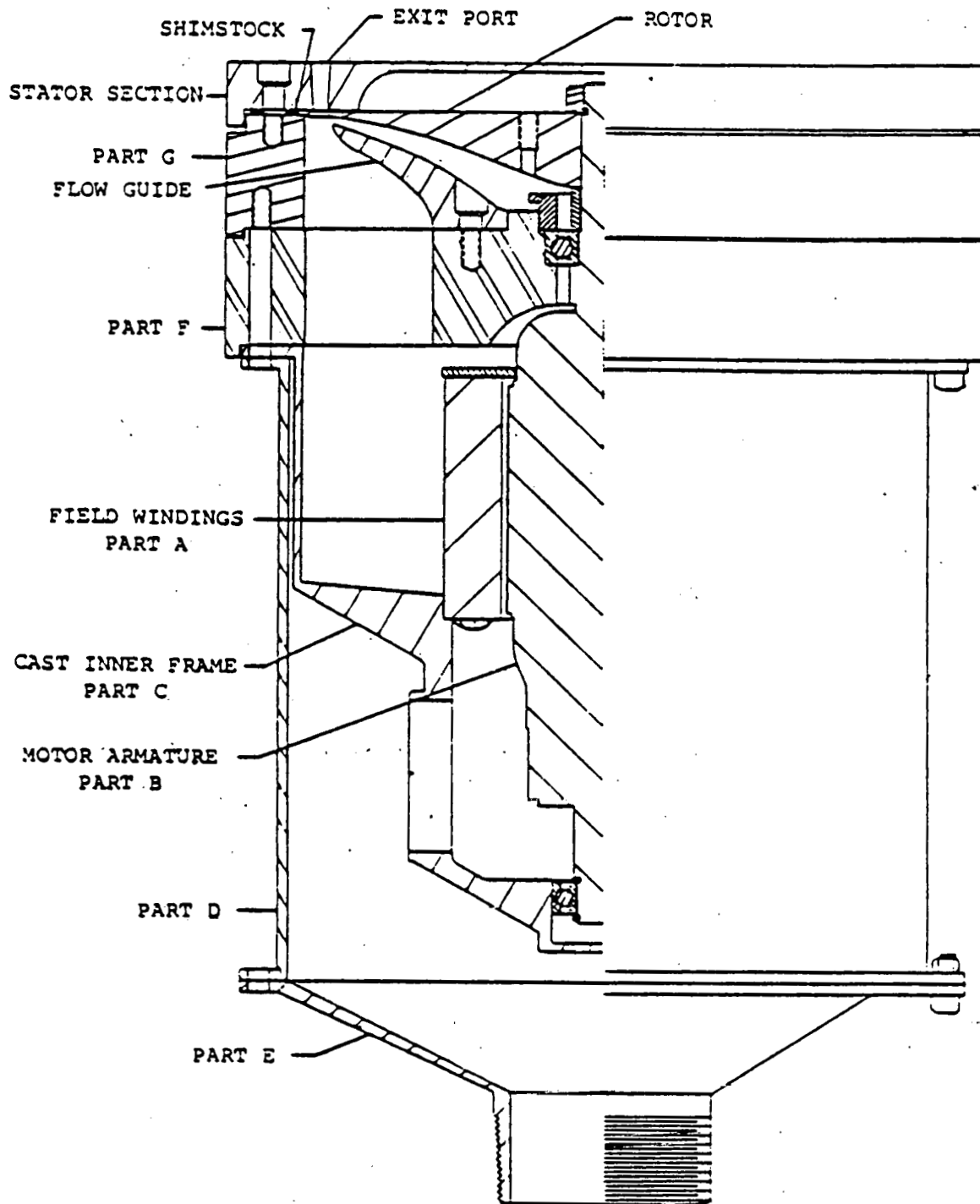
Figure 28. Full View of the Siren

A hardwood exponential cone was attached to the throat section to form the inner surface of the horn. The outer surface was made of molded fiberglass forming a smooth transition from circular to the rectangular cross-section of the agglomeration chamber. A photograph of this siren under test is shown in Figure 29.

The testing was performed in the reverberant room of The Pennsylvania State University's Noise Control Laboratory. The room was calibrated using standard methods. Acoustic measurements were made with 5 microphones. The signals from the microphone amplifiers were analyzed with a Nicolet Scientific Model 660 A Fast Fourier Transform Analyzer (FFT). Twenty frequency domain signals were taken at each microphone position. The frequency spectrum of 100 averages was recorded on a digital plotter. The wave forms were also analyzed by placing one microphone in front of the horn exit. Siren mechanical performance was monitored with an accelerometer mounted on the siren case. The flow rate into the siren was measured by means of an A.S.M.E. orifice meter. Electric power to the siren was measured as were the necessary air pressures and temperatures.

The siren met both the acoustic power output and acoustic efficiency requirements. Figure 30 gives a plot of acoustic power as a function of air flow for the four frequencies tested. We noted, however, that the output was very frequency dependent which is attributable to the exponential horn characteristics. The analytical model of the siren system was programmed on Penn State University's digital computer. The predicted dependency of acoustic power on frequency is given in Figure 31. The wide fluctuations in output are indeed present. Interesting in this regard, is the computer solution of the normalized impedance of the horn and stator port combination as shown in Figure 32. The normalized impedance is found to be largely resistive, which is to be expected for all frequencies above the horn's cut-off frequency.
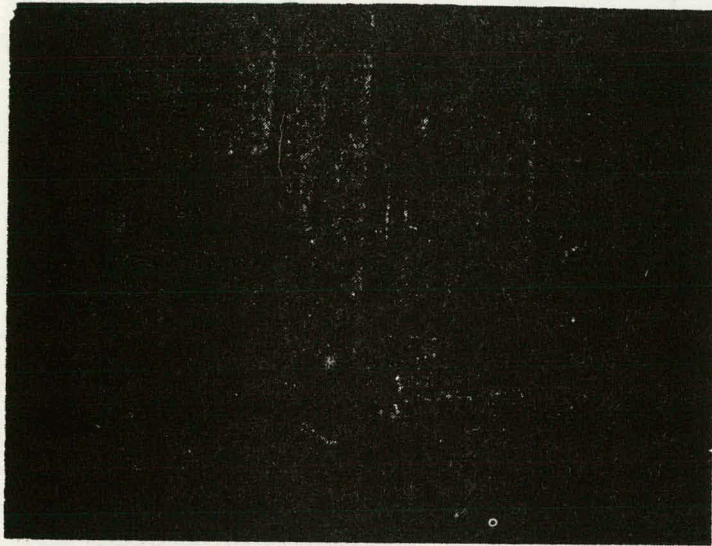
Figure 29.   P.S.U. 600 Acoustic Watt Siren Under
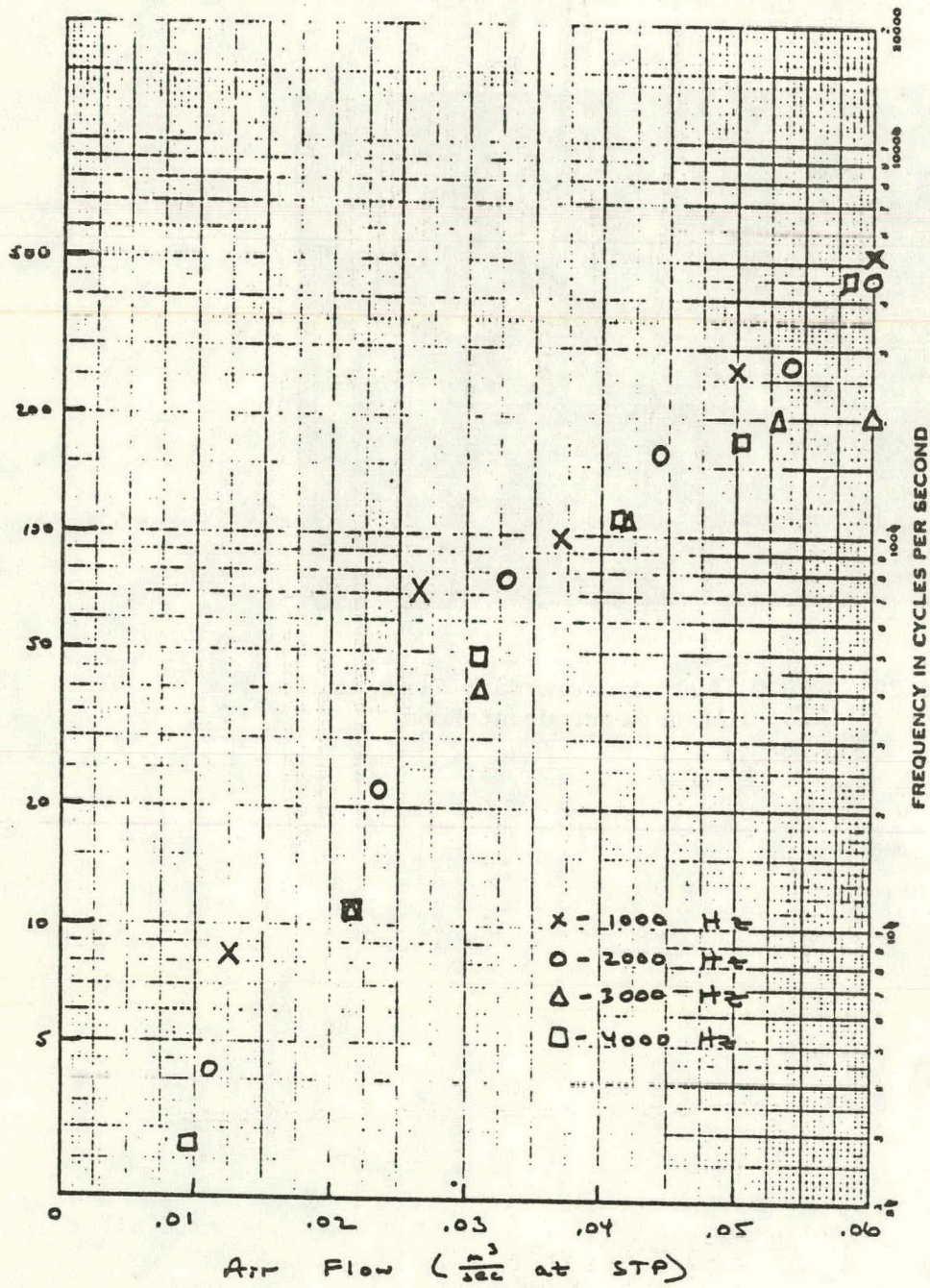   Test in the Reverberant Room

FIGURE 30

Acoustic Power as a Function of Measured Siren Air
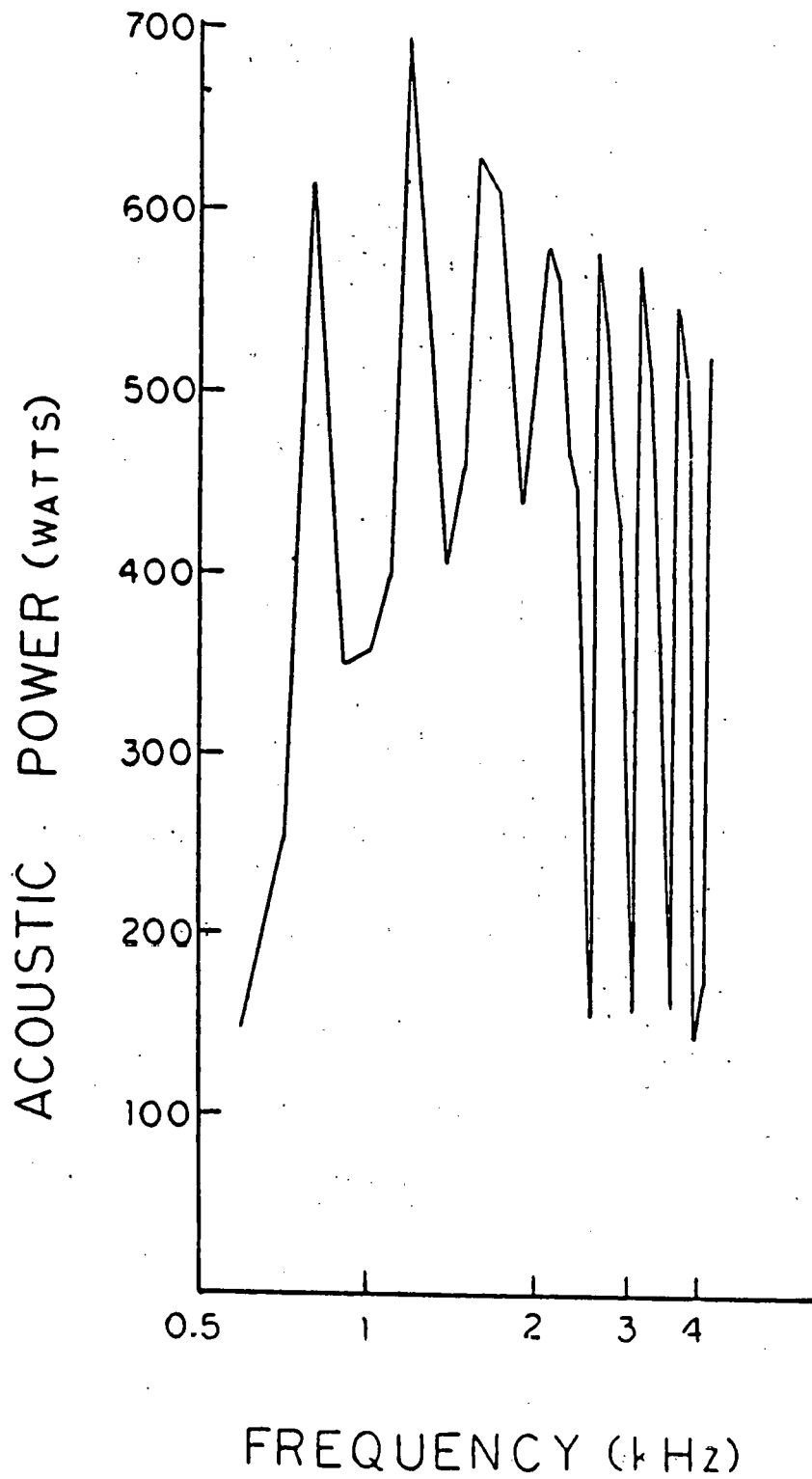Flow for Various Frequencies

FIGURE 31

Predicted Acoustic Power as a Function of Frequency at a Chamber
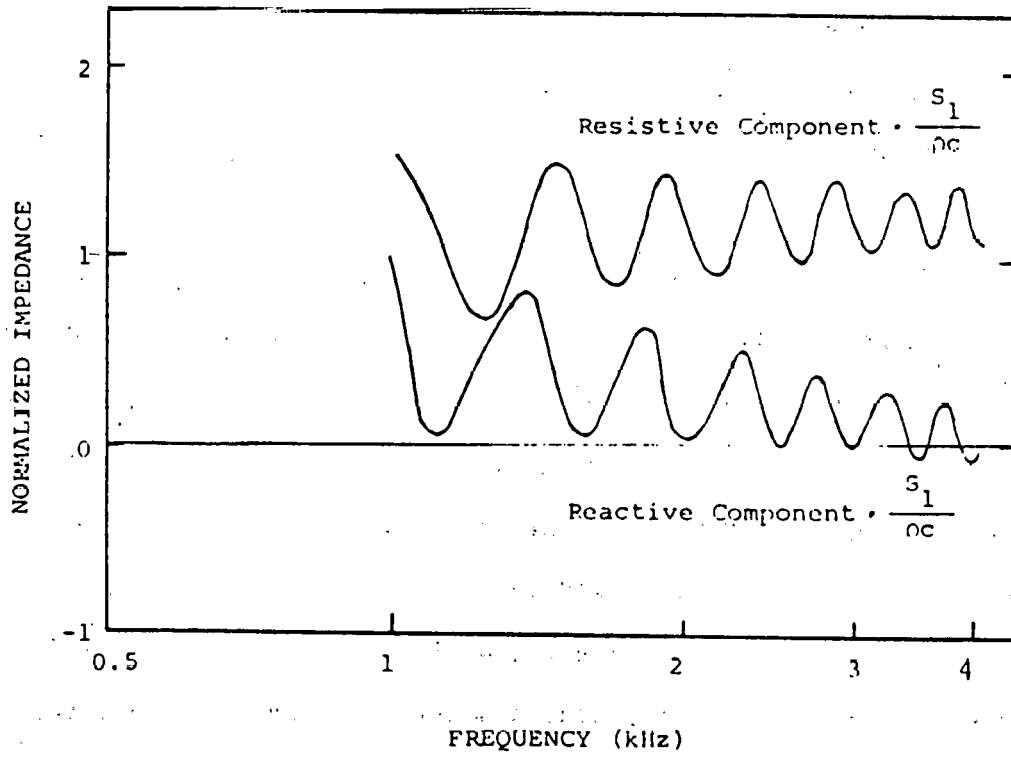Pressure of 1.4 Atmospheres in Increments of 100 Hz

Figure 32. Normalized Impedance of Exit Port-Exponential Horn Combination

The normalized inductive portion is oscillating and decreasing toward zero, typical of an exponential horn. The sharp predicted output drops at 2500, 3000, 3500 and 4000 Hz, occur whenever the reactive portions become negative, thus capacitive at these frequencies because of a term containing the length of the exit port. Thus, phase differences between inlet and outlet of the stator exit port interfere with sound propagation. We do not believe that this effect is as pronounced in the real siren because of the idealizations in the model.

The computer results also predict a drop in airflow rate with drops in acoustic power which is verified by the siren measurements.

Figure 33, is a typical plot of siren acoustic power output as a function of chamber pressure. The agreement is indeed encouraging with the trends comparing very well.

Note must be taken of the fact that the acoustic levels which were generated were in the 160 to 180 dB range resulting in significant non-linear effects which, of course, were not included in the analytical model.

A study of the wave forms measured 20 inches from the exit plane and the narrow band spectra shows that the second harmonic is typically 10 to 20 dB below the fundamental showing that essentially all of the acoustic power is in the fundamental, which was anticipated as a result of the circular stator port design. Figure 34 gives such a typical narrow band spectrum of the siren output.

We also studied the effect of rotor-stator axial clearance on siren power output. As expected, the leakage flow rate increased with increasing clearance, meaning of course, that siren efficiency would drop as clearance increases. Thus, for an axial clearance of 0.006", the static leakage flow rate became a significant fraction of the modulated air flow. This leakage
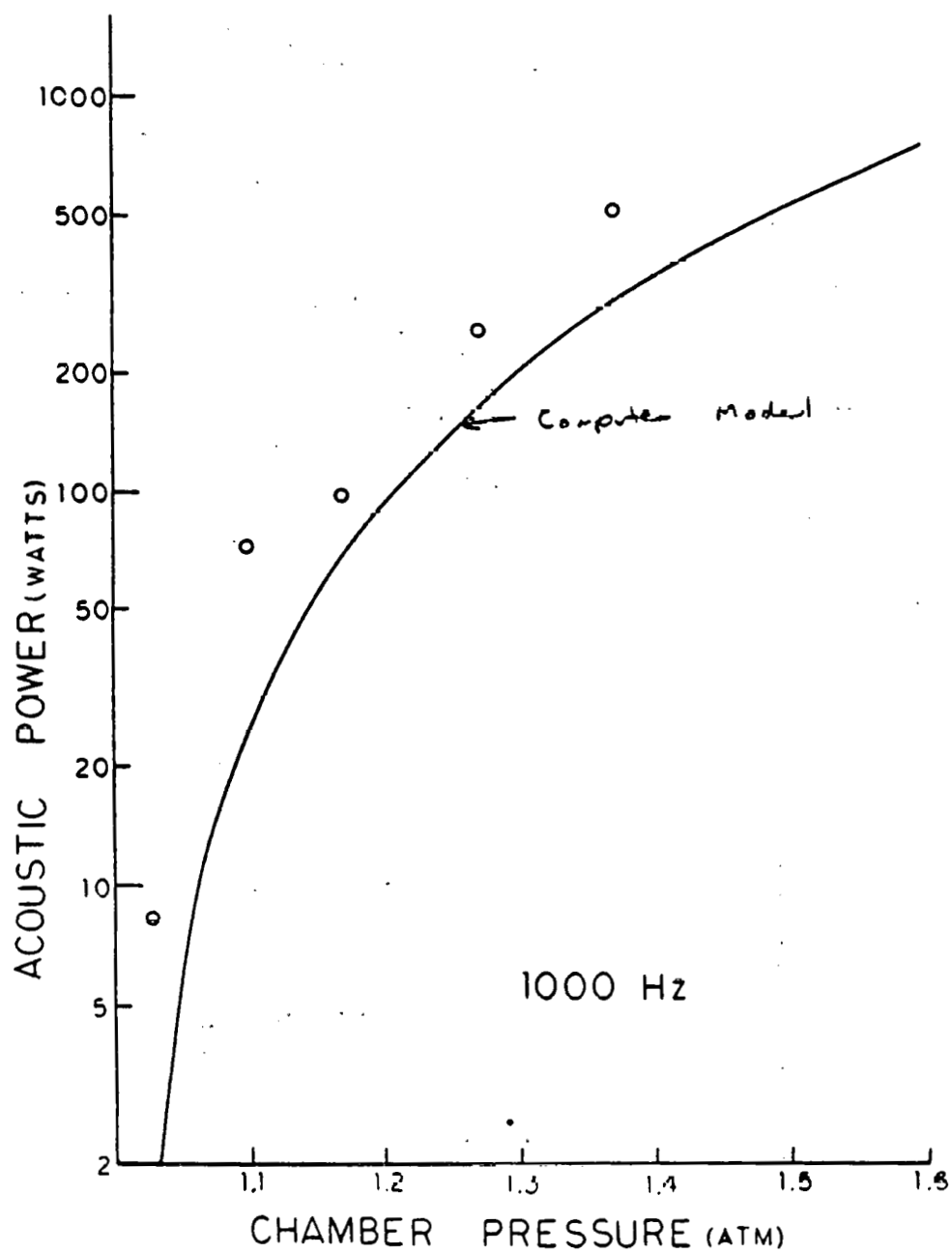
FIGURE 33

Plots Predicted and Measured Acoustic Powers As A
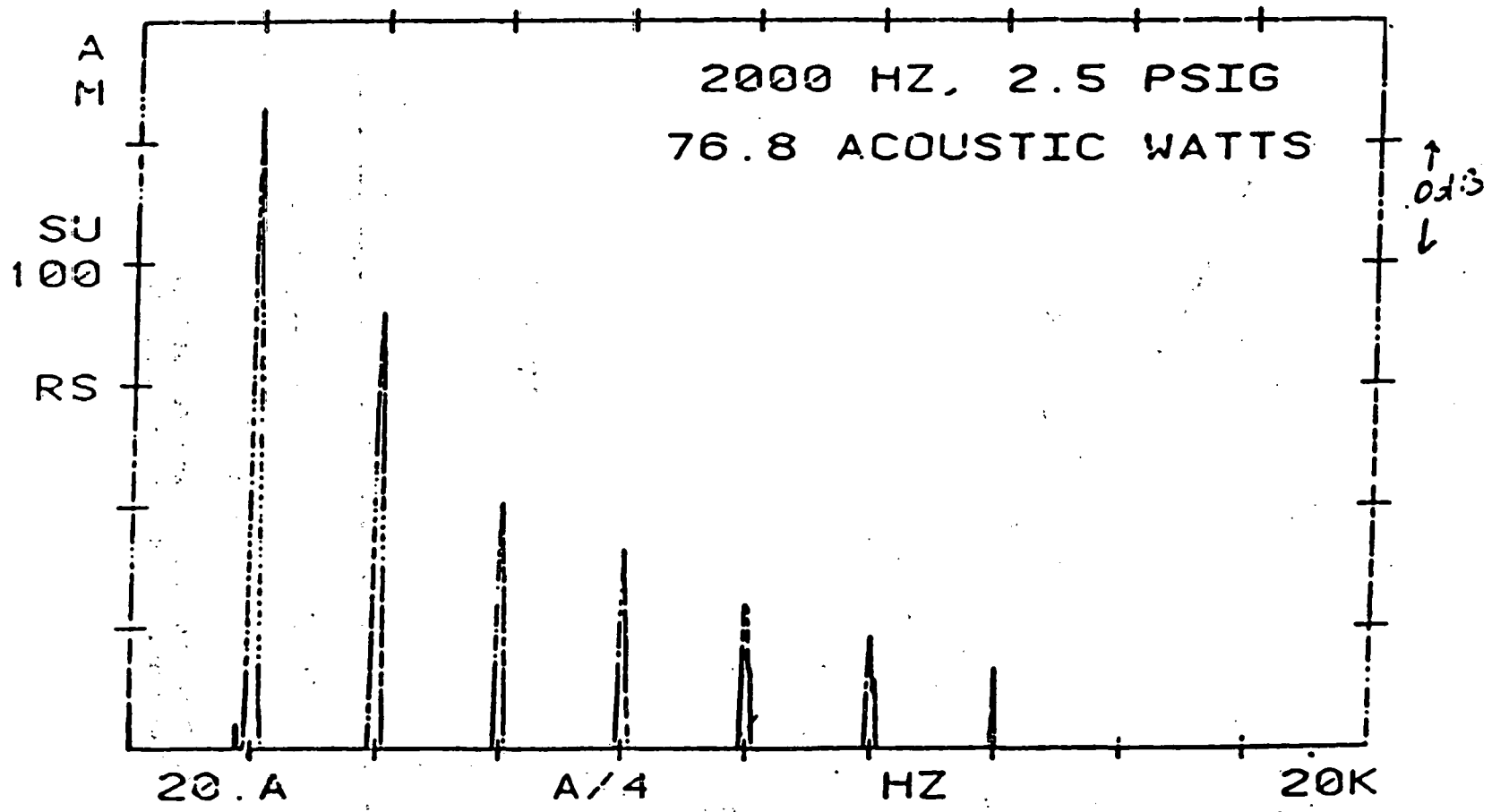Function of Chamber Pressure at 1000 Hz

FIGURE 34

Narrow Band Spectrum of Siren Output

flow is of course not modulated and will not produce sound at the siren frequency. Decreasing the clearance from 0.006 inches to 0.002 inches for the same chamber pressure, resulted in a 3-fold increase in sound power produced. Our latest build-up of the siren with true running rotors (< 0.001" wobble) and 2 preloaded bearings to assure minimum axial separation under chamber pressure has permitted us to operate consistently with clearances of 0.001" and obtain power outputs in excess of 800 acoustic watts at 6 psig chamber pressure.

The measured acoustic efficiencies ranged from a low of 5% up to a high of 27.8% at 1.1 atm and our lowest test frequency of 1000 Hz. We did not observe the theoretically predicted increase in efficiency with decreasing chamber pressure. The highest efficiencies generally occured in the 1.25 to 1.35 atmosphere chamber pressure range as predicted. On the other hand, from the analytical relationships, we may expect to see a decrease in efficiency with increasing frequency as is also predicted by the model. With the improved siren we are using today as compared to the results presented here, we are obtaining considerably higher acoustic power levels and, therefore, should expect efficiencies closer to our prediction of 37.9% for a pressure of 1.3 atmospheres.

The siren which we have developed for our acoustic agglomerator has performed reliably and predictably over close to 1000 hours. We have built two units and both show the same strong dependency of output acoustic power with frequency which we have predicted. The wave form of the round ported siren shows that the fundamental frequency is dominant.

The power output of the siren is essentially identical to the design value. The rather complex analytical model of the siren system predicts siren

output, siren efficiency, and siren speed response rather well. We thus, have developed confidence in our ability to scale siren designs and operation in different environments.

The design was not optimized with regard to rotor-stator flow passages, clearances and chamber impedances. Much higher output powers thus acoustic efficiencies can be obtained by the use of rectangular stator ports and circumferentially long rotor openings thereby generating square wave flow patterns with twice the efficiencies thus twice the powers that are obtainable with sinusoidal modulation. Although it is recognized that substantial portions of the acoustic power are shifted into the higher harmonics for the sharp cut-off conditions existing with the rectangular ports.

2.5.4 MEASUREMENT, CONTROL AND COMPUTATION

The operation of the 700°F agglomerator system required the frequent monitoring of many measurements and the operation of several valves and controls.

The following parameters are measured as shown in Figure 20 during each run:

Siren Pressure (Valedyne Pressure Sensor);

Siren Temperature (Iron - Constantan Thermocouple);

Barrier Pressure Drop (Valedyne Differential Pressure Sensor);

Heater Blower Pressure (Pressure Gauge);

Heater Line Flow - A Pressure Differential (Valedyne Differential Pressure Sensor);

Heater Blower Air Temperature (Iron - Constantan Thermocouple);

Dust Generator Air Pressure (Pressure Gauge);

Dust Generator Pulse Rate;

Dust Generator Reservoir Level (Visual);

Heater Fin Temperature (Chromel-Alumel Thermocouple);

Agglomerator Air Temperature Upstream;

Agglomerator Air Temperature Downstream;

Sound Pressure Level in Agglomerator Upstream;

Sound Pressure Level in Agglomerator Downstream;

Frequency of Sound (Digital Counter);

Wave Form of Sound Wave (FFT Analyzer);

Stak Sampler Flow Rate (Indicator);

Stak Sampler Flow Temperature (Indicator);

Stak Sampler Sampling Time.

The following controls have to be activated, monitored and changed during each run:

Siren By-pass Valve;

Siren Blower Switch;

Siren Frequency Control;

Cooling Water Valve to Main Jacket;

Cooling Water Valve to Sensor Jackets;

Cooling Water Valve to Siren Air Cooler;

Heater Blower Switch;

Heater Controls;

Dust Generator Air Pressure Regulator;

Dust Generator Pulse Rate Control;

Heater Air Blower By-pass Valve;

Heater By-pass Valve;

Staksampler Controls;

Attach and Remove the Heated Impactor and the Necessary Connections. (Details are discussed in a following section).

A microcomputer based data acquisition system was chosen in order to assure that operations are performed in the proper sequence and that all parameters are at their desired values and are recorded. A Commodore Model 4016 microcomputer with 16 K of random access memory is used for this system. Important parameters are computed and displayed on the computer screen and updated periodically. Analog DC signals from thermocouples and pressure transducers are signal conditioned to nominal maximum 5 volt levels and applied to a PSU modified Connecticut Microcomputer AIM 16 digitizing system. This system consists of a 16 channel multiplexer and an 8-bit successive approximation analog to digital converter. Input and output functions are controlled through the IEEE-488 bus and user port of the Commodore Computer. The digital data are then converted to engineering units with software and stored in memory. The AC analog signals from two microphones are digitized using Keithley Model 179 digital multimeters, also controlled from the computer's IEEE-488 bus. These data are converted to sound pressure level with software and stored in memory.

Any desired quantities can be displayed on the computer screen and can be updated at a maximum rate of once every three seconds. The digital data can be recorded on cassette tape when a permanent record is desired. The data acquisition system can be readily modified with simple software changes in BASIC language from the computer keyboard. Programs written to control the system are stored on cassette tape and can be rapidly loaded into computer memory prior to the beginning of tests. (See Figure 25).

Without a doubt, one of the most important operations in the program is the determination of the particle size and size distribution before and after agglomeration at various temperatures.

We used only Anderson Mark III high temperature in stack impactors.
The technology of the sampling procedures which involves the careful pre-
paration of the impactor, the proper use of the Staksampler made by
Research Appliance Company in drawing the sample, the proper disassembly
of the impactor followed by the careful procedures of cleaning all the dust
on to the impactor substrate, weighing the container and the careful weighing
of the packet are well developed. In the data processing and procedures
we have followed the instructions contained in EPA report number EPA-600/
2-77-004 January 1977 titled: "Procedures for Cascade Impactor Calibration
and Operation in Process Streams".

Several details of our procedures are, however, worthy of discussion.
In order to permit valid comparisons of particle size data from different
agglomeration tests, it is important to follow a standardized procedure
for the preparation, handling and disassembly of the fly ash impactors. The
importance of careful handling to prevent loss of dust particles or
pieces of the substrate cannot be over-stated; on the lower stages, total
mass loading per stage may be as little as 10 or 20 micrograms. The loss of
even a small amount of dust or part of the substrate paper itself can cause
errors that are larger in magnitude than the actual mass loadings. The
purpose of this write-up is to summarize the procedures which have been
established to date.

Glass Fibre Substrate and Filter Papers. Substrate and Filter Types:
There are nine stages using ten perforated plates in each impactor: plate
numbers '0' through '8' plus a final 'F' plate at the bottom of each impactor.
The '0' plate does not require a substrate.

Two different glass fibre substrate types are used each time the
impactors are assembled for a test; they differ in geometry and correspond
to different stages of the impactor:

1. Perforated substrates with large outer ring (4 required); This type of substrate is used in the even numbered stages of the impactor to collect the impacted dust particles.

2. Perforated substrates with narrow outer ring (4 required); This type of substrate is installed in the odd numbered stages of the impactor to collect the impacted dust particles.

3. Solid (non-perforated) glass fibre filter (1 required); This is the back-up filter which is installed in the final 'F' stage of each impactor.

The word "filter paper" will be henceforth used to refer both to the glass fibre substrates (decribed in (1) and (2)), and the glass fibre filter paper (described in (3)). Strictly speaking, however, the glass fibre substrates used in Stages '0' to 'F' act as collectors of impacted dust, rather than as "filters".

Filter Preparation: To reduce the mass effects of absorbed moisture, the filter papers are stored in a sealed container which contains fresh dessicant. When the indicator dessicant changes color, it is replaced.

If the impactors are to be used for high temperature tests, further conditioning of the filter papers is necessary. The filters contain a chemical binder which is volatile at the temperatures encountered during high temperature tests. The mass of the binder which is lost from the filters during the impactor preheat procedure, may be in excess of 1.5 milligrams, an amount which is significant relative to the typical mass loadings encountered. To minimize this effect, the filter papers must be baked before they are pre-weighed. Baking the filters for 6 to 8 hours at the intended test temperature has been found to ensure that the majority of the volatile filter constituents are removed; this minimizes any mass loss from the filters during the actual test and prevents negative biasing of the mass loadings.

Filter Weights: After the filters have been baked and properly dessicated, their initial weights must be recorded. Since loose dust will be weighed along with the filters after the test, each filter is pre-weighed along with a numbered aluminium foil packet to contain the dust. The packet numbering system identifies the test number, impactor number and the individual filter stage. When each filter is removed from the impactor after the test, it is replaced in the proper foil packet to be re-weighed. Since the packet and filter are weighed together, great care is taken not to damage or lose portions of the packet.

The balance used is capable of a resolution of 0.01 milligram. To ensure accuracy, the 'zero' or 'tare' of the balance is before weighing each filter. It is time consuming and tedious, but absolutely necessary.

The preweights are recorded in an orderly fashion in a lab notebook with all necessary identification information. The technician signs and dates the page under the weights, so that discrepancies may be more easily resolved by the person who weighed the samples.

Impactor Assembly. Stage Components: There are nine stages in each impactor, lowest number on top. Each stage has a number of parts which are repeated throughout. A description of these parts follows:

Spacer Ring - Installed between the orifice plate and filter retainer to maintain proper spacing between stages.

Filter Retainer - This is the thin sheet-metal piece which is shaped like a cross. It serves to keep the filter flat and in place.

Orifice Plate - These are the numbered, perforated disks against which the substrates lie. These are numbered '0' through '8' plus one stamped 'F'.

Stage Assembly: The top, or '0' plate is assembled slightly different than the lower plates. The plates are arranged as follows, from the top of the impactor:

Stage 0	Substrate retainer
(No Filter)	Orifice Plate '0'
	Spacer Ring
Stage 1	Substrate Retainer
	Perforated Substrate (large outer ring)
	Orifice Plate '1'
	Spacer Ring
Stage 2	Substrate Retainer
	Perforated Substrate (narrow outer ring)
	Orifice Plate '2'
	Spacer Ring

Stages '1' through 'F' are assembled identically, with care taken to use the appropriate type of substrate as outlined earlier. Note that stage 'F' uses a solid type of filter and also has a spacer ring beneath the orifice plate.

In practice, the stages are loaded in reverse order into the impactor base, beginning with the spacer ring below the final stage 'F'. When the orifice plates are inserted in the impactor base, they must be aligned correctly. Each plate has a notch in its outer edge, which is aligned with one of the vertical edges of the impactor base. The paper filter is placed on top of the orifice plate and aligned so that none of the holes in the orifice plate are covered. Finally, the filter retainer is placed on the filter, again aligned so that the holes are unobstructed.

Impactor Disassembly. General Information: Disassembly is not quite as simple as just taking the pieces out. The filter papers must be replaced in the proper foil packets, along with the loose dust that has been collected on the metal parts of that stage. Disassembly is accomplished from the top of the impactor down. Extreme care must be taken to prevent dust loss, carefully brushing the loose dust into the foil packets. Overly aggressive

brushing will result in airborne dust . . . which is very hard to weigh accurately. Work is done on a clean piece of white paper, so that small dust spills may be caught and placed in the foil packets. The contents of the stage packets are described below.

Stage Packet Contents: As in assembly, the top stage is treated differently than the lower stages; in this case, the dust from plates '0' and '1' are placed together in the foil packet marked '1'. This corresponds to stage '0'.

The stage '0' packet should contain dust that is loosened from the thread area and interior of the diffuser portion of the impactor. Carefully brush the dust from these regions into the foil packets. Also brush off the dust from the plate '0' filter retainer and the stage '0' orifice plate (tap the dust from within the holes of the orifice plate). Continue with the same packet by brushing the dust from the spacer ring and filter retainer of stage '1'. Carefully place the stage '1' filter into the packet and then bursh the contents of the stage '1' orifice plate into the packet. Carefully fold the foil packet shut and seal the edges.

The stage '1' packet should contain the dust from the spacer ring above plate 2, the filter retainer, the filter, and the loose dust collected on orifice plate marked '2' (including the dust in the holes).

Stages '2' through 'F' are disassembled and cleaned with identical procedures. In general, the packet for each stage contains dust from the parts down to and including the orifice plate for that stage. This pattern is continued until all of the stages have been cleaned. There is no need to brush the spacer ring that fits beneath stage 'F'.

Cleaning and Re-assembly: After all of the filters have been removed and placed in packets, the impactors are prepared for the next set of filters. All parts of the impactor diffuser, base and stage components are cleaned with compressed air. Care is taken to ensure that all loose dust has been removed from the holes of the orifice plates.

After cleaning, the impactor is re-assembled with clean filters according to the procedures outlined earlier.

Next we have developed a computer program for the determination of the many measures of the particle size distribution that we feel are important. The program uses the following inputs:

Test section temperature;

Temperature of gas as it goes through the dry gas meter (meter temperature);

Ambient temperature;

Static Pressure in agglomerator test chamber (static pressure);

Calculated tested section absolute pressure (Test Section Pressure);

Barometric pressure;

Average pump vacuum;

Average pressure differential across meter orifice in stak sampler (Average Delta H);

Sampling nozzle diameter (nozzle diameter);

Volume as measured by dry gas meter (meter volume);

Test section inside diameter;

Number of points sampled;

Sample time;

Staksampler flow calibration (meter delta H);

Total weight collected (total mass).

(Note: this is calculated from the individual stage weights).

The computer calculates the volume of gas sampled at standard conditions; the mass loading in milligrams per normal cubic meter and grams per standard cubic foot.

Furthermore, the computer calculates several different measures of the size distribution such as:

The three cut point diameters. Namely: the Stokes arithmetic mean diameter (D-50-S) is calculated using the actual particle density and the Cunningham correction factor in an interactive manner where:

$$D = \left(\frac{18 \, \psi \, \mu \, D_j}{c \, \rho_p \, V_j} \right)^{1/2}$$

$$C = 1 + \frac{2\ell}{D} \left[1.23 + 0.41 \exp\left(-\frac{0.44D}{\ell} \right) \right]$$

D = diameter of particle impacting on the stage for the 50% cut-off condition.

$\psi = 0.1 - 0.3$ (empirical constant for particular impactor type). The aerodynamic mean diameter (D50-A) is calculated using the actual Cunningham correction factor with a particle density of 1.0. The aerodynamic impaction diameter (D50-AI) is calculated with both the Cunningham correction factor and the particle density as 1. The percent mass in each stage (pc Mass) and the cumulative percent mass for the impactor (CUM pc).

Also the differential particle size distribution (a probability density function of the size) is calculated using Stokes diameter. Thus, we show a column marked D50-S (50% cut-off of each stage) followed by the midpoint diameter.

(MID DIAM) which is the arithmetic mean of the range. Then follows the measure which have chosen to plot for results. The D%M/D LOG D column

gives the ratio of the percent mass in each stage divided by the difference of the logarithm to the base 10 of the upper and lower diameters for the particular stage. The results of such computations in a computer print out sample is given in Figure 35 followed by the plot of D%M/D LOG D versus midpoint diameter in Figure 36.

2.5.5 TEST RESULTS

The 700° agglomerator appears to meet the design objectives which we had set although we have not as yet completed a full study of its behavior.

Sound pressure levels as high as 168 dB were achieved at certain frequencies. Most of the runs were performed in the 145 to 165 dB range.

Frequency control and stability over the desired range of 1000 to 4000 Hz was attained after some of the developmental problems in the solid state frequency controller were solved.

The aerosol generator worked well in the range from 2 gm/m^3 to 20 gm/m^3 loading although repeatability presented some problems particularly at high temperatures. Repeatability of about ± 20% for the same pressures and pulse rates was noted. We do, however, believe that this variability is serious enough to warrant further development.

The 18 KW heating system generally functioned well. We experienced several instances of internal short circuits which caused the fuses to open in the controller. We believe that this problem has been solved by careful attention to detail in the assembly of the heating unit connections. In a follow-on program, we would do well to incorporate several improvements to increase the reliability of the heater. The impactor results at room temperature are quite repeatable for similar conditions in the agglomerator. Typical samples are given in the following Figures and are discussed in detail in the accompanying treatment.

```
FILE NAME:   DOE130.IMP
TITLE     :  RUN#2 2530HZ 158DB AMB TEMP
TEST DATE:   8/16/82
TEST TIME:   MON NIGHT
```

INPUT TEST DATA

Test Section Temp=	77.5 Deg F	Static Pressure	=	+2.800 In H2O
Meter Temp =	82.4 Deg F	Test Section Press. =		29.08 In Hg
Ambient Temp =	77.5 Deg F	Barometric Pressure =		28.87 In Hg
		Average Pump Vacuum =		0.000 In Hg

Average Delta H = 1.0000 In H2O

Nozzle Diameter = 0.5000 In   Meter Volume   = 0.208 Cu Ft

Test Section ID	=	7.90 In
Number Of Points Sampled	=	1.0
Sample Time	=	0.3 Min
Meter Delta H	=	1.700 In H2O
Total Mass	=	115.24 Milligrams

FIGURE 35

```
FILE NAME:   DOE130.IMP
TITLE     :   RUN#2 2530HZ 158DB AMB TEMP.
TEST DATE:   8/16/82
TEST TIME:   MON NIGHT
```

TEST RESULTS

Volume Of Dry Gas Sampled At STP;	=	0.006 NCM
21 Deg C (68 Deg F)	=	0.197 SCF
760 Mm Hg (29.92 In Hg)		
Test Section Temp	=	25.3 Deg C
	=	77.5 Deg F
Static Pressure	=	+5.23 Mm Hg
	=	+2.80 In H2O
Sample Time	=	0.3 Min
Molecular Weight Of Stack Gas, Dry Basis	=	28.8 Gm/Gm-Mole (Lb/Lb-Mole)
Total Mass	=	115.24 Milligrams
Concentration, Dry Basis At STP	=	20,715.90 Mg/NCM
	=	9.03 Grains/SCF

```
FILE NAME:   DOE130.IMP
TITLE    :   RUN#2 2530HZ 158DB AMB TEMP
TEST DATE:   8/16/82
TEST TIME:   MON NIGHT
```

Andersen Instack 9 Stage Impactor Analysis

Cumulative Particle Size Distribution

STAGE	CATCH (Mg)	DIST MAS (Mg)	D50-S	D50-A	D50-AI	PC MASS	CUM PC
F	0.240	0.240	0.296	0.492	0.579	0.208	0.208
7	0.400	0.400	0.459	0.739	0.826	0.347	0.555
6	0.770	0.770	0.769	1.210	1.298	0.668	1.224
5	0.570	0.570	1.574	2.431	2.521	0.495	1.718
4	0.150	0.150	2.470	3.792	3.882	0.130	1.848
3	0.310	0.310	3.642	5.569	5.659	0.269	2.117
2	0.430	0.430	5.388	8.217	8.307	0.373	2.490
1	21.010	21.010	8.672	13.198	13.288	18.232	20.722
0	91.360	91.360	50.000	50.000	50.000	79.278	100.000

Differential Particle Size Distribution

STAGE	D50-A	MID DIAM	D %M/DLOGD	DC/DLOGD MG/NCM/DLOGD
F	0.492	0.251	0.123E+00	0.255E+02
7	0.739	0.615	0.197E+01	0.407E+03
6	1.210	0.974	0.312E+01	0.646E+03
5	2.431	1.821	0.163E+01	0.338E+03
4	3.792	3.111	0.675E+00	0.140E+03
3	5.569	4.680	0.161E+01	0.334E+03
2	8.217	6.893	0.221E+01	0.458E+03
1	13.198	10.707	0.886E+02	0.184E+05
0	50.000	31.599	0.137E+03	0.284E+05

```
Total Volume Sampled (Dry STP)  =      0.006 DNCM
Total Mass Collected            =    115.24 Milligrams
Plate Wash                      =      0.000 Milligrams
Front End Wash                  =      0.000 Milligrams
Assumed Density Of Particles    =      2.300 Grams/CC
Arbitrary Smallest Diameter     =      0.010 Micrometers
Arbitrary Largest Diameter      =     50.000 Micrometers
Sample Flow Rate                =    290.685 Actual CC/Sec
Impactor Vacuum                 =     16.608 Millimeters Hg
```

All Diameters Reported In Micrometers

Dp vs % MASS

DOE130 2530hz 158db   Amb Temp

% MASS

MIDPOINT AERODYNAMIC DIAMETER (Micrometers)
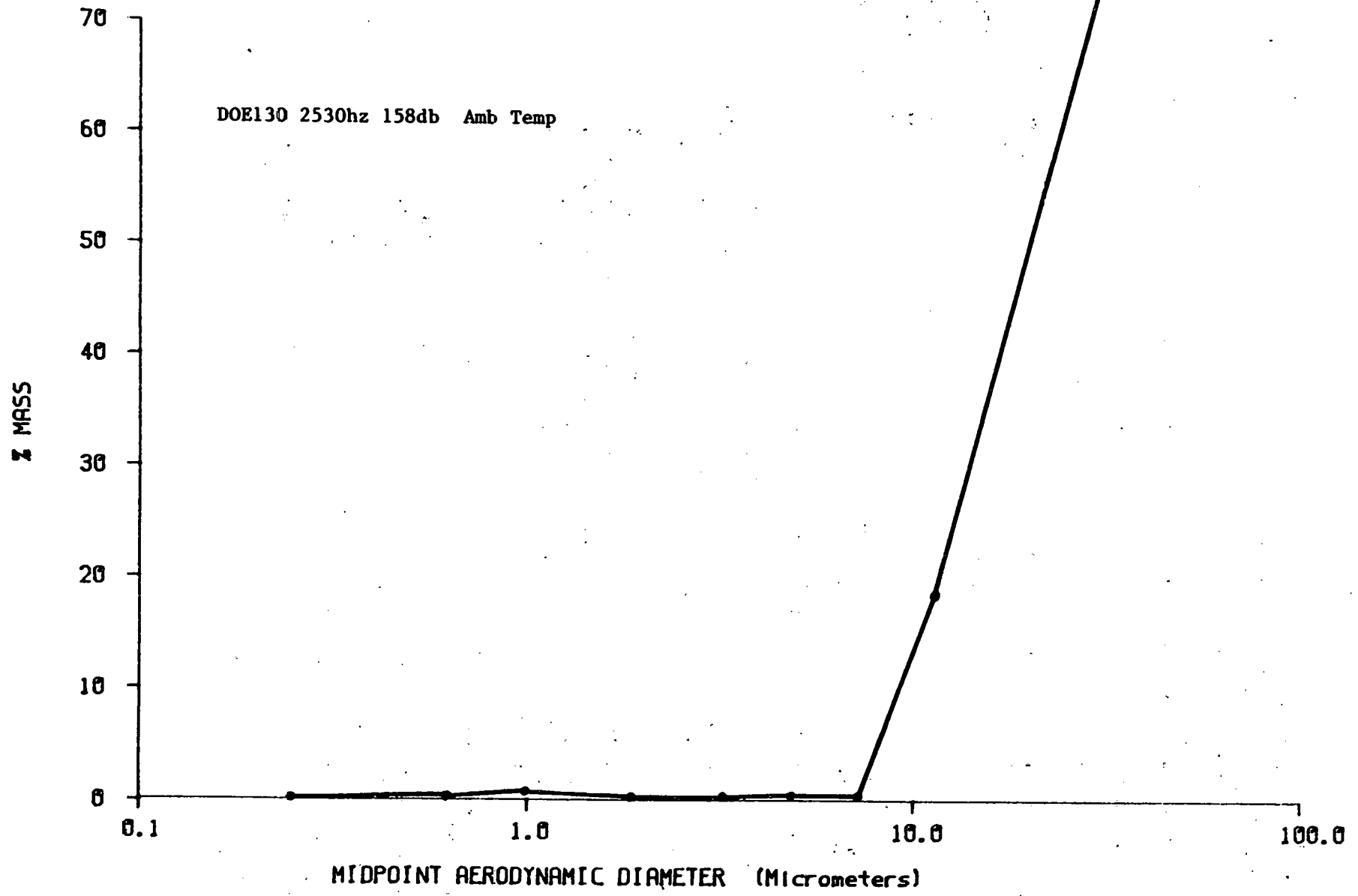
Figure - 36

The plots present the percent mass collected in each stage as a function of the stages midpoint aerodynamic diameters. The data from the nine stages are thus plotted on a semi-logarithmic particle size scale on the abscissa and a linear % differential mass scale on the ordinate. For each figure we show the no sound particle size distribution which was measured before and after the particular series of runs. During each series, we varied one or more parameters such as frequency, loading and sound pressure levels. In some cases we attempted to hold all the variables constant to test for the repeatability. All the runs were performed with a residence time of 10 seconds which means that we had a convection velocity of about 0.8 ft/sec.

We are presenting samples for our very extensive ambient temperature runs in Figures 37 through 41 representing a total of 20 runs of a total experience well in excess of 100 room temperature runs. The results are indeed encouraging. In Figure 37 (runs 128 through 150) we note that the no sound particle distribution has a mean aerodynamic diameter of about 8 microns (which would be about a 5 micron Stokesian diameter). With sound pressure levels in the 150 to 160 dB range and frequencies of 2530 Hz and 4080 Hz, and a rather large loading of 13.1, 18.6 and 30.2 g/m^3, we note very substantial agglomeration. In fact, we appear to have agglomerated most of the particles below about 8 microns. We also observe that the 4080 Hz at 151 dB gave us somewhat less agglomeration than the 2530 Hz at 158 dB case. We note that the two 2530 Hz, 158 dB runs are indeed very similar attesting to the repeatability of the process.

Figure 38 (runs 160 through 190) gives us some very interesting results. We again, have the no sound curve with a loading of 2.39 g/m^3 as a reference.

The two 2400 Hz curves at 164 and 156 dB show very substantial agglomeration at loadings of 8.33 g/m³. The slightly reduced agglomeration at 164 dB, based on other data, may actually show some de-agglomeration although this is not conclusive. The considerably lower agglomeration at 1290 Hz and 166 dB is most likely due to the lower frequency rather than the smaller loading of 2.73 g/m³.

Figure 39 (runs 200 through 230) shows almost the identical agglomeration at 1290 Hz, 166 dB and a larger loading of 4.03 g/m³ than we saw in Figure The other two curves at 2500 Hz and 3050 Hz show that in this frequency range both frequency and loading effects appear to be small. Agglomeration theory predicts an optimum frequency of about 2800 Hz for fly ash dust in the 5 micron range. The 1290 Hz results, therefore, are most likely due to frequency effects. The effect of frequency on agglomeration here agree well with earlier findings by us as reported in the works of Volk [14], Miao [47], and Dwyer [48].

Figure 40 (runs 470 through 500) shows the rather significant improvements in agglomeration due to higher sound pressure level at representative loadings. Clearly a 150 dB level gives us much better results than 140 dB.

Figure 41 (runs 510 through 540) gives further substantiation for the need to agglomerate at sound pressure levels of 150 dB or above and frequencies in the 2500 to 3000 Hz range.

We can summarize these and many similar results from other tests at ambient temperature conditions as follows:

a) Best results are obtained at frequencies in the 2500 to 3000 Hz range for fly ash dust with about a 5 micron mean size and a two population logarithmic size distribution.

Dp vs % MASS

+ DOE128	No Sound	Amb Temp	18.6 g/m^3
x DOE130	2530hz 158db	Amb Temp	20.7 g/m^3
□ DOE140	4080hz 151db	Amb Temp	13.1 g/m^3
○ DOE150	2530hz 159db	Amb Temp	30.2 g/m^3

Residence Time: 10 seconds

% MASS (vertical axis)

MIDPOINT AERODYNAMIC DIAMETER (Micrometers) (horizontal axis)
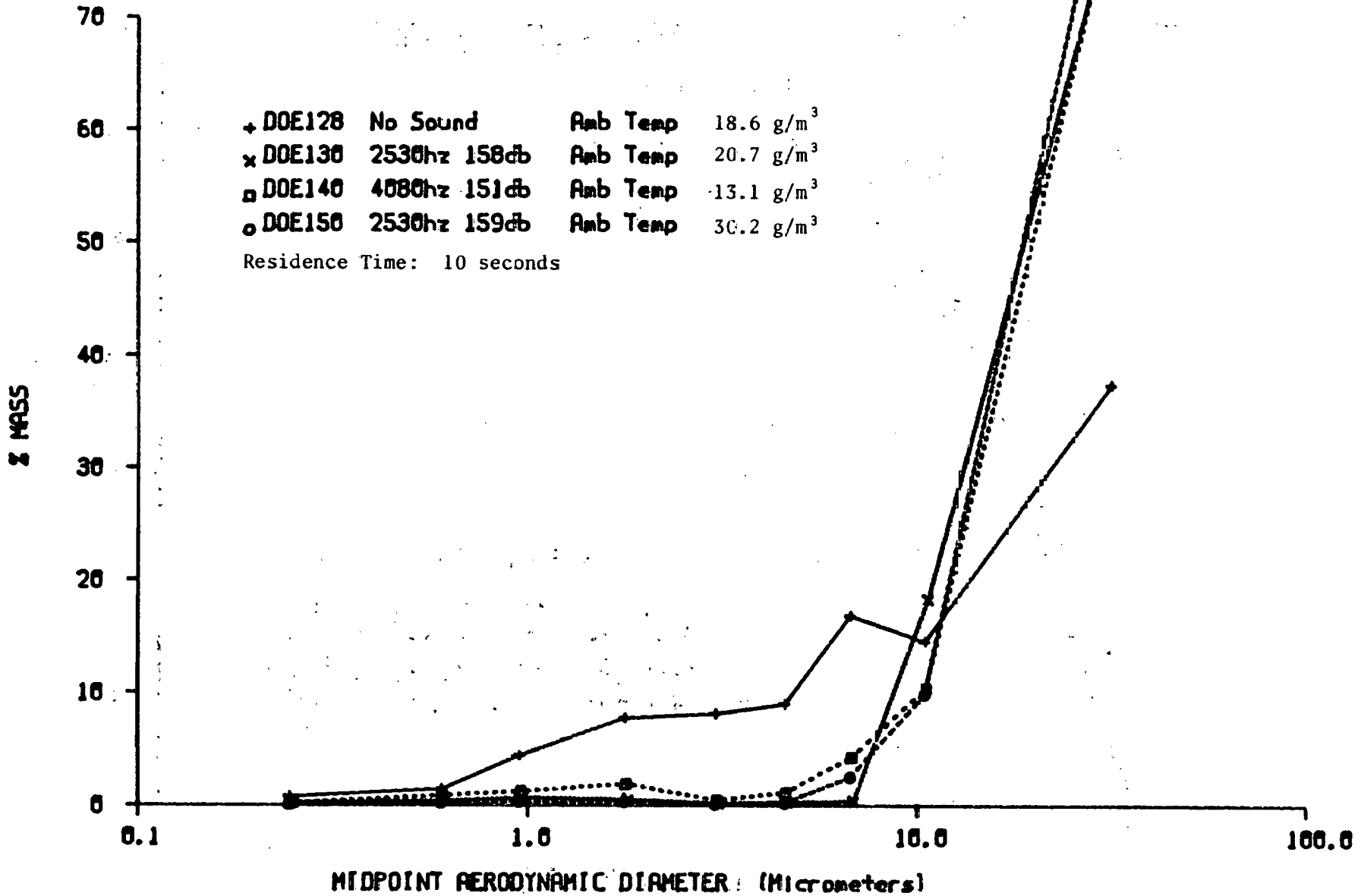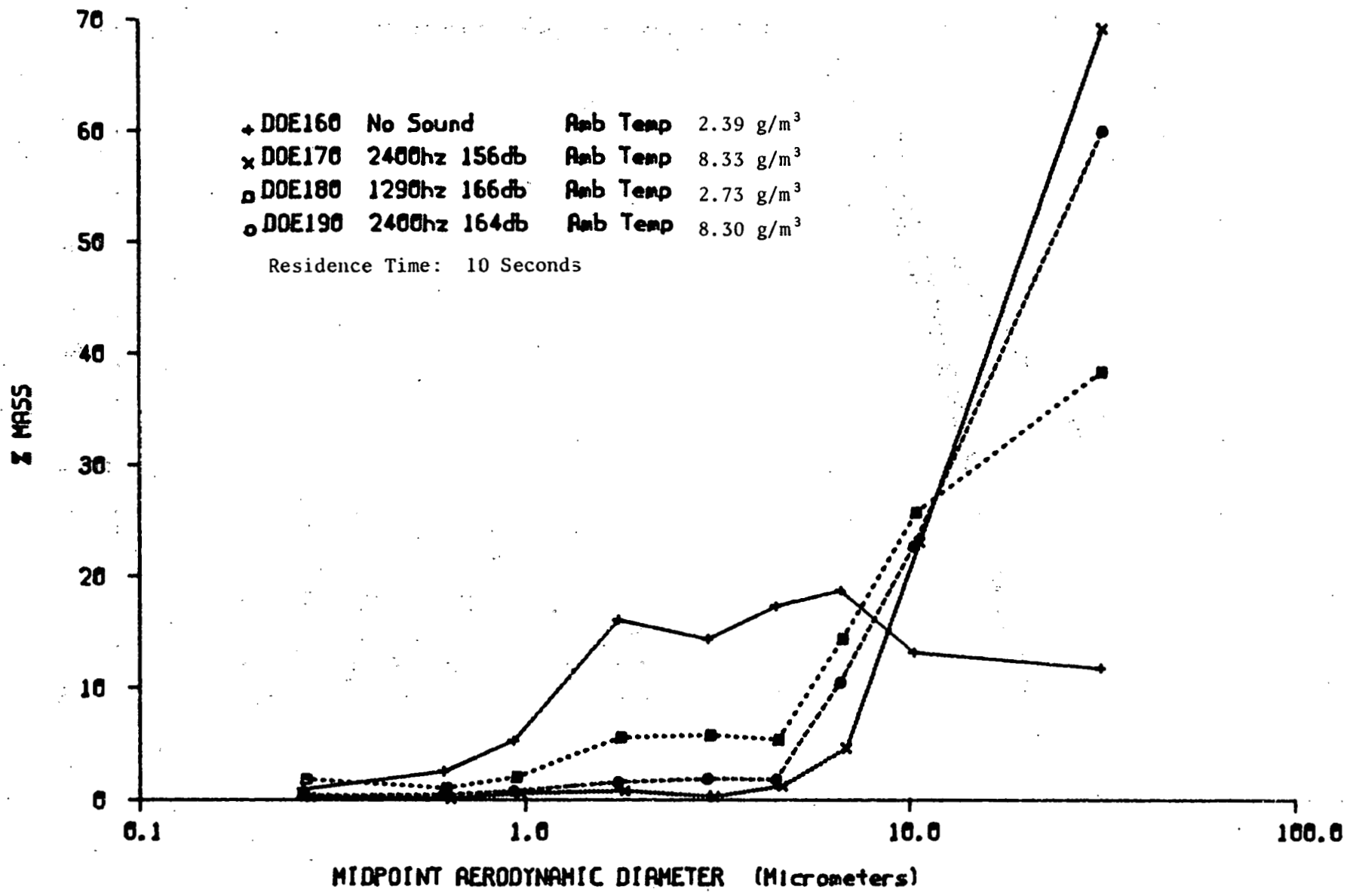
Figure 37

Dp vs % MASS

Figure 38

Dp vs % MASS
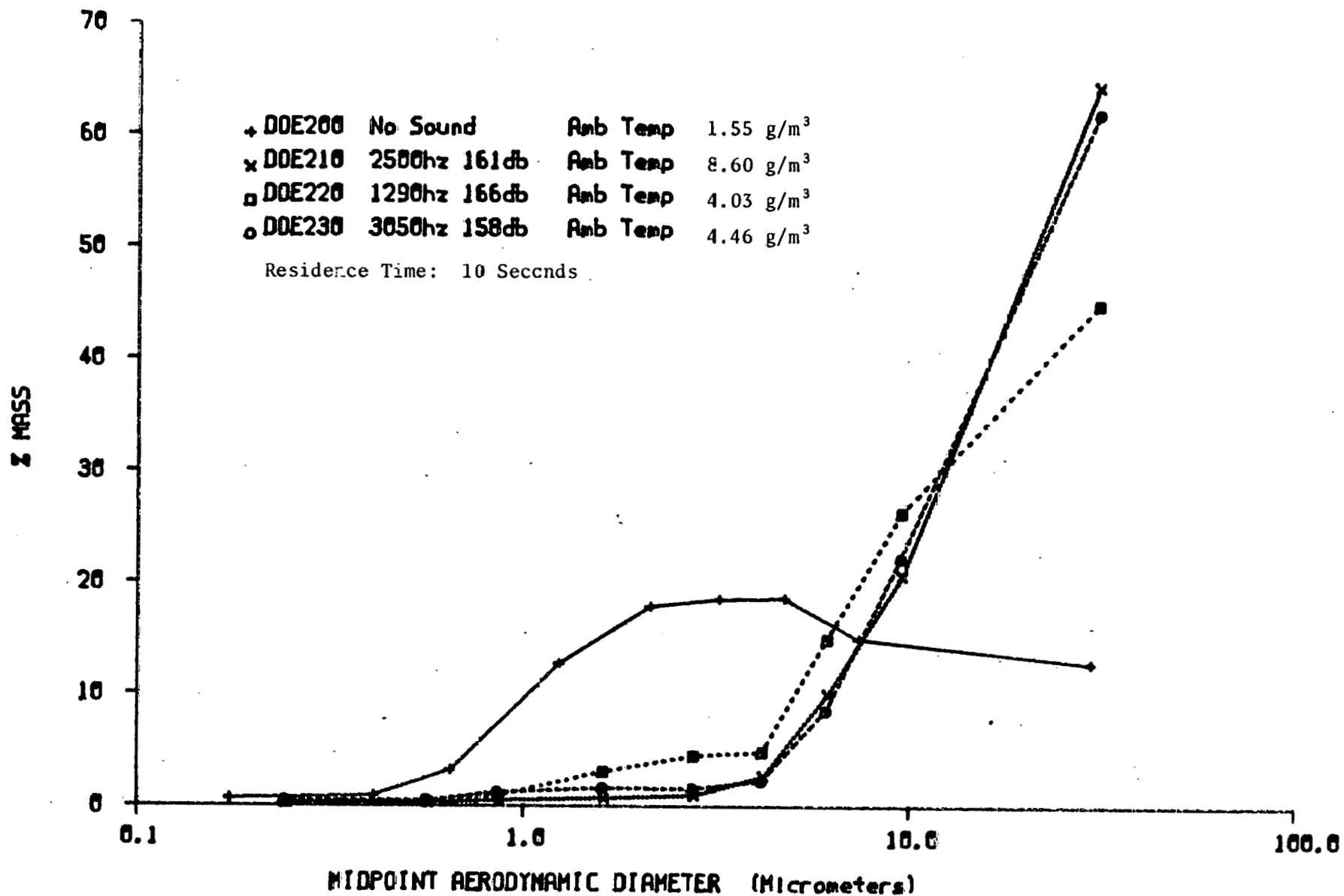
Figure 39

Dp vs % MASS

Figure 40

Dp vs % MASS

+ DOE500	No Sound	Amb Temp	16-4	3.5 g/m³
x DOE470	2000hz 139.8db	Amb Temp	16-1	4.9 g/m³
□ DOE480	2120hz 149.9db	Amb Temp	16-2	10.7 g/m³
○ DOE490	2910hz 136.7db	Amb Temp	16-3	2.3 g/m³

Residence Time: 10 Seconds

% MASS
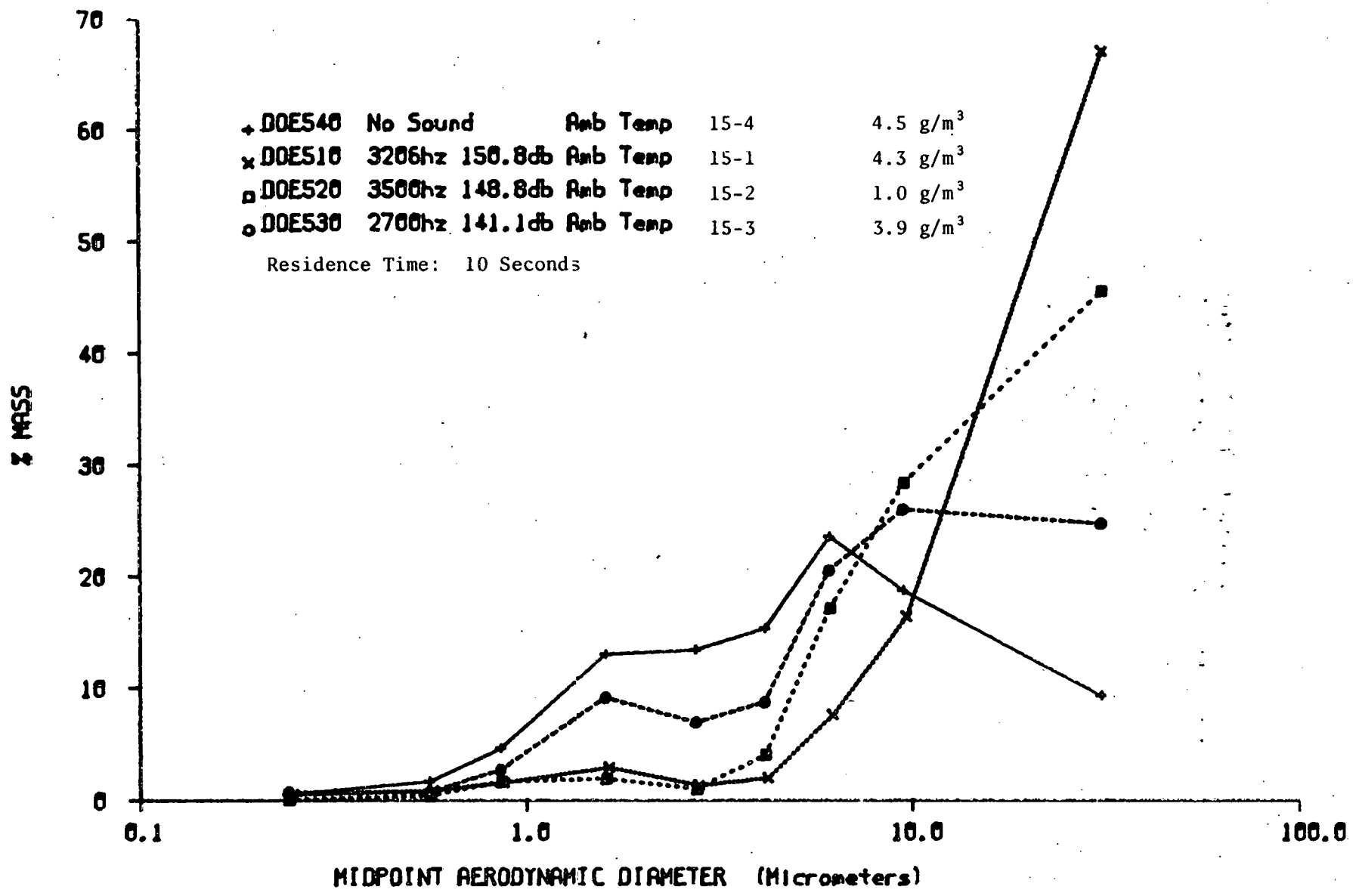
MIDPOINT AERODYNAMIC DIAMETER (Micrometers)
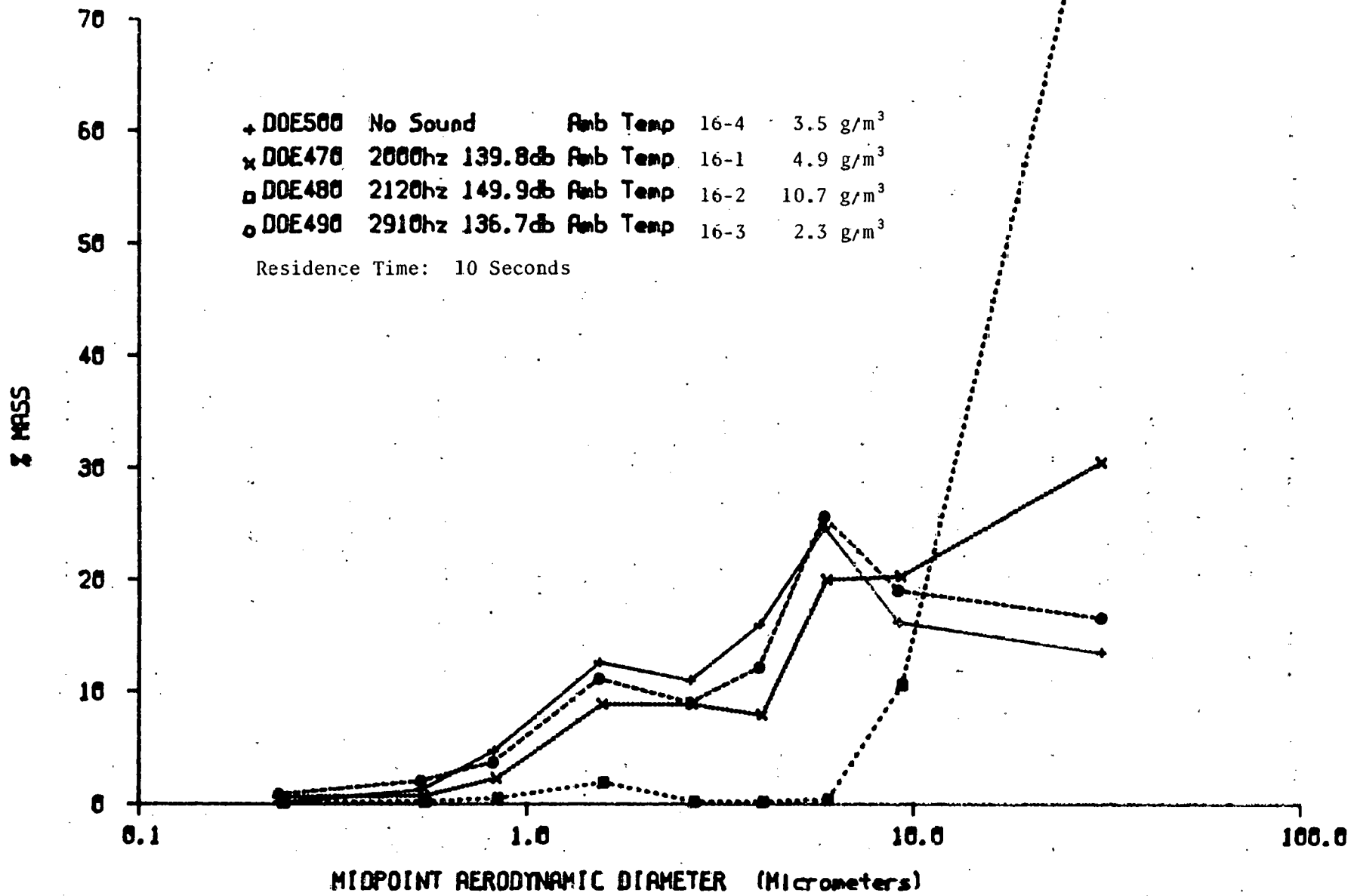
Figure 41

b) There is indication that higher loading gives better agglomeration with experience ranging from 1 g/m³ to 30 g/m³.

c) Sound pressure levels in the 155 to 160 dB range appear to give excellent results for the 10 second exposure times.

d) There is some indication that at levels above 160 dB and 10 second exposure times, we may actually de-agglomerate the samples.

We have actually only just begun to run high temperature tests and do not feel that we have fully developed the test and sampling techniques. The results have not been as repeatable as the ambient temperature runs. We have encountered some rather disturbing inconsistencies which were not resolved at the time of this report preparation.

We present two figures, Figure 42 (runs 680 through 710) and Figure 43 (runs 720 through 740) for conditions where we have had reasonable acceptable repeatability at temperatures of 270°F and 350°F. As we would expect, the results generally agree with the ambient condition results. Figure 42 in particular, verifies our earlier experience that an optimum frequency exists at about 3000 Hz. Up to 350°F the agglomeration appears to be little affected by increased temperatures.

We have, unfortunately, not made as much progress with the high temperature testing as we had hoped. We have progressed with caution to be sure that our results are repeatable and of course, are in agreement with our understanding of the processes.

We have not as yet taken the time to explore the conditions existing in the agglomeration tube at both the ambient and elevated temperatures. We should measure both the acoustic field, the convection flows, as well as local velocity fluctuations resulting from the siren sound source, the convection flows from the flow through the barrier between siren and heater

Dp vs % MASS

+ DOE710	No Sound		270 Deg F	9.725 g/m^3
x DOE680	2500hz	147 dB	260 Deg F	7.224 g/m^3
□ DOE690	3000hz	144 dB	270 Deg F	12.655 g/m^3
○ DOE700	4000hz	144 dB	270 Deg F	11.996 g/m^3

Residence Time: 10 Seconds

% MASS (y-axis)

MIDPOINT AERODYNAMIC DIAMETER (Micrometers) (x-axis)

Figure 42

114
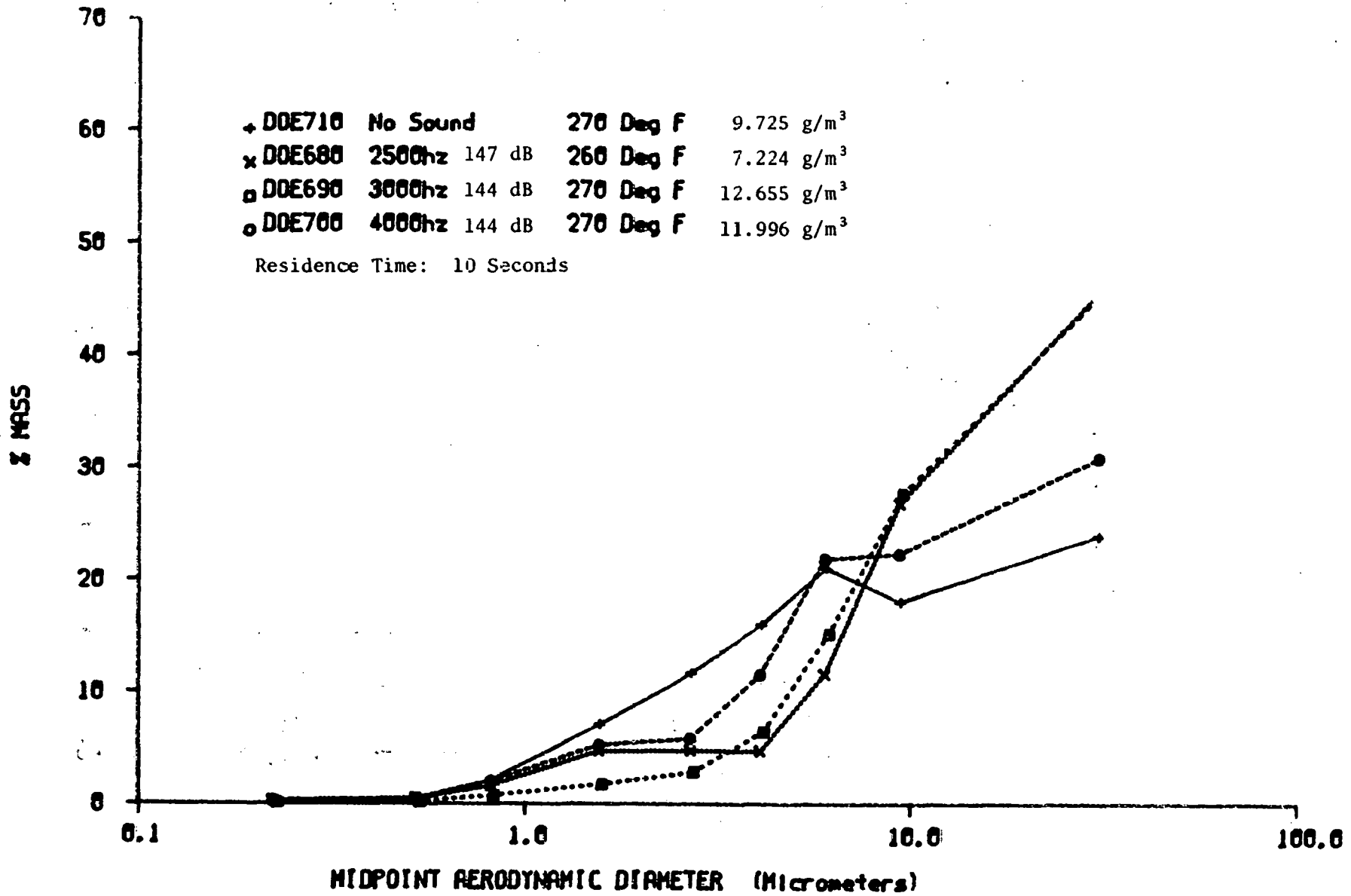
Dp vs % MASS
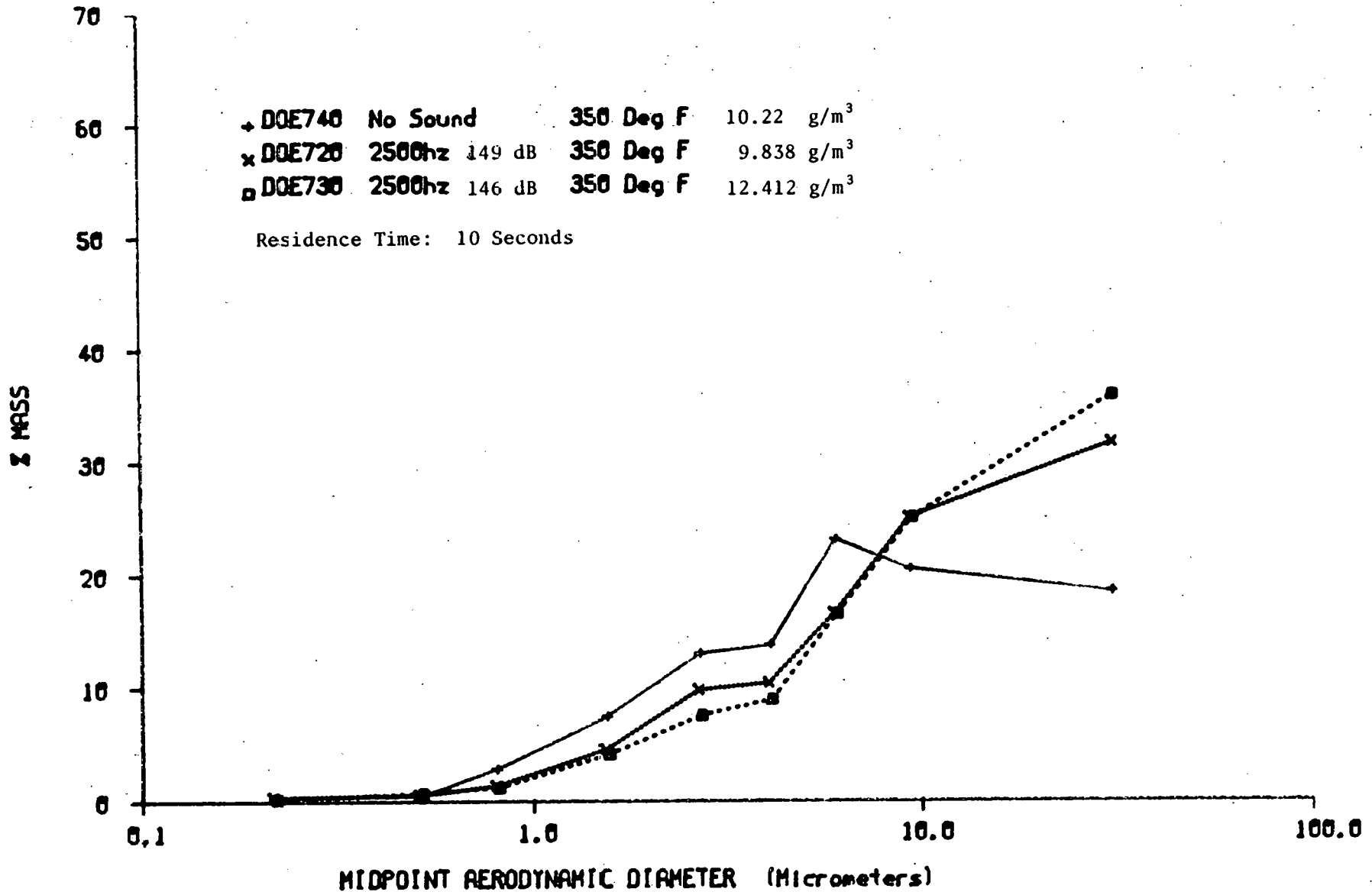
Figure 43

sections, and the flows from the heater as well as the aerosol generator. We should explore the spatial distribution of the aerosol concentration throughout the agglomerator by extensive radial and some axial sampling. We have chosen not to conduct these rather time consuming but necessary efforts in order to gain some preliminary experience at high temperatures to guide our further work.

We have encountered some tenacious difficulties with the aerosol generation system at higher temperatures which have affected the consistency of the feed rates resulting in unacceptably wide dust loading variations and predictability. We have learned that we must pressure balance the dust feed container with the agglomerator and other related matters.

The sampling of the agglomerated aerosols also requires further development to assure consistency and reliability. Simply the problem of heating, handling, attaching and removing the impactor and maintaining impactor temperature during these runs while taking care of other idiosycracies presented uncontrolled variables.

Thus we can say that we have made good progress but that further development in hardware and particularly techniques is required in the continuing program.

2.6 ACOUSTIC ABSORPTION CONSIDERATIONS IN THE SONIC AGGLOMERATION PROCESS

In both the environmental and hot has clean-up applications of sonic agglomeration to small particulate removal, significant amounts of acoustic power must be generated. It is, therefore, important that any acoustic energy losses in the system be minimized. Losses through the walls of the agglomeration chamber can be minimized by proper mechanical design to make the surfaces as reflective as possible to sound. The remaining loss mechanism is acoustic absorption. Acoustic absorption results from irreversable thermodynamic and chemical processes whereby a portion of the acoustic energy is converted into heat.

In the usual textbook derivations of the equations governing the behavior of sound waves, the thermodynamic process is assumed to be adiabatic and in addition the acoustic wave is assumed to be an infinistesimal disturbance of the medium. This results in a linear second order dissipationless wave equation:

$$\nabla^2 p = \frac{1}{c^2} \frac{\partial^2 p}{\partial t^2}$$

where ∇^2 is the Laplacian operator, p is the sound pressure, t is time and c is the sound speed. This wave equation can be used to solve a large majority of the problems in acoustics. For a plane progressive sinusoidal wave, this equation has the solution of the form:

$$p = P_o e^{j(\omega t - kx)}$$

where P_o is the wave peak amplitude, ω is the angular frequency, $k = \omega/c$ and x is distance. The wave propagates at constant amplitude and the above equation is a good approximation for a low frequency acoustic wave propagating in a pipe.

It was, however, recognized many years ago by Stokes [59], that viscosity effects could result in energy loss and by Kirchoff [60], that heat conduction should also be considered. When these effects are considered, the plane wave equation for a single component gas becomes:

$$\frac{\partial^2 p}{\partial t^2} = c^2 \frac{\partial^2 p}{\partial x^2} + \frac{1}{\rho} \left[\frac{K}{c_p} (\gamma - 1) + \frac{4}{3} \eta \right] \frac{\partial^3 p}{\partial x^2 \partial t}$$

where ρ is the density, K is the coefficient of heat conduction, c_p is the specific heat at constant pressure, η is the shear viscosity, and γ is the ratio of specific heats. For a sinusoidal wave this equation has the solution $p = P_0 e^{j(\omega t - kx)} e^{-\alpha_c x}$ so that the wave is exponentially damped. The term α_c, called the classical absorption coefficient is given by:

$$\alpha_c = \frac{1}{2} \frac{\omega^2}{c^3 \rho} \left[\frac{K}{c_p} (\gamma - 1) + \frac{4}{3} \eta \right]$$

The classical coefficient was widely accepted as representing the total loss mechanism in an acoustic medium although Stokes recognized the possibility of an additional volume viscosity (see Reference 61 page 38). The classical theory went unchallenged until instruments were developed which were capable of measuring absorption coefficients. Measurements revealed that, with few exceptions, the acoustic absorption coefficients in gases and liquids are in excess of values calculated from this equation and also do not have the simple frequency squared behavior. Herzfeld and Rice [62], first proposed that the additional absorption was due to relaxation phenomena, that is, due to the finiteness of time required for energy exchange between the translational and internal degrees of freedom of the

molecules. Tisza [63], has shown that the excess absorption can be treated with the introduction of a bulk or volume viscosity and Herzfeld and Litovetz (reference 61, page 91) demonstrate that this concept has physical validity.

The rotational and vibrational relaxation processes can be treated separately [64] and for the frequency range of interest in this study the rotational absorption coefficient can be written as:

$$\alpha_r = \frac{1}{2} \frac{\omega^2}{c^2 \rho} \frac{\gamma(\gamma-1)R}{1.25 \, c_p} K \, Z_r$$

where R is the gas constant and Z_r is the number of molecular collisions required to establish rotational equilibrium [64] and is also referred to as the De-excitation probability [65]. The above equation is approximate since there is a relaxation frequency associated with rotational excitations, however, for the gasses considered in this study, it is several orders of magnitude higher than the frequencies of interest. The previous two equations have the same frequency dependence and the rotational relaxation absorption can be considered as an additional term to the classical absorption.

For vibrational relaxation in a single component gas, the absorption coefficient α_v will have the general form:

$$\alpha_v = A(T) \, (\omega^2/\omega_r) \, / \, (1+(\omega/\omega_r)^2) \quad \text{and} \quad A(T) = \frac{R(\gamma-1)}{4\pi c \gamma c_p}$$

where A(T) is a function of temperature, where c_p is the high frequency limit of the specific heat at constant pressure (see reference [64]) and ω_r is the relaxation frequency, also a function of temperature and of pressure.

For a constant temperature and pressure, this equation can be arranged in normalized terms as:

$$\frac{\alpha_v}{A(T)} = \omega \ \Omega \ / \ (1+\Omega^2)$$

where $\Omega = \omega/\omega_r$ and since $\omega = \Omega \ \omega_r$,

$$\frac{\alpha_v}{A(T)} = \omega_r \ \Omega^2 \ / \ (1+\Omega^2)$$

This equation is plotted in Figure 44 for three values of ω_r. The relaxation absorption coefficient increases as Ω^2 for Ω sufficiently below the relaxation frequency and becomes a constant value for Ω sufficiently above ω_r. This is, of course, an oversimplified analysis since $A(T)$ and ω_r are usually highly temperature dependent; however this formulation gives physical insight into the general behavior of the relaxation process as it affects the absorption coefficient.

The term $A(T)$ defined earlier can also be expressed as:

$$A(T) = (R/c_v) \ (T_v/T) \ \exp \ (-T_v/T)$$

where T is temperature and T_v is the characteristic vibrational temperature of the gas.

The total absorption coefficient for a single component gas is the sum of the equations for α_c, α_r and α_v. Rearranging the equations for α_c and α_r in more convenient computational form (as in Reference [64]), results in the total coefficient as follows:

$$\alpha_T = \frac{1}{2} \frac{\omega^2}{\gamma pc} \ (\frac{K}{c_p} \ (\gamma-1) \ + \ \frac{4}{3} \ \eta \ + \ \frac{\gamma(\gamma-1)}{1.25 \ c_p} \ K \ Z_r) \ + \ [(R/c_v) \ (T_v/T) \ \exp$$

$$(-T_v/T)] \ (\omega^2/\omega_r) \ / \ (1+(\omega/\omega_r)^2)$$
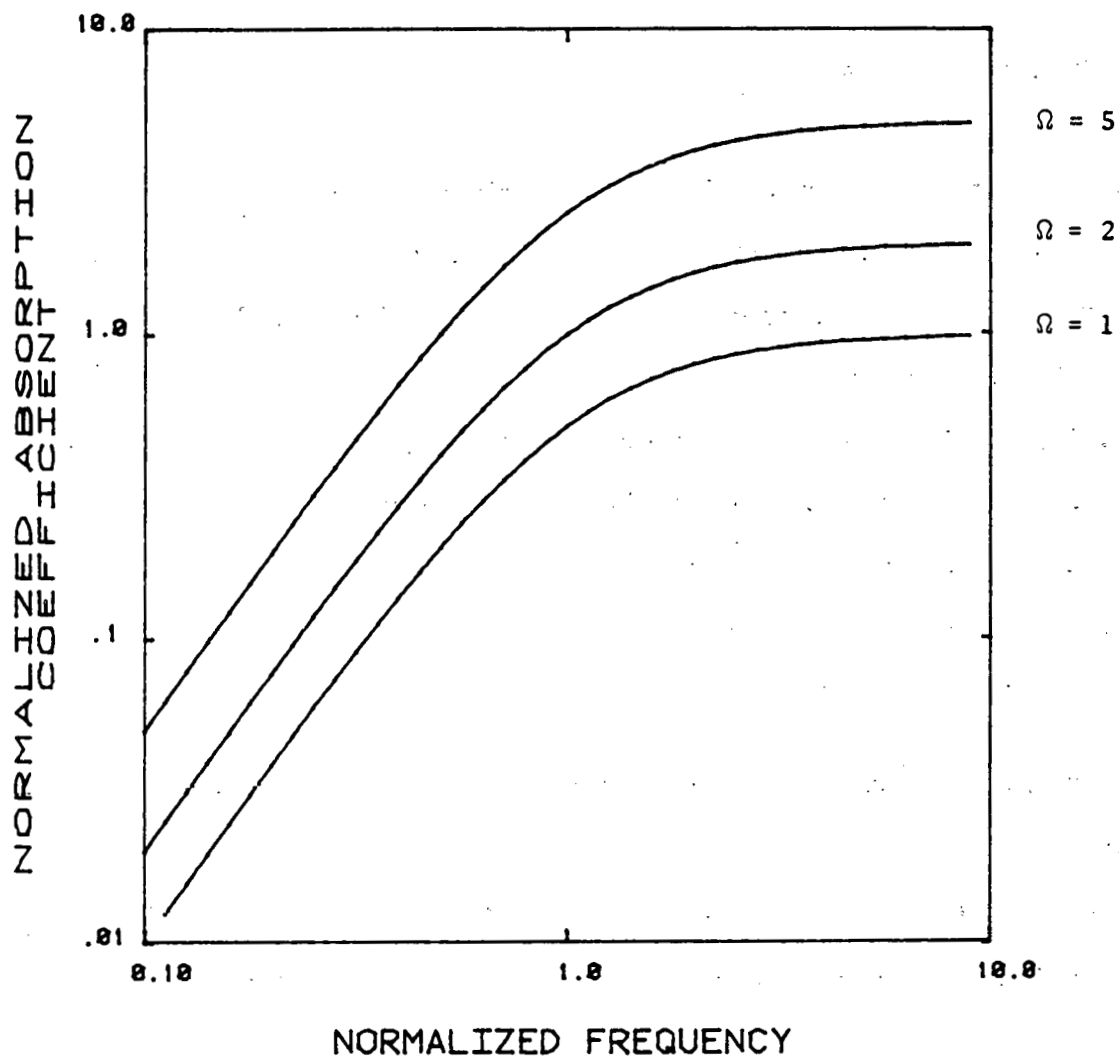
Figure 44. Plot of Normalized Absorption Coefficient Versus Normalized Frequency for a Single Component Gas Considering Vibrational Relaxation.

Most of the quantities involved in this equation are well known for the gases involved in this study. The specific heat at constant pressure c_p, can be found from a polynominal expansion:

$$c_p = A + BT + CT^2$$

where the constants, A, B and C are tabulated in several references and textbooks (see for example Reference [66], page 332). The equation for c_p is accurate to within two percent from 300 to 2000°K.

The behavior of c_p as a function of temperature for nitrogen and carbon dioxide is given in Figures 45 and 46. The ratio of specific heats,

$$\gamma = c_p/c_v$$

can be obtained from the specific heat at constant volume. For monatomic and diatomic gases, c_p is independent of temperature, 5 R/2 and 7 R/2 respectively.

For polyatomic gasses (other than diatomic) c_v is given as follows:

For Linear Molecules

$$c_v = 3 R + \sum_{T_v} R\left(\frac{T_v}{2T}\right)^2 \sinh^{-2}\left(\frac{T_v}{2T}\right)$$

For Nonlinear Molecules

$$c_v = 5 R/2 + \sum_{T_v} R\left(\frac{T_v}{2T}\right)^2 \sinh^{-2}\left(\frac{T_v}{2T}\right)$$

The number of values of T_v for a given gas depend upon the number of vibrational modes present in the specific type of molecule. The number can range from 3 for the triatomic molecules to 9 for higher order polyatomic molecules such as methane. The characteristic vibrational temperatures, T_v are also required in the equation for α_T; however only one vibrational mode

TEMPERATURE IN DEGREES KELVIN
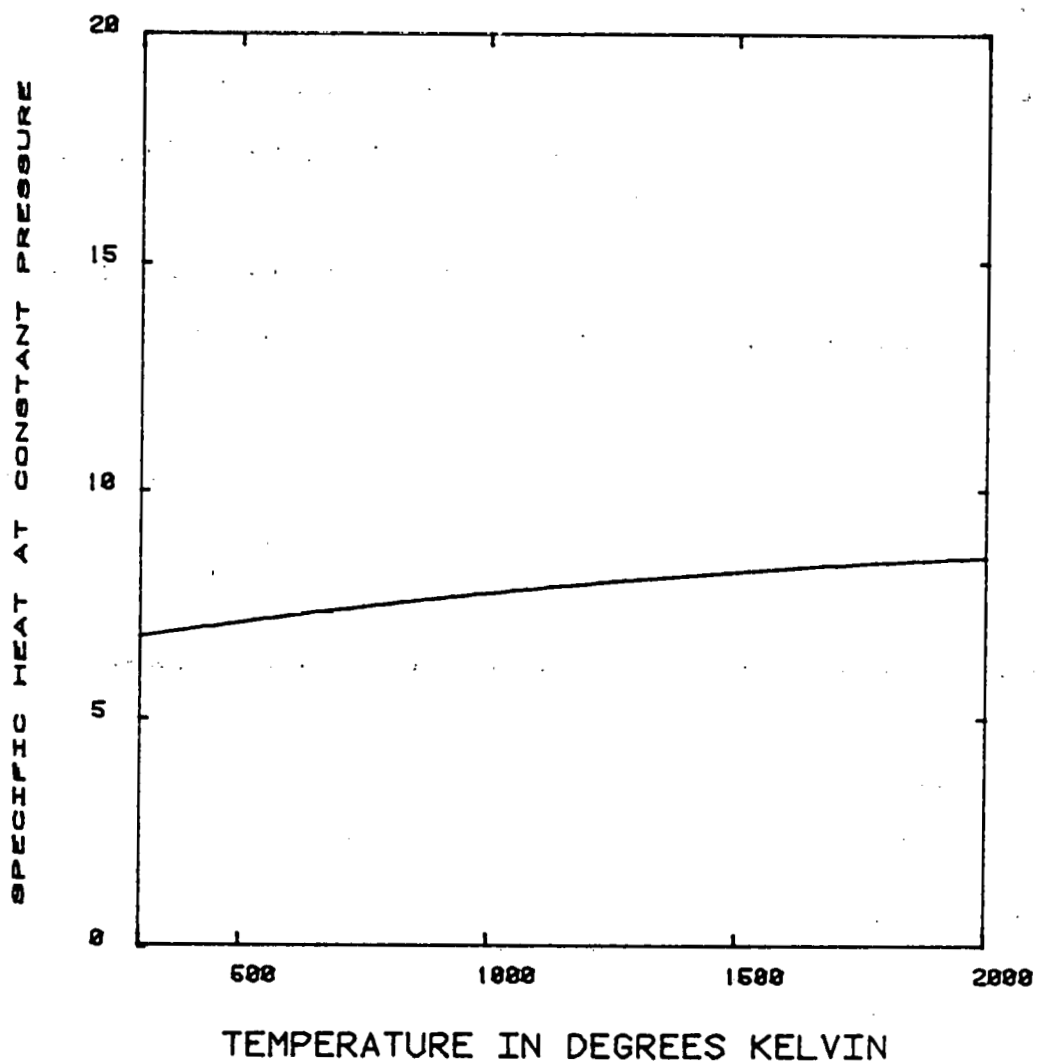
SPECIFIC HEAT VERSUS TEMPERATURE FOR NITROGEN

Figure 45

SPECIFIC HEAT VERSUS TEMPERATURE FOR CARBON DIOXIDE
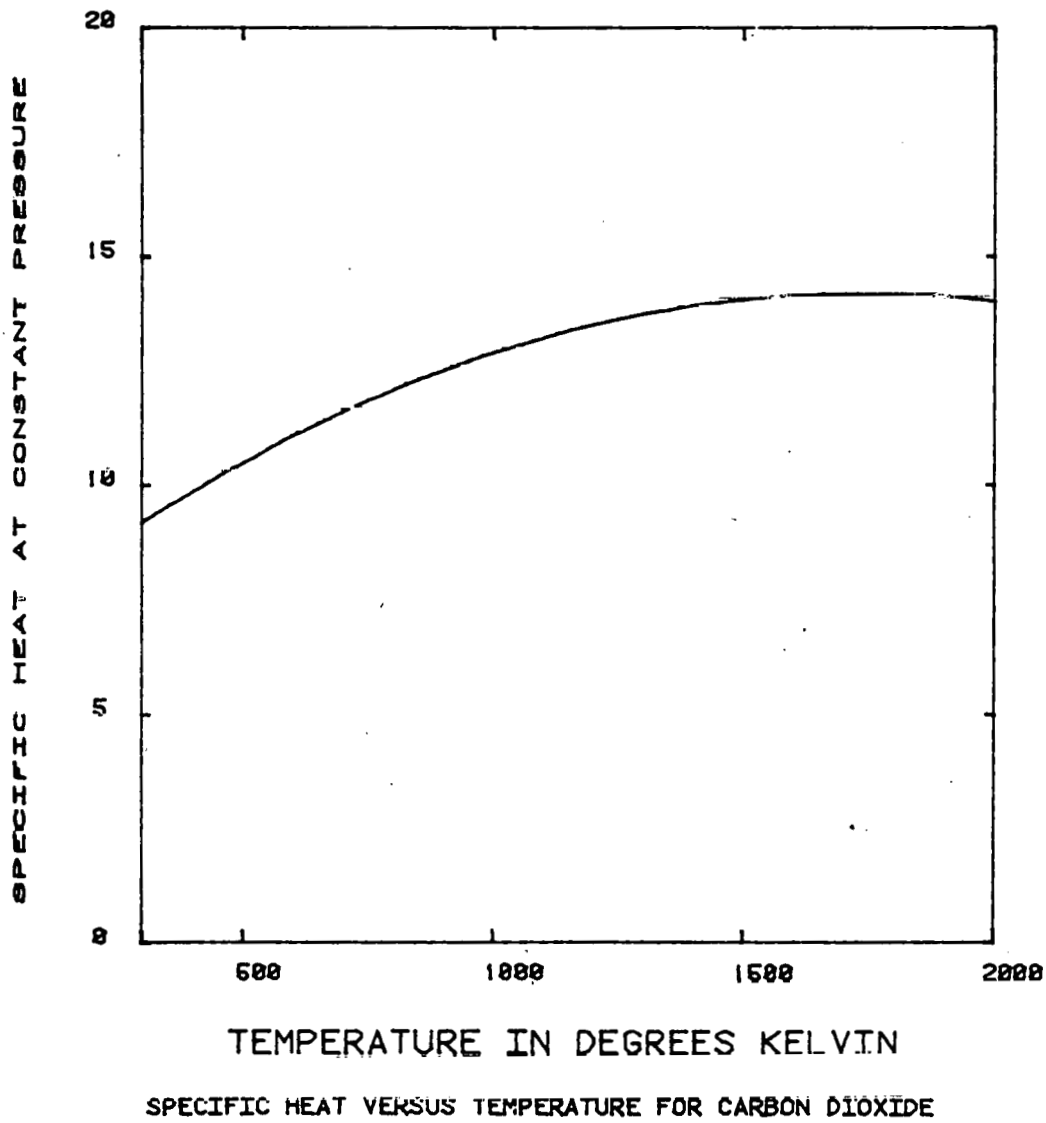
Figure 46

normally contributes to acoustic absorption and, therefore, only one value of T_V is required in the equation for α_T. In determining c_V; however, the two equations for c_V must be summed over all values of T_V.

The viscosity, η, has been extensively measured and tabulated as a function of temperature for most gases and these data are available in reference books [67]. Likewise, the heat conduction coefficient is well documented [68].

The major problem area for a single component gas is in the determination of the relaxation frequency ω_r and the collision parameter Z_r. A number of measurements of ω_r (usually reported as the relaxation time $\tau_r = 1/\omega_r$) and Z_r have been made for many gases at a large number of temperatures. Most of these measurements were made at ultrasonic frequencies by measuring the absorption coefficient and working backwards to obtain τ_r and Z_r. A plot of the natural logarithm of τ_r for carbon dioxide (from Reference [61]), as a function of absolute temperature to the minus one third power for a variety of temperatures is shown in Figure 47. These results are from 16 independent experiments using many different techniques. The data are widely scattered but show a definite trend of decreasing τ with temperature. It has been found that the relaxation time in CO_2 is highly sensitive to impurities, especially water vapor and Herzfeld and Litovitz [61], suggest that this is the cause of the scatter. They suggest that the longest value of τ_r for each temperature are more representative of pure CO_2.

Similar measurements have been conducted for other gases of interest in this study and in most cases the scatter problem of CO_2 also exists for these gases. In most cases the studies were conducted to determine the molecular properties of the gases and the publications rarely are in the
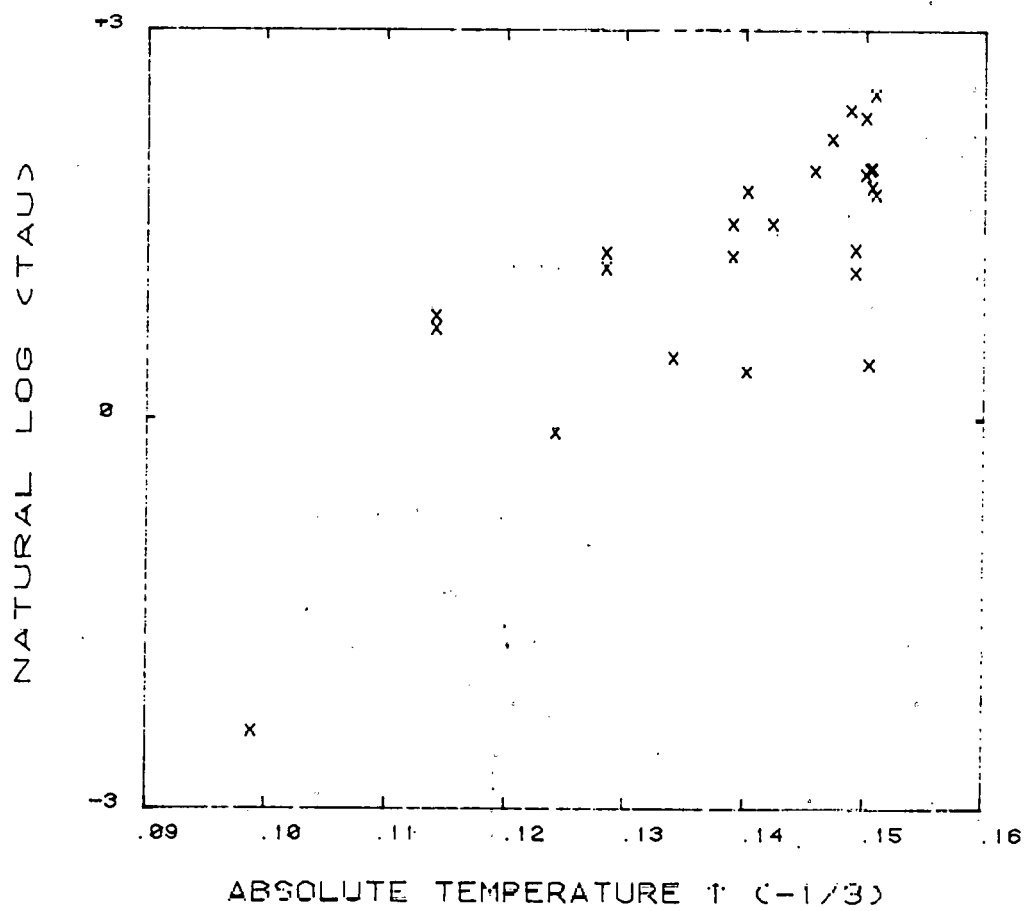
Figure 47

Measurement of Relaxation Time as a Function
of Temperature for Carbon Dioxide

acoustics literature. An extensive literature search will be required to collect all the data available.

The most extensive and carefully conducted experiments to measure relaxation times in gases have been with nitrogen and oxygen, the major components of air. This results from the considerable interest in absorption of sound in the atmosphere.

The total absorption coefficient α_T calculated for N_2, using the relaxation time and Z_r data from Reference [64], is shown as a function of frequency ($f = \omega/2\pi$) in Figure 48, for five temperatures. The contribution due to relaxation (the third term in the equation for α_T) is shown in Figure 49. The relaxation frequency is below 100 Hz for all but the two highest temperature. Relaxation effects are predominant except for the 300°K case above 1 KHz and the 400°K case above 10 KHz.

Up to this point we have only considered the single component gas. The total absorption can be readily determined provided that τ_r and Z_r are known. The problem becomes considerably more complicated for the case where acoustically induced chemical reactions can occur. A typical reaction is:

$$N_2^* + H_2O \rightleftarrows N_2 + H_2O^*$$
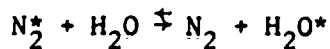
where * denotes the quantum change in the molecular vibrational excitation and ⇌ denotes that the reaction is oscillating back and forth at the frequency of acoustic excitation. Figures 50 and 51 illustrate the importance of this phenomenon.

Figure 50 presents the absorption coefficient in dry air as a function of frequency for 5 temperatures using data from Reference [64]. These curves are similar to the nitrogen curves of Figure 48, which is understandable
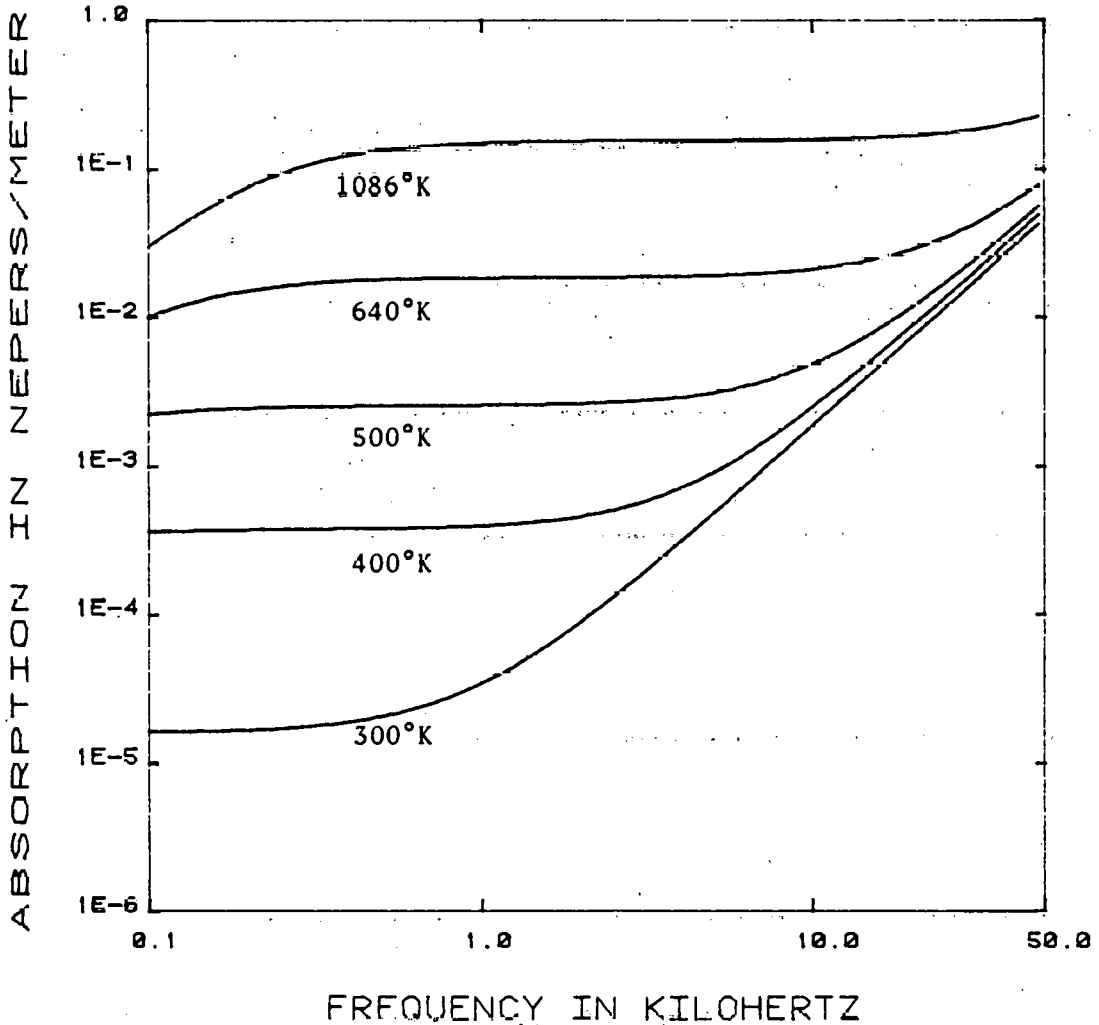
TOTAL ABSORPTION COEFFICIENT FOR
NITROGEN AT ONE ATMOSPHERE

Figure 48
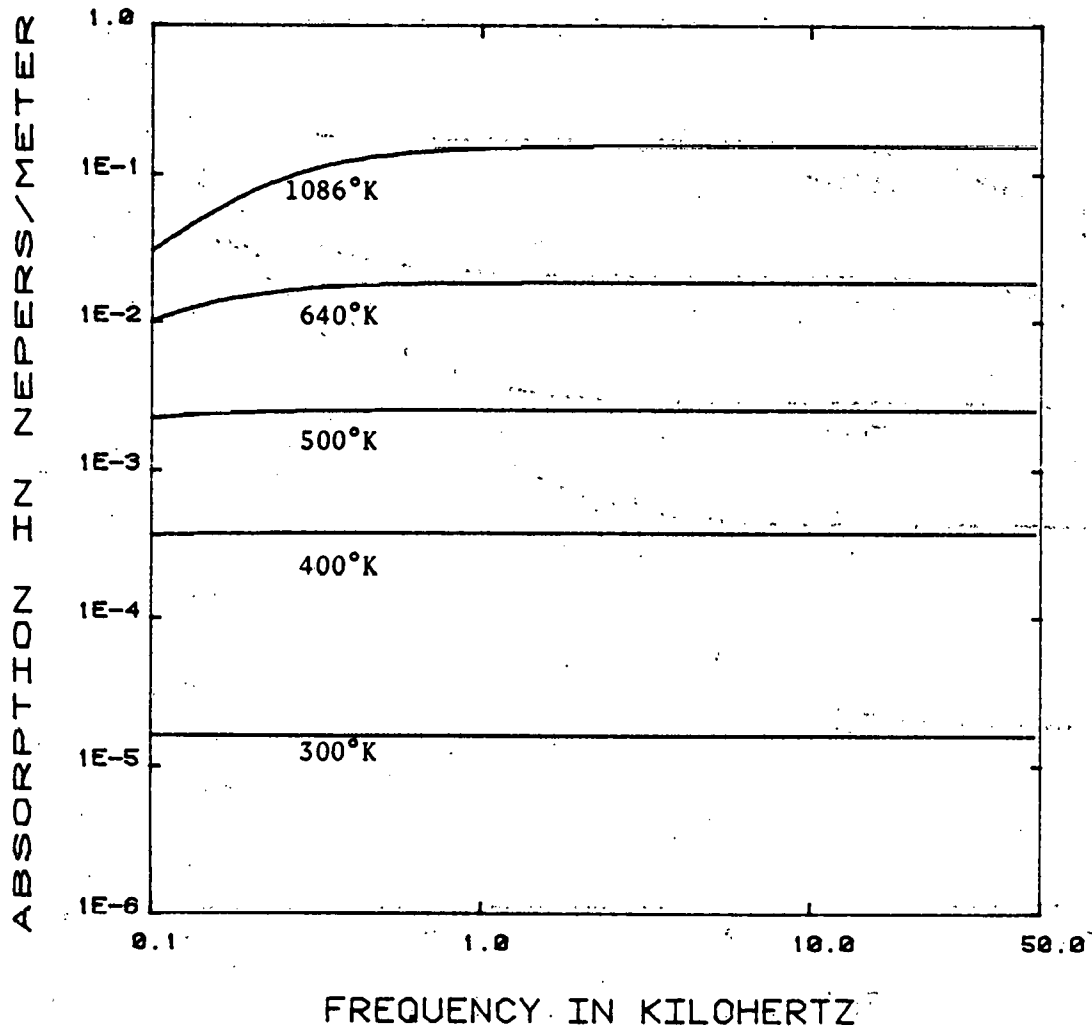
RELAXATION CONTRIBUTION FOR NITROGEN
AT ONE ATMOSPHERE

Figure 49
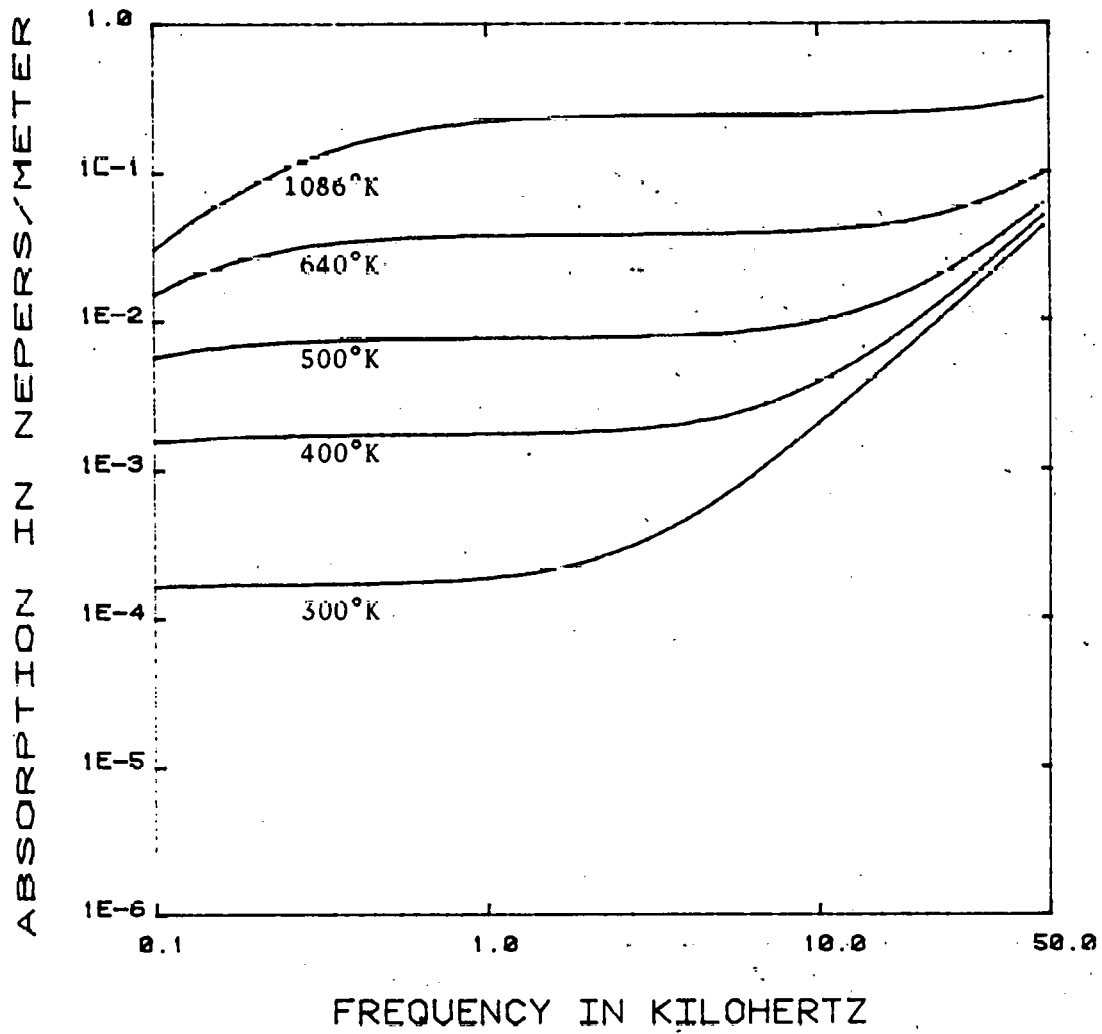
TOTAL ABSORPTION COEFFICIENT FOR
DRY AIR AT ONE ATMOSPHERE

Figure 50
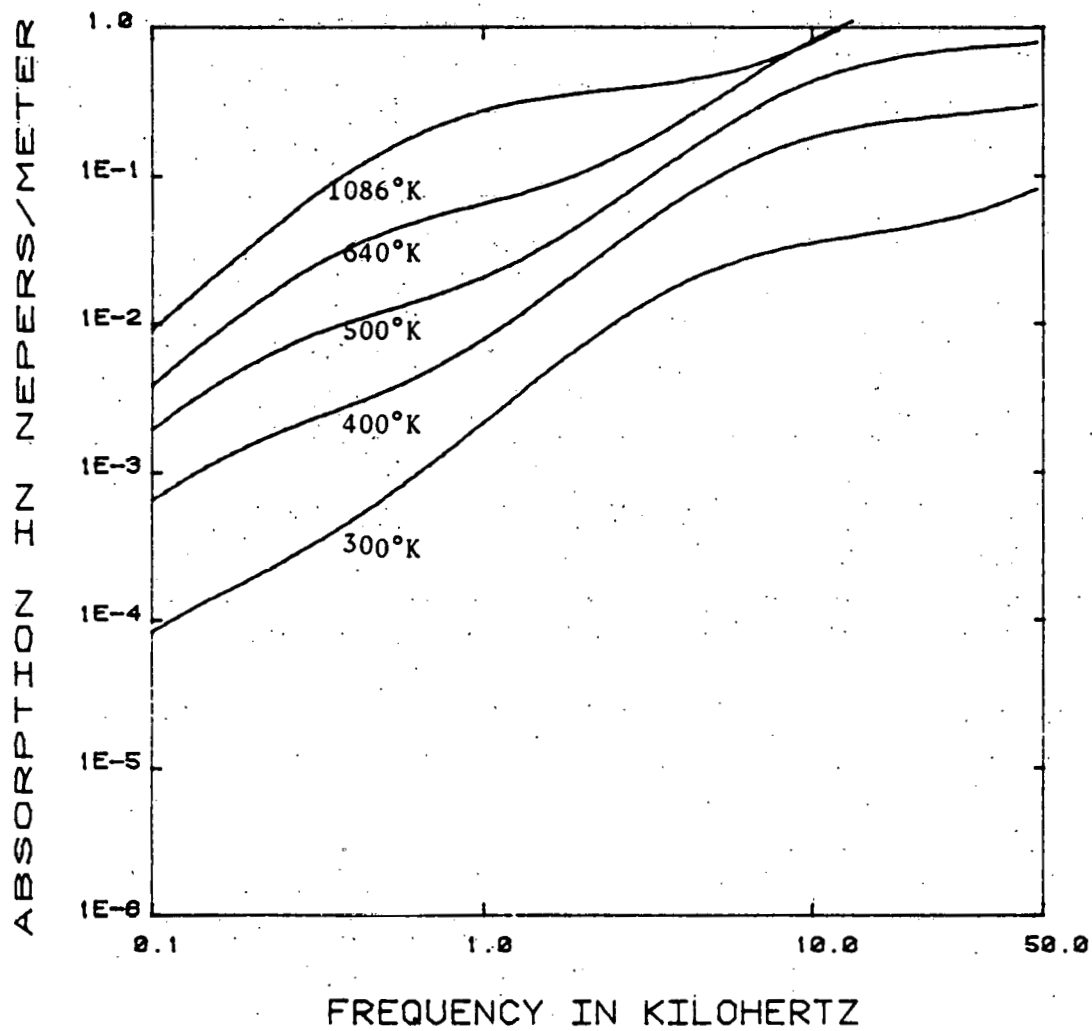
TOTAL ABSORPTION FOR AIR AT 0.5% ABSOLUTE
HUMIDITY AND ONE ATMOSPHERE

Figure 51

since air is 78% nitrogen. Figure 52 illustrates the drastic change which occurs when water vapor is added to a 0.5% absolute humidity. This change occurs because the relaxation frequencies of nitrogen (N_2) and oxygen (O_2) are changed by the presence of water vapor. This is illustrated in Figure 51 which shows the dependence of the relaxation frequencies of N_2 and O_2 on the water vapor content. This dependence for N_2 is shown over a wide humidity range and at three temperatures in Figure 53. Figures 54, 55, and 56, present the absorption coefficients for air as a function of frequency for absolute humidities of 0.0, 1.0 and 5.0 percent respectively, the curves labled 0 and N are the oxygen and nitrogen relaxation contributions to the total absorption. The curves labeled CR are the classical-rotational contributions and the curves labeled T are the total absorption coefficient α_T. Air was chosen for this illustration of absorption in a gas mixture since the most accurate data are available for air.

A considerable number of additional investigations have been conducted in gas mixtures and those up to 1962 are summarized in Table 4, which is from Reference [65].

We can only conclude from this study that although much work has been done and reported on the acoustic energy absorption of gases, most of the data and theory pertains to air at atmospheric conditions. Since the aerosols from coal combustion contain many other gas constituents and since the temperatures are much higher we are convinced that additional theoretical and experimental work remains to be done.

RELAXATION FREQUENCY AS A FUNCTION OF
HUMIDITY AT ONE ATMOSPHERE AND 500 DEG.K
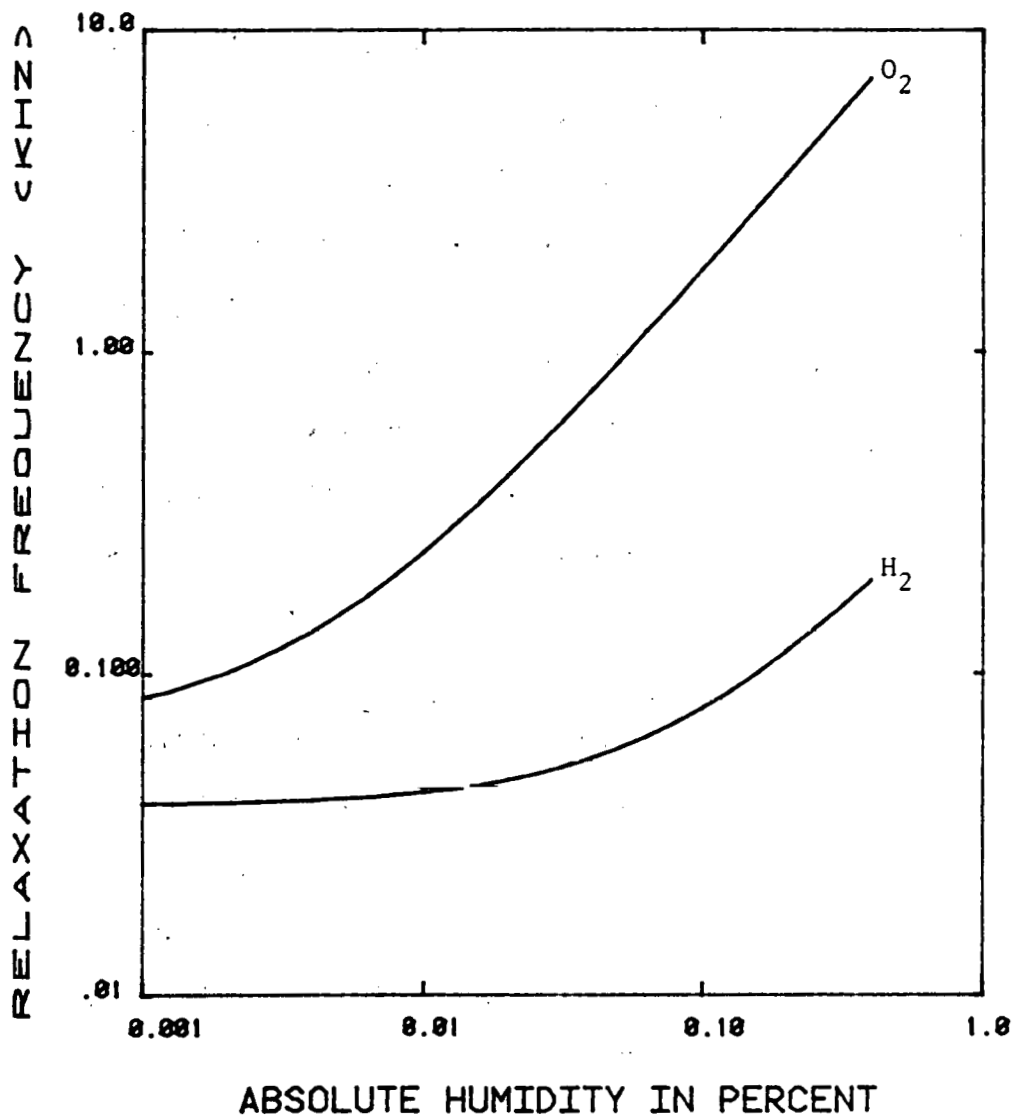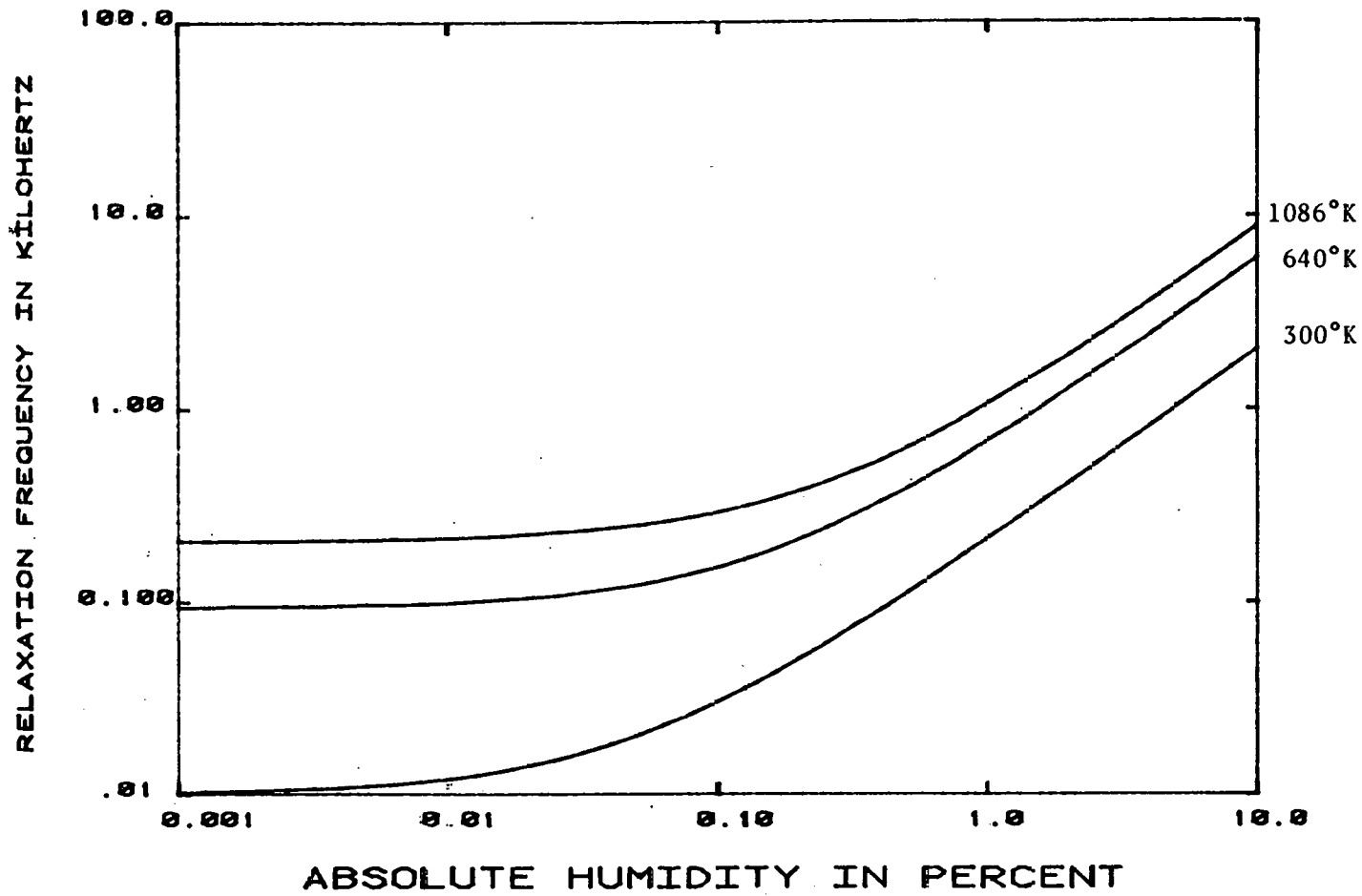
Figure 52

NITROGEN RELAXATION FREQUENCY VERSUS
HUMIDITY AT 14.7 PSI

Figure 53

FREQUENCY IN KILOHERTZ
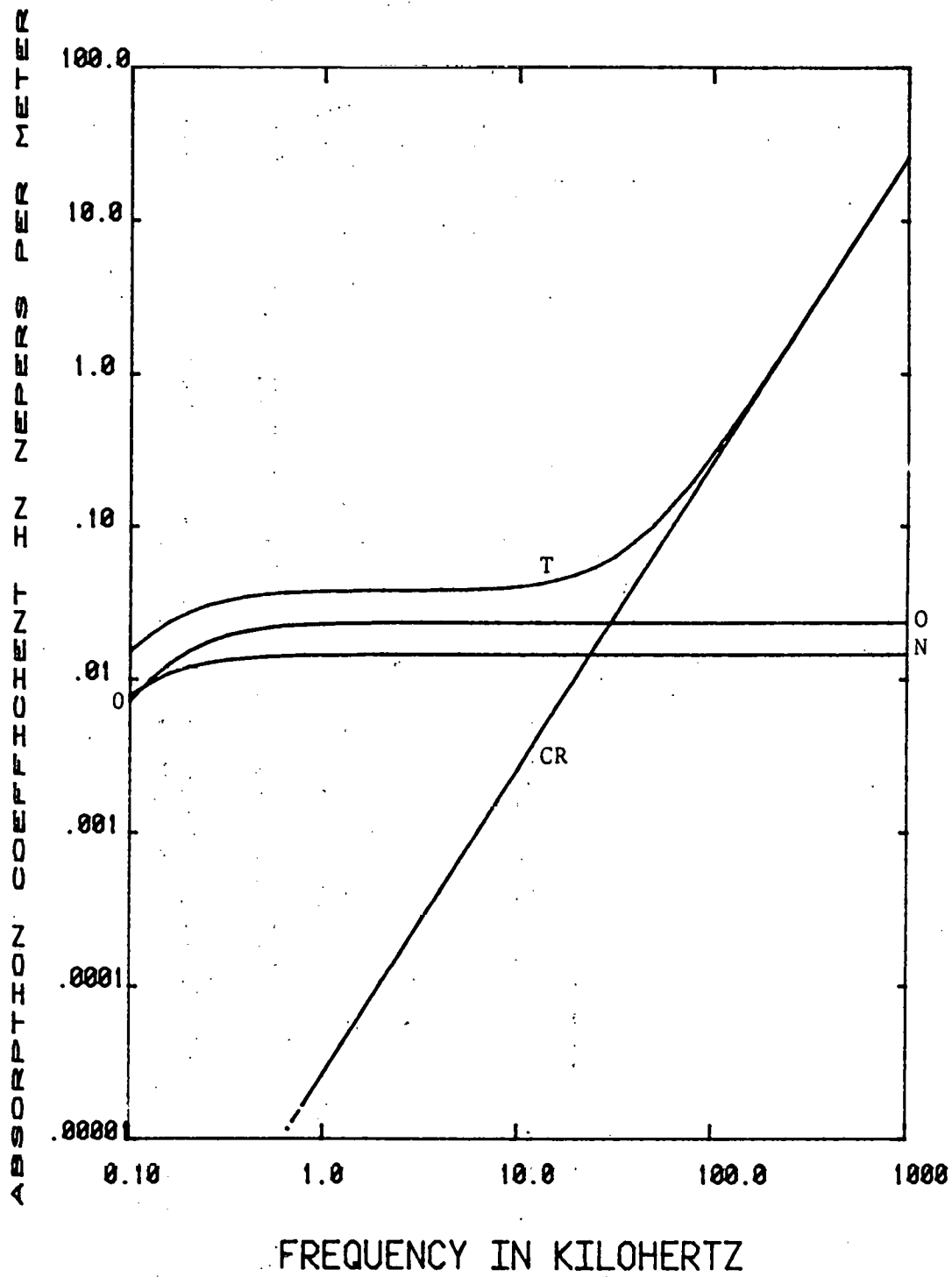
ABSORPTION COEFFICIENT AT 700 DEG. F
14.7 PSI AND 0.00% ABSOLUTE HUMIDITY

Figure 54

FREQUENCY IN KILOHERTZ
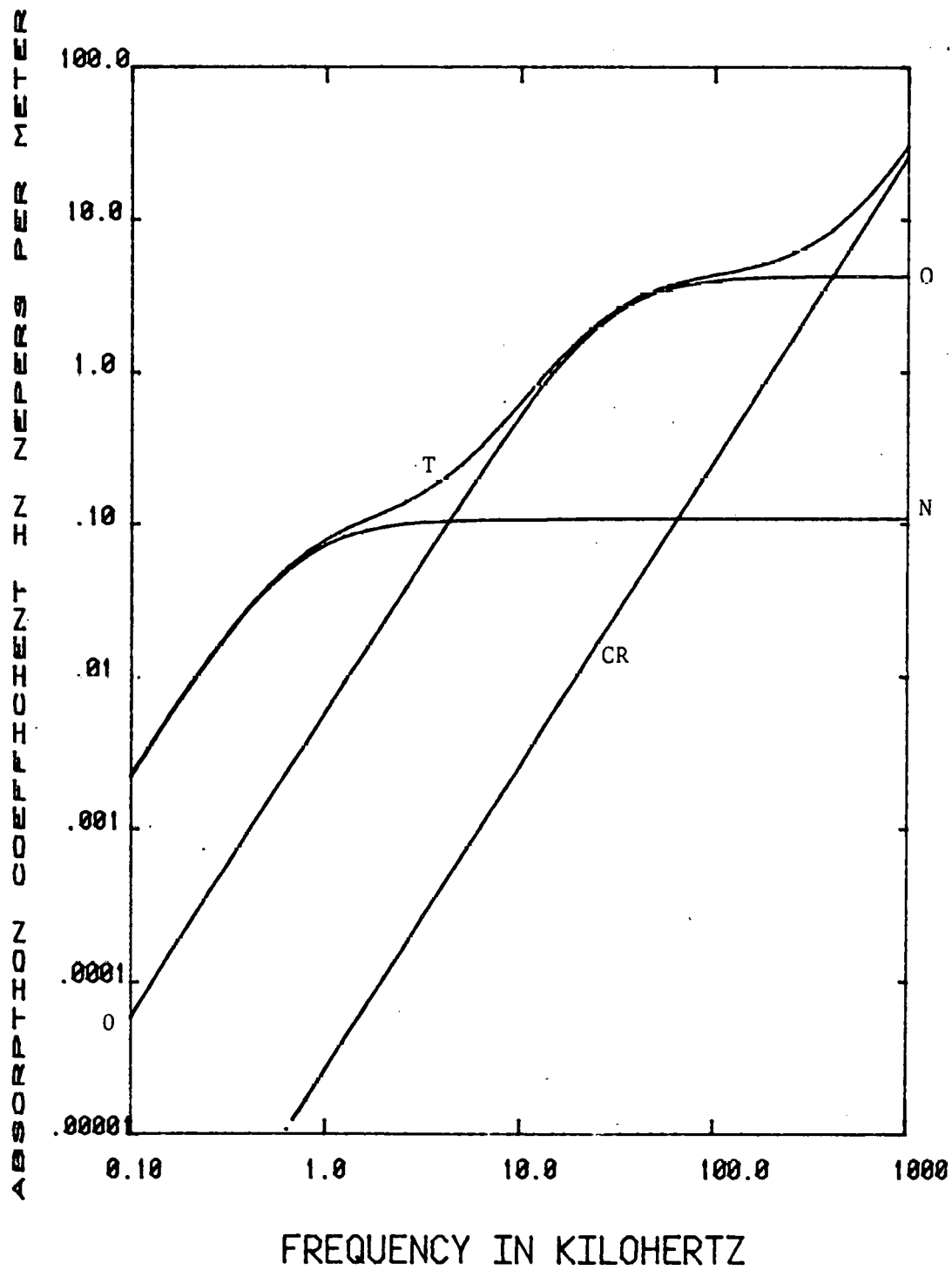
ABSORPTION COEFFICIENT AT 700 DEG. F
14.7 PSI AND 1.00% ABSOLUTE HUMIDITY

Figure 55
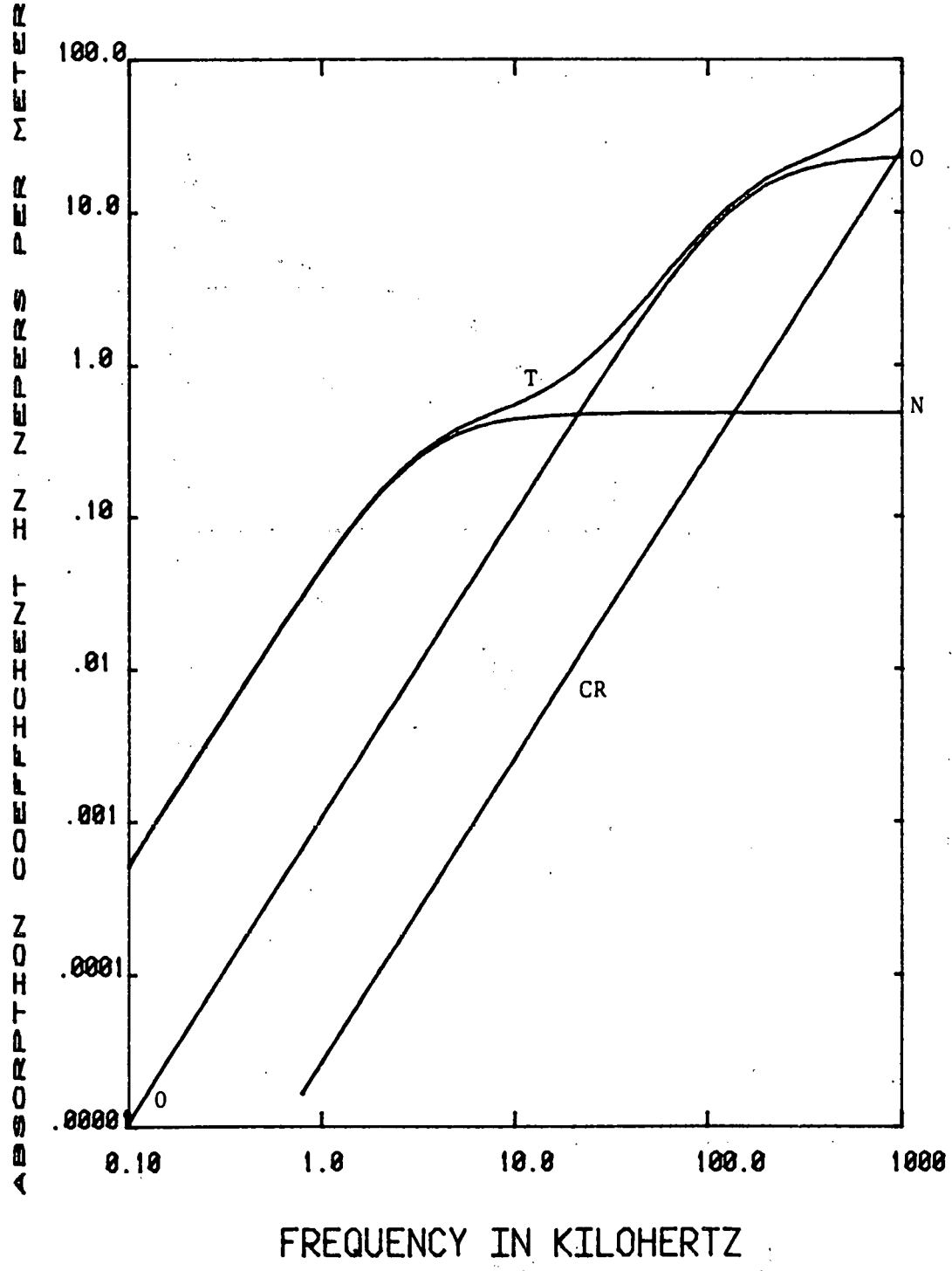
ABSORPTION COEFFICIENT AT 700 DEG. F
14.7 PSI AND 5.00% ABSOLUTE HUMIDITY

Figure 56

TABLE 4   138

REFERENCES FOR INVESTIGATIONS CARRIED OUT ON GAS MIXTURES

Added gas	Base gas										Air
	N_2	O_2	Cl_2	CO_2	COS	CS_2	N_2O	CH_4	C_2H_4O	C_2H_4	
He	—	g, h, i	m, n, o, p	m, n, o, p, q, r, s, t	cc	—	o, p, s, t, cc, dd, ee	—	--	ff	—
Ne	—	j	—	j, m, n	—	--	—	—	--	—	—
Ar	—	i	m, n, o, p	m, n, o, p, q, u, v	cc	—	o, p, s, ee	—	—	ff	—
H_2	a	g, h, k	m, n, o, p	l, m, n, o, p, t v, w, x, y, z	y, cc	y	o, p, y, dd	cc	--	ff, gg	—
D_2	—	h	—	z	—	—	dd	—	—	gg	—
N_2	—	a, k	n, o, p	d, f, g, v, aa	cc	—	ee	—	ff	ff	—
O_2	b, c	—	—	a, f	cc	—	--	—	—	—	—
CO	—	a, g, l	n, o, p	aa	cc	—	o, p, dd	—	—	—	—
HCl	—	—	m, n, o, p	m, n, o, p	·	—	—	—	--	—	—
CO_2	d, e, f	a, d, f, g	—	—	—	bb	—	cc	bb	—	—
COS	—	—	—	—	—	—	—	—	—	—	—
CS_2	d, e, f	d, f, g	—	d, f, bb	—	—	—	—	bb	—	f
N_2O	e	—	—	—	—	—	—	—	—	—	—
H_2O	k	j, k, cc, hh, ii	—	d, f, j, m, n, p, s, r, w, y, aa, jj, kk, ll, mm,	y	y	o, p, s, y, dd, oo	—	—	pp, gg, rr	k, ss, tt
SO_2	e	—	—	—	—	—	—	—	—	—	--
NH_3	—	k, hh, u	—	—	—	—	o, p, dd	—	—	—	—
O_3	—	g	—	—	—	—	—	—	—	—	—
H_2S	—	g, k	—	y	—	—	—	—	—	—	—
D_2O	—	—	—	j, z, kk	—	—	dd, oo	—	—	—	—
CH_4	—	—	m, n, o, p	m, n, o, p	—	—	o, p, cc	—	—	pp	—
C_2H_4O	—	—	bb	—	—	bb	—	—	—	—	—
CH_3OH	—	d, f	—	d, f, w, y	y	y	y	—	—	—	—
C_3H_7OH	—	d, f	...	d, f, w, y	y	y	y	—	—	—	—
C_2H_5OH	—	d, f, g, k	—	d, f	—	—	—	—	—	—	—
$C_6H_5CH_3$	—	—	—	y	—	y	y, pp	—	--	pp	

a Henderson (1962a).
b Ener et al. (1952).
c Zartman (1949).
d Alleman (1938).
e Fricke (1940).
f Knudsen and Fricke (1938).
g Kneser and Knudsen (1934).
h Parker (1961).
i Holmes et al. (1962a).
j van Itterbeck and Mariens (1940).
k Knudsen (1933, 1935).
l Henderson and Klose (1959).
m Eucken and Becker (1933).
n Eucken and Becker (1934).
o Eucken and Küchler (1938).
p Patat and Bartholomé (1936).

q Kneser and Roesler (1959b).
r Bauer and Liska (1962).
s Eucken and Nümann (1937).
t Küchler (1938).
u Kneser and Roesler (1959a).
v Wallmann (1934).
w Knudsen and Fricke (1940).
x Pielemeier and Byers (1943).
y Knudsen and Fricke (1940).
z van Itterbeck et al. (1939).
aa Metter (1937).
bb Angona (1953).
cc Eucken and Aybar (1940).
dd Eucken and Jaaks (1935).
ee Walker et al. (1954).

ff Richards and Reid (1934).
gg Richards (1936).
hh Knötzel and Knötzel (1948).
ii Knudsen and Obert (1936).
jj Pielemeier et al. (1940).
kk Sette and Hubbard (1953).
ll Gutowski (1956).
mm Widom and Bauer (1953).
nn McCoubrey et al. (1954).
oo Wight (1956).
pp Arnold et al. (1958).
qq McCoubrey et al. (1954).
rr McGrath and Ubbelohde (1954).
ss Evans and Bazley (1956).
tt Pöhlmann (1959).

III. CONCLUSIONS AND RECOMMENDATIONS

3.1 INTRODUCTION

The twenty five months research and development program on acoustic agglomeration of power plant fly ash produced important results which will add considerably to our understanding of the processes of sonically induced agglomeration of submicron and micron sized particles. The work has also shown that the process is both technically and most likely, economically viable. As is so common with research at the cutting edge of technology, the results have pointed the way to several additional or continuing investigations which should follow to further our understanding and to develop much needed new insight and advanced technology such as the development of advanced more efficient sound generation technology.

3.2 ACOUSTIC MODELING OF THE AGGLOMERATION PROCESSES

The physics of agglomeration in high intensity sound fields at such levels as 150 - 160 dB has been found to be very complex because of the additional effects of nonlinear acoustics phenomena on local velocity fluctuations. The P.S.U. model was tested at 140 dB levels and found to give fairly good results considering the limited features which are included. At 140 dB we would not expect these nonlinear aspects of acoustic fields to significantly affect the processes. Our current computer code includes Stokesian viscous drag forces, Brownian motion, radiation pressure, Oseen forces, hydrodynamic (Bernoulli) forces, and turbulent diffusion.

We investigated the potential effect of turbulence on agglomeration considering the hydrodynamically and acoustically generated random motions. A study of the work reported by Dr. Shaw on turbulence at the State University of New York at Buffalo in several publications prompted us to start some

independent investigations because of several rather perplexing inconsistencies. As a result of these uncertainties, we questioned the validity of the turbulent diffusion model in our computer code and decided to postpone further runs until clarification of the issues was obtained. Also, and with the concurrence of the technical program monitor, we decided not to continue the further development of the computer code in order to be able to concentrate on the turbulence and fragility studies.

We recommend that the further development of the computer code be made an important aspect of the follow-on program with inclusion of the spatial and spectral characteristics of the sound field from nonlinear acoustic and absorption phenomena. The nonlinear effects will include acoustic streaming, and wave steepening or shocks due to plane wave components.

3.3 BASIC ACOUSTIC INVESTIGATIONS

Our results of the parametric acoustic studies at high intensity levels showed that the parametric acoustic effect could be used to provide both ultrasonic and sonic frequency acoustic energy for a rather unique agglomeration system. However, upon considering the absorption of acoustic energy at the high frequencies by the flue gases, we had to conclude that the concept is simply not economically viable.

We concentrated our efforts in this phase on the investigation of the quite controversial subject of acoustically generated turbulence. The investigation was largely experimental involving acoustic levels up to 170 dB and frequencies in the range of 1000-3500 Hz. We developed a rectangular chamber test set-up such that we dealt with an essentially two-dimensional propagation situation. Since the lowest mode cut-off frequency was 290 Hz, we excited only higher order modes in the chamber. The location and direction of the two sound sources resulted in considerable acoustic streaming velocities

of the order of 5 m/sec. The resulting high Reynolds numbers indicate that turbulent convection flows existed, similar to what we expect to see in agglomerators. Should any significant hydrodynamic turbulence - acoustic turbulence interactions occur, our test results would reflect these interactions.

We conclude from the extensive tests that some acoustically generated turbulence of sorts exists but that such turbulence energies are on the order of 3 orders of magnitude lower than the acoustic energies at the excitation frequencies and harmonics. Furthermore, the spectral characteristics are not truly speaking random in that they appear as a broadening of the bases of the spectra at the acoustic frequencies. We have been successful in modeling this phenomenon electronically and believe it to be akin to an intermodulation distortion due to the simultaneous presence of the low frequency turbulence due to the acoustic streaming and the multiple pure tones components.

We conclude, therefore, that although some acoustically generated turbulence exists, it will not be a significant factor in acoustic agglomeration. The results of this study are documented in our report to DOE/METC number CAES No. 673-83 entitled: "Research on Acoustically Generated Turbulence".

3.4 FRAGILITY STUDIES

We used the predictable fluid shear phenomena taking place in the Anderson Mark III impactors to prove that the agglomerates formed are indeed sufficiently robust to withstand the shear stresses that such agglomerates would experience in typical cyclones. Based on our theoretical studies of the flow phenomena in impactors compared to cyclones and observations of the agglomerates from scanning electron microscope photo-micrographs, we conclude that agglomerates are indeed sufficiently robust to withstand

the less severe conditions in typical industrial cyclones. The results of this study are documented in our report to DOE/METC number CAES No. 655-82 entitled: "Fragility of Acoustically Agglomerated Submicron Fly Ash Particles".

3.5 DESIGN & DEVELOPMENT OF THE 700°F ACOUSTIC AGGLOMERATOR AND SOME TEST RESULTS

An acoustic agglomerator was designed and developed which has a tubular test section of 8" diameter and 8 feet length. The specification of the system were as follows:

Sound Pressure Levels: 130-160 dB.
Sound Frequencies: 1000-4000 Hz.
Aerosol Flow Rates: 0.1 - 1 ft/sec.
Aerosol Loading: 2 gr/m^3 - 20 gr/m^3.
Aerosol Temperature: Controllable to 700°F.

The Sound source was the Penn State University designed and developed 600 acoustic watt siren. Aerosol particle size measurement was performed using Anderson Mark III impactors. The 18.6 KW electric heating system provided the energy to heat the aerosol to the desired temperatures. A Penn State developed ejector type, pulsed aerosol generator provided the proper particle size and loading to the agglomerator. The measurement of the required physical qualities was performed by conventional methods. Data acquisition and reduction was performed by a central microcomputer based system. The Commodore PET Model 4016 microcomputer, the digitizers, multiplexers and displays all functioned well. The design of the agglomerator is documented in a Master of Science in Mechanical Engineering Thesis by Peter An Lu entitled: "Design and Analysis of a Moderate Temperature Acoustic Agglomeration Facility", Nov. 1982.

The 700°F agglomerator met or exceeded all specifications and functioned well. Several desirable improvements became apparent particularly in the particle size measurement system and the siren sound source. Our studies on siren technology have shown that siren efficiency could almost be doubled compared to our current design by optimizing the aerodynamic, porting and acoustic design.

The extensive results at room temperature at acoustic levels above 150 dB and frequencies near 2500 Hz were indeed most encouraging. It is clearly evident that at these conditions the acoustic agglomerator eliminates most of the submicron particles. Our tests also verified that an optimum frequency exists even at these high acoustic levels. For the size distributions and the fly ash density used a frequency of about 2500 Hz appears best. This result agrees with earlier studies at Penn State and results from our current computer code. As previously noted, it appears that increased loadings up to 30 g/m^3 give better agglomeration than lower loadings which again agrees with theory.

We have only performed very few runs at elevated temperatures at the time of this writing. Runs at temperatures of 260°F and 350°F with acoustic levels in the 145 dB range gave similar results to equivalent room temperature runs with an indication that there will be a small decrease in agglomeration due to the increased gas viscosity at the higher gas temperatures.

We conclude that we have a well functioning, valuable test facility. Furthermore, very significant agglomeration of submicron particles occurs at practical levels, loadings and frequencies. We recommend that we first of all, improve our existing facility from lessons learned, that we complete the high temperature tests and that we perform much needed detailed performance explorations of the agglomerator. We also recommend that we use the agglomerator for several basic investigations.

3.6 ACOUSTIC ABSORPTION CONSIDERATIONS IN THE SONIC AGGLOMERATION PROCESS

The literature on the absorption of acoustic energy by atmospheric gas constituents was studied, the theoretical relationships were programmed, considerable new insight was gained and a program for follow on research

was developed. The design specification of acoustic agglomerators in terms of frequency and acoustic level trade-offs depend on the in-depth knowledge of the absorption processes of the flue gas constituents. From our study, we conclude that a follow-on program should include such an investigation involving oxides of nitrogen, carbon and sulfur at temperatures and pressures expected in power plant flues.

IV. REFERENCES

1. 1981 Annual Report to Congress, Energy Information Administration,
    U.S. Department of Energy, Volume 3, Energy Projections, February
    1982 (DOE/EIA-6173(81)/3 pg. 79.

2. National Air Pollution Control Administration, "Air Quality Criteria
    for Particulate Matter," AP-69, 1969.

3. Davies, R. N., "Dust is Dangerous," Faker & Faker Limited, London,
    1953.

4. Proceedings of the Second Annual Contractor's Meeting on Contaminant
    Control in Hot Coal Derived Gas Stream, February 17-19, 1982,
    Morgantown, West Virginia.

5. Dittenhoefer, A.C., and De Pena, Rosa G., "Sulfate Aerosol Production
    and Growth in Coal Operated Power Plant Plumes," Jour. Geophys.
    Research, Vol. 85, No. C8, pg 4499-4506, August 20, 1980.

6. Brandt, O., Freund, H. and Hiedemann, E., "Schwebstoffeim Schallfeld,"
    Z. Phys., Vol. 104, No. (7-8), 511-533, (1937).

7. Kundt, A., "Ueber eine neue Akt akustischer Staubfiguren and iiber die
    Anwendung der Selben zur Bestimmung der schall gesch windigkeit infesten
    Kur pern und Gasen," Annalen Der Physik, Vol. 127, 495-522, (1866).

8. Smoluchowski, M.V., "Versuch Einer Mathematischen Theorie der
    Koagulationskinetik Kolloider Losungen," Z. Physik Chem., Vol. 195,
    129-168, (1918).

9. Brandt, O., Freund, H. and Hiedemann, E., "Zur Theorie der akustischen
    Koagulation," Kolloid Z, Vol. 77, No. 1, 103-115, (1936).

10. St. Clair, H. W.,"Agglomeration of Smoke, Fog or Dust Particles by Sonic
     Waves," Industrial Engineering Chem., 2434-2438, (1949).

11. Stokes, C. A., "Sonic Agglomeration of Carbon Black Aerosols," Chemical
     Engineering Process, Vol. 46, No. 8, 423-432, (1950).

12. Mednikov, E. P., "Acoustic Coagulation and Precipation of Aerosols,"
     Translated from Russian, Consultants Bureau, (1965).

13. Volk, Jr., M and Moroz, W. J., "Aerosol Coagulation in an Acoustic Field,"
     CAES Technical Report Number 354-74, The Pennsylvania State University,
     University Park, Pennsylvania, 80 pages, (1974).

14. Volk, Jr., M. and R. Hogg, "Sonic Agglomeration of Aerosol Particles"
     CAES Report 465-77, The Pennsylvania State University, March 1977.

REFERENCES (Continued)

15. Levich, V. G., Physico-Chemical Hydrodynamics, Moscow, Fizmatgiz, (1959).

16. Black, A. P., "Basic Mechanisms of Coagulation," Journal American Water Works Association, 492-501, (1960).

17. Fuchs, N. A., The Mechanics of Aerosols, Pergamon Press, New York, (1964).

18. Andrade, E. N. dac, "The Coagulation of Smoke by Supersonic Vibrations," Pro. Royal Society, Vol. 134, 1111-1115, (1936).

19. Davidson, G. A. and Scott, D. S., "Finite-Amplitude Acoustics of Aerosols," J. Acoustic Soc. Am. 53(6), pp. 1717-1729, (1973).

20. Shaw, D. T., "Recent Developments in Aerosol Science," Wiley Inter-Science, pp. 279-319, (1978).

21. Shaw, D. T., and Tu, K. W., "Acoustic Particle Agglomeration Due to Hydrodynamic Interaction Between Monodisperse Aerosols," SUNY at Buffalo, NY (1979).

22. Lee, P.S., Cheng, M. T. and Shaw, D. T., "The Acoustic and Hydrodynamic Turbulence - Turbulence Interaction and Its Influence on Acoustic Particle Agglomeration," Report DOE/MC/11842-T9, 1982.

23. Braxton Corporation, "Sonic Agglomeration," Report to Environmental Protection Agency, Report No. PB234146, 1974.

24. Neumann, E. P., Soderberg, C. R. and Fowle, A. R., "Design Application, Performance and Limitations of Sonic Type Flocculators and Collectors," International Committee on Air Pollution, Washington, D.C., Air Pollution Proc. - U.S. Technical Conference, 388-393, (1950).

25. Neumann, E. P. and Norton, T. L., "Application of Sonic Energy to Commercial Aerosol Collection Problems," Chem. Eng. Progr. Symp. Sec. 1, Vol. 47, No. 1, 4-10, (1951).

26. Danser, H. W., "Eliminate Stack Dusts and Mists," Chemical Engineering, 158-160, (1950).

27. Danser, H. W. and Neumann, E. P., "Industrial Sonic Agglomeration and Collection Systems," Industrial Engineering Chem., Vol. 41, No. 11, 2439-2442, (1949).

28. Soderberg, C. R., Jr., "Industrial Application of Sonic Energy," Iron Steel Engr., Vol. 29, No. 2, 87-94, (1952).

REFERENCES (Continued)

29. Neumann, E. P. and Norton, J. L., "Application of Sonic Energy to Commercial Aerosol Collection Problems," Chemical Engineering Symposium Series No. 1, Vol. 47, 4-10 (1951).

30. Kolmogorov, A. I., Leontovich, M., Physik Z. Sovjetunion, 4, 1 (1933).

31. Goldberg, Z. A., "The Propagation of Plane Waves of Finite Amplitude, Soviet Physics Acoustics, 3(4), pp. 322-328 (1957).

32. Morris, P. J. and Baltas, C., "Measurements and Prediction of Turbulence in Sound Excited Jets," AIAA Seventh Aeroacoustics Conference, Palo Alto, 1981.

33. Staffman, P. G. and Turner J. S., "On the Collision of Drops in Turbulent Clouds," Journal of Fluid Mechanics, Vol. 1, 1956.

34. George, Wallace, "Fragility of Acoustically Agglomerated Submicron Fly Ash Particles," Special Report to DOE, CAES Report No. 655-82, August 1982.

35. Miao, Hsu-Chiang, "Aerosol Coagulation in an Acoustic Field," A Thesis in Mechanical Engineering, The Pennsylvania State University, Master of Science Thesis, August 1981.

36. Lu, Peter An., "Design and Analysis of a Moderate Temperature Acoustic Agglomeration Facility," A Report in Mechanical Engineering, CAES Report No. 649-82, November 1982.

37. Shane, S. Joseph, "Design and Development of a High Intensity Siren as a Noise Source for Acoustic Agglomerators," Master of Science Thesis in Mechanical Engineering, The Pennsylvania State University, November 1982.

38. Reethof, G. and Shane, S. J., "Analysis and Design of a 600 Acoustic Watt Siren for an Acoustic Agglomerator of Submicron Particles in Gas Streams," Presented at the Winter Annual Meeting of the A.S.M.E., Phoenix, Arizona, November 1982.

39. R. C. Jones, "A Fifty Horsepower Siren," JASA, 18, 2, October 1946 pp. 371-387.

40. C. H. Allen and I. Rudnick, "A Powerful High Frequency Siren," JASA 19, 5 pp. 857-865, September 1947.

41. Neumann, E. P., and Norton, J. L., "Application of Sonic Energy to Commercial Aerosol Collection Problems, Chem. Eng. Symp. Series No. 1, Vol. 47, 4-10, (1951).

42. Cole, N. J., Powell, R. G., Oesterjober, H. L., and Giericki, H. E., "Acoustic Siren for Generating Wide Band Noise," JASA, 35, 2, 173-191, (1963).

REFERENCES (Continued)

43. Puch, A., "The Effect of the Shape of the Holes of the Rotor and
Stator on the Acoustic Parameter of a Dynamic Axial Generator,"
Arch. of Acoustics, 5, 4, 369-380, 1980.

44. Puch, A., "Generalized Model of an Axial Dynamic Generator," 3, 1,
17-34, (1978).

45. Hueter, T.F., and Bolt, R.M., Sonics, John Wiley & Sons, Inc., New
York, N.Y., (1955).

46. Daily, J.W., and Nece, R.E., "Chamber Dimensions Effects on Induced
Flow and Frictional Resistance of Enclosed Rotating Disks," Jour.
Basic Engrg., Trans. A.S.M.E., Series D, Vol. 82, March 1960.

47. Miao, Hsu-Chiang, "Aerosol Coagulation in an Acoustic Field," A Thesis
in Mechanical Engineering, The Pennsylvania State University, Master
of Science Thesis, August 1981.

48. Dwyer, Thomas J., "An Investigation of Several Special Problems for
the Agglomeration of Fine Particulate with Low Intensity Acoustic
Energy," A Report in Mechanical Engineering, CAES Report No. 659-82,
The Pennsylvania State University, November 1982.

49. Morse, P.M., and Ingard, K.U., "Theoretical Acoustics", McGraw-Hill
Book Company, New York, N.Y. 1968.

50. McDaniel, O.H., "Propagation of Sound at Moderate and High Intensities
in Absorbant and Hard-Walled Circular Ducts," Ph.D. Thesis in Engineering
Acoustics, The Pennsylvania State University, March 1975.

51. Wyerman, B.R., "A Theoretical and Experimental Study of Acoustic
Propagation in Multisectioned Ducts," Ph.D. Thesis in Engineering
Acoustics, The Pennsylvania State University, March 1976.

52. Walter, J.L., "Coincidence of Higher Order Modes - A Mechanism of the
Excitation of Cylindrical Shell Vibrations via Internal Sound,"
Ph.D. Thesis in Mechanical Engineering, The Pennsylvania State
University, May 1979.

53. Reethof, G., "Turbulence - Generated Noise in Pipe Flow," Am. Rev.
Fluid Mech., Vol. 10, 333-368, 1978.

54. Eckart, C., Phys. Rev. 73, 68, 1948.

55. Lighthill, J., "Waves in Fluids," Cambridge University Press, Cambridge,
England, 341-342, 1978.

56. Nyborg, W., "Acoustic Streaming," Physical Acoustics, Vol. II, Part B,
Edited by W. R. Mason Chapter 11, Academic Press, 1965.

REFERENCES (Continued)

57. Lieberman, L. N., Phys. Rev. 75, 1415 (1949).

58. Walker, J. P. and Allen, C. H., "Atmospheric Physics and Sound Propagation," Chapter 10, Report by Acoustics Laboratory, Dept. of Physics at The Pennsylvania State University, September 1950.

59. Stokes, G., Trans. Cambridge Phil. Soc., 8, 287, (1845).

60. Kirchoff, G., Am Phys. 134, 177, (1868).

61. Herzfeld, K.F., and Litovitz, T. A., Absorption and Dispersion of Ultrasonic Waves, Academic Press, 1959.

62. Herzfeld, K. F., and Rice, F. O., "Dispersion and Absorption of High Frequency Sound," Phys. Rev. 31, 91, (1928).

63. Tisza, L. T., "Supersonic Absorption and Stoke's Viscosity Relationship," Phys. Rev. 61, 531 (1942).

64. Bass, H. E., "Absorption of Sound by Air: High Temperature Predictions," J.A.S.A. 69, (1), 124-138, (1981).

65. Kneser, H. O., "Relaxation Processes in Gases," Chapt. 3 in Physical Acoustics, Vol. II, Part A, Edited by W. P. Mason, Academic Press 1965.

V. LIST OF FIGURES

LIST OF FIGURES (Continued)

LIST OF FIGURES (Continued)

LIST OF FIGURES (Continued)

VI. LIST OF TABLES

STATEMENT OF WORK
Acoustic Agglomeration of Power Plant Fly Ash

Scope

The proposed project is to further investigate some of the basic phenomenas associated with the acoustical treatment of aerosols, and in particular, fly ash suspensions, to ascertain the behavior of these systems under a variety of parameter variations. This project would be undertaken in order to better develop and evaluate potential gas stream cleanup technologies encountered in coal utilization schemes.

Objectives

The goals of the proposed work are to further the understanding of the agglomeration phenomena in both cool and hot particle-laden gas streams. Specifically, the effect of ultrasonic sound on collision frequency, the fluid dynamics associated with acoustically generated turbulence and nonlinear acoustical effects, the spatial and temporal aspects of sound fields and chambers, and the fragility of agglomerated particles are to be investigated. Thus, so armed with this knowledge, more sound developmental designs and evaluations will be possible.

Work Statement

The proposed contractor is to provide the necessary equipment and personnel required for the accomplishment of the below listed tasks:

Task I -- Acoustic Modeling

Modification and further development of the computer code is developed under the current contract. Specifically, the existing model is to be extended to include the effects of: (a) spatial and temporal characteristics of the sound field on agglomeration, (b) nonlinear acoustic phenomena generated at high acoustic pressures, (c) using parametric acoustics to generate high sound intensities, and (d) particle configuration on diffusional processes.

Deliverables for Task I -- A documented computer program incorporating the modifications effected under Task I. The results obtained in running the program over the parameter ranges attained in Tasks II are to be included in the topical reports required under Task II.

Task II -- Basic Acoustic Investigations

Design and conduct tests to experimentally examine the phenomena of acoustic streaming in the existing PSU test facility to ascertain the characteristics of this phenomena related to agglomeration. Experimentally investigate the mechanism by which turbulence is acoustically induced and compare the scale and magnitude of that turbulence to hydrodynamically induced turbulence. Experimentally investigate the nonlinear phenomena of wave-steepening in reverberant space. Characterize and investigate the spatial and temporal aspects of the sound field in the existing PSU agglomeration chamber.

Deliverables for Task II -- A design plan for each type of experiment is to be submitted to the TPO for approval prior to experimental execution. All results of these tests are to be incorporated into a series of reports describing in detail the results and conclusions and submitted as topical reports.

Task III -- Room Temperature Particle Fragility

Devise a methodology or technique for measuring particle agglomerate fragility using velocity shear flows. Originate a test plan to produce fly ash agglomerates at room temperature in the existing PSU acoustic agglomerator and to extract and classify the fragility of the agglomerates using the technique developed above. Execute the test plan.

Deliverables for Task III -- A test plan for testing the fragility of acoustic agglomerated fly ash particles is to be submitted to the TPO for approval prior to execution. A topical report describing the methodology for testing agglomerate fragility and describing the test results, and conclusions of room temperature agglomerate fragility testing is to be sumbitted.

Task IV -- Moderate-Temperature Agglomeration Tests

Design and construct an approximately 6-inch diameter acoustic agglomeration chamber to be operated over a range of elevated temperatures from 300°F up to 700°F. Design and conduct tests of acoustic agglomeration of fly ash at elevated temperatures. These tests are to include tests of agglomerate fragility using the technique developed in Task III. Design a similar facility for operation at temperatures up to 1500°F.

Deliverables for Task IV -- Design of high-temperature agglomeration chamber is to be submitted for approval prior to construction. Design of high-temperature acoustic agglomeration of fly ash tests is to be submitted to the TPO prior to execution. The results of all tests and a topical report describing in detail the high-temperature agglomeration experiment, results, conclusions, and recommendations for future work. Design of high-temperature acoustic agglomeration facility.